UiO Satellite Ground Station: Simulation, Implementation and Verification

Eirik Vikan

November 2011

CUBESTAR

UNIVERSITAS OSLOENSIS · MDCCCXI ·
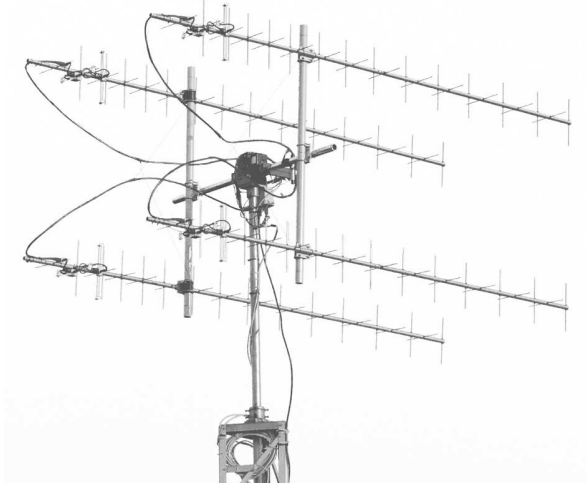
Abstract

This thesis has documented the work of implementing the new UiO ground station which is situated at the University of Oslo. The station is fully operational and it meets the needed requirements for a communication link with satellites in low earth orbit.

The antenna arrangement consists of four stacked Yagi-Uda antennas mounted on a frame with vertical booms made of fiberglass. The choice of fiberglass over metal minimize degradation of the antenna radiation pattern and the antenna input impedance. The effects of stacking antennas have been simulated in FEKO simulation software which is based on Method of Moments (MoM) integral formulation of Maxwell's equations.

To master all the details of the ground station requires a wide range of knowledge. The first chapters present some very useful background theory for gaining a better understanding of how the system works and how it was tested. There has been a strong emphasis on providing the reader with a clear picture of the complete system and the theoretical foundation needed to understand this. Hopefully this will motivate future students to take part in working with and improving the ground station.

Acknowledgements

This master thesis concludes my degree in Electronics and Computer Technology at the Department of Physics. This was done in the timeperiod from September 2010 to Desember 2011 under the supervision of Associate professor Torfinn Lindem.

First of all I want to thank Professor Torfinn Lindem for his enthusiasm in his teachings and his belief in us students. Without Torfinn we would not have our great student assoiciation SEF (Students Electronics Association) which has given many students another good reason to thrive at campus.

I am gratefull to Jonas Ringnes, Thor Arne Agnalt and the rest of the team from the mechanical workshop at the Department of physics for their swift assistance in making the neccesary parts needed to complete this task. I also want to thank Halvor Strøm for ordering needed parts. I have enjoyed the company of all the CubeSTAR members and in particular Johan Tresvig who has been very helpful and excellent office room mate during this time.

I want to dedicate this work to my girfriend Christel, who I believe is the reason i made it this far. Thank you for giving me back faith in the future. You are a truly beautiful girl.

Norway, Oslo, November 2011
Eirik Vikan

Contents

List of Figures

List of Tables

Chapter 1

Introduction

A small student built nano satellite is under development at the University of Oslo. The satellite has the dimensions of 20 cm · 10 cm · 10cm and can have a maximum weight of 2.66 Kg. This is based on a standard developed at the California Polytechnic State University (Cal Poly) through the CubeSat Project.

To establish and verify an operational ground station early in the project phase should have a high priority. Without any means of communicating with the satellite while in orbit, the mission objective is rendered useless. In the spring of 2008 two students began work on what would be the first ground station established under the CubeSTAR project [22]. This development was kick-started by a workshop at Andøya august that same year. Then six students from the university of Oslo went to the Andøya Rocket Range and set up a ground station in coordination with staff from Norwegian Centre for Space-related Education (NAROM).

This thesis present the new improved ground station at the University of Oslo.

1.1 The CubeSTAR Project

In 2006, NAROM in coordination with Andøya Rocket Range (ARR) decided to initiate a norwegian student satellite program called ANSAT [3]. The first student satellite would be HinCube developed at the Narvik university college. The second satellite is under development at the University of Oslo and is called CubeSTAR (also the name of the project). The CubeSTAR project was initiated December 2008 and is expected to be launched, in a polar low earth orbit (LEO) orbit at an altitude between 450 and 500 km, sometime in the spring of 2014 [10].

There will be a scientific experiment on board the satellite as payload. This payload is called a fixed-bias multi-Needle Langmuir Probe system (m-NLP). This is a novel instrument invented at the University of Oslo. It's purpose

onboard the satellite is to measure the electron density structures in the iono-
sphere at much greater resolution (a few meters) than todays standards. It
has been flown and tested on several rockets, ICI-2 being the first [4]. When
this instrument is flown on the CubeSTAR satellite it can measure the electron
density over the polar cusps. Theses measurements can possibly be used to
understand and give better predictions of the space weather phenomenon.

Besides the scientific experiment on board, the project also aims at making
most of the satellite subsystems locally. Through the work of master thesis
several reports have been delivered with work related to the electronic power
system, communication, attitude determination and control system and more
of the parts needed for the CubeSTAR satellite. An early physical model of
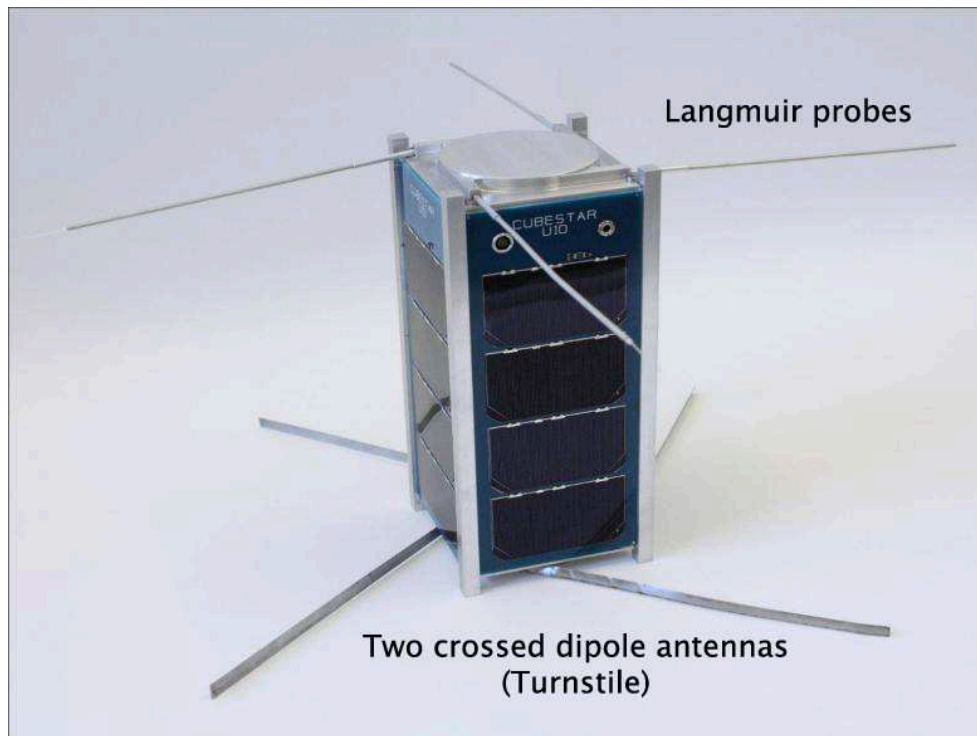
Figure 1.1: An early model of the CubeSTAR satellite

the CubeSTAR satellite model is presented in figure 1.1.

1.2 GENSO

Global Educational Network for Satellite Operations (GENSO) is a project of
the European Space Agency (ESA) under the Education Office. The university
of Vigo in Spain hosts the european node and coordinate access to the GENSO
network. The objective if this project is to realize a world wide network of radio

amateur and university ground stations to support the operations of university satellites.[24] The benefit of such a network is to increase the coverage and timeframe for which data is downloaded from the satellite. A LEO satellite has only a few passes per day. The individual student ground stations remains idle for most of the time. When connected to the GENSO network the ground station can then be used to track and download data from other passing by satellites when it would otherwise just stand idle. This will greatly increase the overall efficiency of all the stations involved and give all members a much greater amount of valuable downloaded scientific data from the experimental payload on board the satellite.

At the 2010 international astronautical congress in Prague, GENSO was reported to be in an early operational phase [15]. Only a handful of operational ground stations was allowed to take part at this stage. Revision 2 of the software is to be released under open source license, but a release date has not yet been published.

1.3 The Goals of this Thesis

The previous ground station consisted of two Yagi-Uda antennas, one for the ultra high frequency (UHF) band the other for the very high frequency (VHF) band. As the CubeSTAR progressed a decision fell on using a single frequency in the UHF communication link between the satellite and ground station. For this reason the ground station was determined to be upgraded to a antenna rig consisting of four UHF antennas stacked at appropriate distance to increase the antenna gain. At that time there was also an acquisition of a higher quality of test equipment (vector network analyzer (VNA) and signal generator) which gave the opportunity to perform testing and verification of all the components in the physical implementation of the ground station. The goals to be achieved in this thesis are:

- Build and verify the new satellite ground station for the purpose of future communication with the CubeSTAR satellite.

- Simulate the behavior of the antenna radiation pattern for the four stacked Yagi-Uda antennas.

- Ensure continued compatibility for GENSO.

- Ensure that that this report can be used as a reference to the ground station for future students and participants in the CubeSTAR project.

1.4 Outline of this Thesis

This document is a report of the work on the new ground station as well as a reference and user guide for future students of the CubeSTAR project involved

in work on the communication link. For this reason some of the chapters have a lot of attention on details and procedures which might prove useful for further work and development on this system.

The first fours chapters present a lot of theory which give a foundations for understanding the simulation and measurement results presented in later chapters. It is intended mainly for those readers which are unfamiliar with these subjects. The report phase of this document starts at chapter 6 on page 47.

The general description of the ground station is presented in chapter 8 and the link budget results can be seen in appendix B. Below is a brief description of each chapter.

`Chapter 2` present the reader to some key aspects within transmission line theory. The basic notion of simply connecting a cable between two points for optimal transportation of current or voltage only holds true when certain conditions are met. The chapter explains these conditions and some other important subjects needed for making a precise analysis of the transmission lines role in the performance of the ground station.

`Chapter 3` describe the scattering parameters which is used to describe the performance of the different device under test (DUT) in the system. The basic concept and some definitions used while doing measurements with a VNA are explained.

`Chapter 4` focuses on basic antenna theory and describe the Yagi-Uda antenna. The principles presented here are highly relevant for understanding the work presented in chapter 6 on page 47.

`Chapter 5` gives the background theory needed for the link budget calculations.

`Chapter 6` present the antenna simulation results and implementation. These simulations are performed with the FEKO simulation software tool. The antenna radiation pattern of the four stacked yagi antennas have been evaluated in different arrangements.

`Chapter 7` present the downlink budget calculation for data transmission. This is the only scheme presented at this level of detail because all the other scenarios such as uplink and downlink beacon will have a higher link margin due to more available power at the transmitter for uplink and a much lower required signal to noise ratio (SNR) for the downlink beacon for successful reception.

`Chapter 8` gives the reader an complete overview of the UiO ground station.

The component selection is explained as well as details regarding the installation. The different physical connections that are currently needed for receiving CW morse code or sending or receiving AX.25 data is described.

`Chapter 9` present the methods and results from all the measurements done at the station.

`Chapter 10` gives a summary and conclusion of the work as well as future work and recommendations.

Chapter 2

Transmission Line Theory

The content of this chapters is intended for the audience without prior knowledge of transmission line theory. This chapter will review selected parts from transmission line theory that is useful for understanding the behavior of a signal travelling from a radio transmitter to an antenna load connected through transmission lines. The level of detail used here is intended to give the readers that are unfamiliar with these subjects a foundation for understanding the testing and measurement conducted on the station in later chapters.

As the frequency of electromagnetic waves in a circuit increase, the wavelength decrease. In Lumped Circuit Theory the circuit elements are assumed to have zero spatial extent where voltages and currents are considered spatially uniform. Kirchhoff's circuit laws can be applied. But when circuit elements become comparable to the wavelength of the propagating wave, distributed theory must be used. This theory models the circuit elements as having finite size relative to the wavelength of voltage and current waves. The transition from lumped theory to distributed theory occurs gradually and has no explicit value for when to use one or the other. As a rule of thumb, distributed theory should be applied when the average size of the discrete circuit components is more than a tenth of the wavelength [13].

2.1   Transmission Lines

The most basic transmission line is the two-wire line. But it has poor performance in radio frequency (RF) applications. At high frequency changing electromagnetic field lines will be induced between and around the two conductors causing it to radiate. This makes it sensitive to incoming radiation just as an antenna is. The coaxial cable on the other hand has an outer conductor that encloses the center conductor and the electric and magnetic fields. This means that coaxial cable has very low radiation loss and is highly resistant to intereference from other fields.
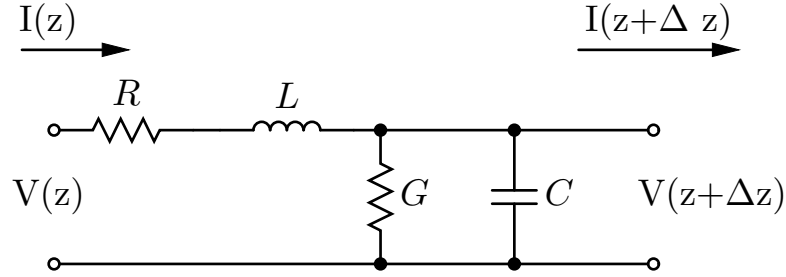
Figure 2.1: Electrical equivalent of a infinitely small transmission line segment

2.1.1   Equivalent Circuit Representation

Transmission lines longer than 10% of the signal wavelength should not be considered to have spatially uniform voltages and currents when performing calculations. The results of these calculations will give inaccurate results. But if the line is divided into infinitesimal segments, Kirchoff's circuit laws can then be applied on each of these segments. An infinitesimal segment of a transmission line can be seen in figure 2.1. To make an analogy with a coaxial cable. The elements in the circuit can be described the following way. The resistor is the center conductor wire resistance per unit length. The inductance L is due to the internal and external inductance of the center conductor. The parallel connected admittance G represent the conductance between the center conductor and the outer braid or shield. And the capacitor C is due to the capacitance between the center conductor and the outer braid or shield. Each segment can be said to have a length of Δz. Then the circuit can be described by Kirchoff's voltage and current law in the following way

$$(R + j\omega L)I(z)\Delta z + V(z + \Delta z) = V(z) \tag{2.1}$$

From this relation, many other useful equation can be derived. Some of these are presented in the following sections.

2.1.2   Travelling Voltage and Current Waves

When a lossless transmission line is sourced with a high frequency sinusoidal source, voltage and current waves will propagate along the line. If there are reflections at the load or along the transmission line it selves there will be a reflected wave travelling in the opposite direction of that of the incident wave. The voltage on a single point z on the line can then be described by the combination of the forward travelling wave and the backwards travelling way in the following manner

$$V(z) = V_0^+ e^{-j\beta z} + V_0^- e^{+j\beta z} \tag{2.2}$$

The net current at a single node on the line can equally be described the following way

$$I(z) = I^+ e^{-j\beta z} + I^- e^{+j\beta z} \qquad (2.3)$$

V_0 describe the magnitude of the applied voltage wave from the source and I_0 describe the magnitude of the current applied from the source. The β is known as the phase constant and is given by

$$\beta = \frac{2\pi}{\lambda} \qquad (2.4)$$

For a real transmission line such as a coaxial cable there are losses due to heating of the center conductor and the dielectric material. There are also some loss due to radiation, but this is usually much less than the previous mentioned. This causes the propagating waves to be gradually attenuated along the line. To model this behavior a attenuation constant α is added to the phase constant β to form the complex propagation constant γ given by

$$\gamma = \alpha + j\beta = \sqrt{(R + j\omega L)(G + j\omega C)} \qquad (2.5)$$

The voltage at point z along a lossy line can then be described as [11].

$$V(z) = V_0^+ e^{-\gamma z} + V_0^- e^{+\gamma z} = V_0^+ e^{(-\alpha - j\beta)z} + V_0^- e^{+(\alpha + j\beta)z} \qquad (2.6)$$

2.1.3   Characteristic Impedance

The characteristic impedance,Z_0, of a transmission line is given by

$$Z_0 = \frac{V^+}{I^+} = -\frac{V^-}{I^-} = \frac{R + j\omega L}{\gamma} = \sqrt{\frac{R + j\omega L}{G + j\omega C}} \qquad (2.7)$$

This impedance describe the ratio between the travelling voltage wave and the travelling current wave [13]. For a lossless transmission line, the characteristic impedance is purely real and given by $\sqrt{\frac{L}{C}}$. In this case the voltage and current waves travel in phase along the line.
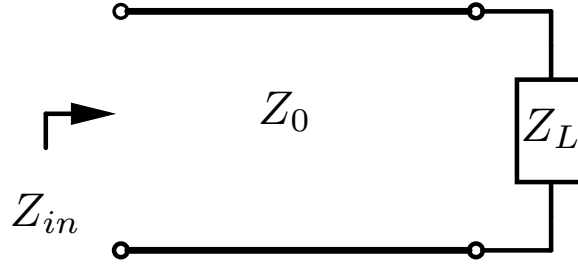
Figure 2.2: Transmission line with load.

2.2   Sourced and Loaded Transmission Lines

2.2.1   Voltage Reflection Coefficient and Voltage Standing Waves

When voltage or current waves are travelling through a discontinous medium, where the characteristic impedance changes, there will be a reflection. The ratio of voltage between the incident and reflected wave can be describe by the voltage reflection coefficient Γ. For a lossless transmission line with characteristic impedance Z_0, connected to a load with impedance Z_L, the reflection coefficient is given by

$$\Gamma = \frac{Z_L - Z_0}{Z_L + Z_0} \tag{2.8}$$

When there is a mismatch (i.e. $Z_0 \neq Z_L^*$), there will be a forward travelling voltage wave and a backwards travelling voltage wave due to the reflection at the load. When there is an open load (i.e. $Z_L = 0$) the reflected wave will be equal in amplitude as the incident wave, but it has a phase change of 180 degrees. The two waves combined will then have fixed zero crossings and form a standing wave pattern where. No energy propagates to any load. A term called the voltage standing wave ratio (VSWR) is often used to describe the quality of match and is usually referred to the input of a device. It is defined as

$$VSWR = \frac{|V_{max}|}{|V_{min}|} = \frac{|I_{max}|}{|I_{min}|} \tag{2.9}$$

In terms of reflection coefficient the VSWR is given by

$$VSWR = \frac{1 + |\Gamma_0|}{1 - |\Gamma_0|} \tag{2.10}$$

2.2.2   Input Impedance of a Loaded Transmission Line

For a lossless transmission line with characteristic impedance Z_0 and a load impedance of Z_L the input impedance at a distance d along the line from the

load is given by the following equation

$$Z_{in}(d) = Z_0 \frac{Z_L + jZ_0 tan(\beta d)}{Z_0 + jZ_L tan(\beta d)} \qquad (2.11)$$

Even though a perfectly lossless transmission line is a physical impossibility, equation 2.11 can be used as a good approximation for low loss line where $R << \omega L$ and $G << \omega C$.

2.2.3 Maximum Power Transfer

For a generator source to deliver the maximum possible power to a load, the impedances in the system must be matched. If a source impedance Z_S is connected to a load though a transmission line, the impedance seen at the input of the transmission line Z_{in} must fulfill the following condition

$$Z_S = Z_{in}^* \qquad (2.12)$$

The input impedance must be the conjugate of the source impedance or vice versa. If the imaginary part of Z_S is zero and $Z_S = Z_0 = Z_L$ the transmission line can be any length without compromising the matched condition. The voltage and current waves will travel in phase as explained in 2.1.3 on page 9. For all other cases the matched condition can be achieved through the use of different line configurations or by adding matching networks.

2.2.4 Power Delivered to a Load

Figure 2.3 on the following page shows a source generator connected to a load impedance through a lossy transmission line. The power delivered to the load (P_L) from the generator with a peak amplitude of V_G is given by

$$P_L = \frac{1}{8} \frac{|V_G|^2}{Z_0} \frac{|1 - \Gamma_S|^2}{|1 - \Gamma_S \Gamma_{in}|^2} e^{-2\alpha \ell} \left(1 - |\Gamma_0|^2\right) \qquad (2.13)$$

Where Γ_S is the reflection coefficient when looking into the source, Γ_{in} is the reflection coefficient looking into the transmission line towards the load and α and ℓ is the attenuation constant and the length of the transmission line. In the case of the circuit in figure 2.3 on the next page half the power will be delivered to the load and the other half will be consumed in Z_S. In a cascaded network the different reflections along the chain ports might interact to give a higher or lower mismatch loss than expected from adding up the individual mismatch losses.

2.3 Transmission Line Applications

2.3.1 Open and Shorted Circuited Transmission Line

The input impedance of a loaded lossless transmission line was given in equation 2.11. When the load is removed we have a line with no load. This is defined
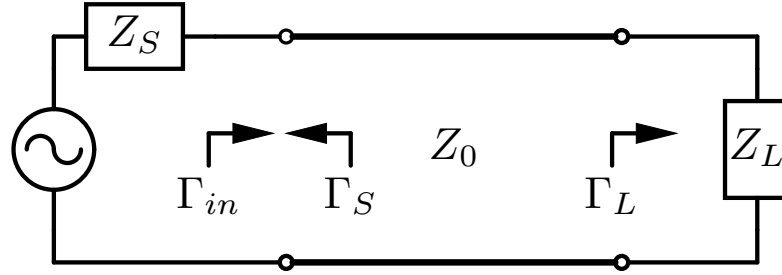
Figure 2.3: Sourced and loaded transmission line

as an open-circuited transmission line. Given that there are no fringe capaci-
tances or any conductance to any surrounding material, the load impedance is
equal to infinity. The input impedance seen at the input of the transmission
line, at a length d away from the open end, is then

$$Z_{in}(d) = -jZ_0 \frac{1}{tan(\beta d)} \tag{2.14}$$

If the transmission line is shorted at the load end, the load impedance will be
zero ($Z_L = 0$). The input impedance is then given by

$$Z_{in}(d) = -jZ_0 \frac{1}{tan(\beta d)} \tag{2.15}$$

These two equations are very interesting as the input impedance change at
the input of the transmission line as a function of frequency, characteristic
impedance of the transmission line and the distance away from the load. If the
frequency is fixed, the length of the transmission lines can be varied to create
both capacitive and inductive behavior as well as the basic open and short
circuit conditions. This means that transmission lines can be used to model
the behavior of lumped capacitors and inductors in a circuit. The different
configurations and their equivalent lumped component behavior is showed in
figure 2.4 on the next page. When the length ℓ of the transmission lines is 0 or
a multiple of $\frac{\lambda}{4}$ the input impedance is either zero or infinite consistent with
equation 2.14 and equation 2.15.

2.3.2   Lambda-Quarter Wave Transformer

A transmission line of a quarter wavelength can be used to transform the load
impedance. The equation for the characteristic impedance for a quarter wave
transmission line is

$$Z_0 = \sqrt{Z_L Z_{in}} \tag{2.16}$$

 In figure 2.5 on the facing page two transmission lines of a quarter wavelength
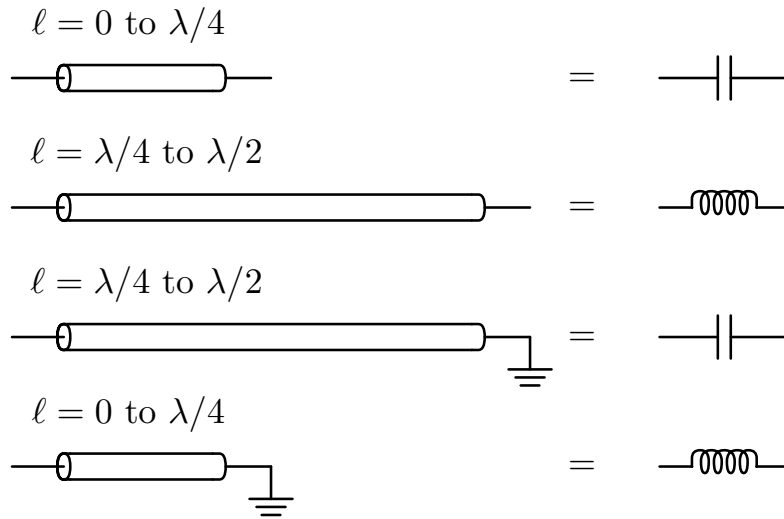
Figure 2.4: Lumped component equivalent of short-circuit and open-circuit transmission lines.
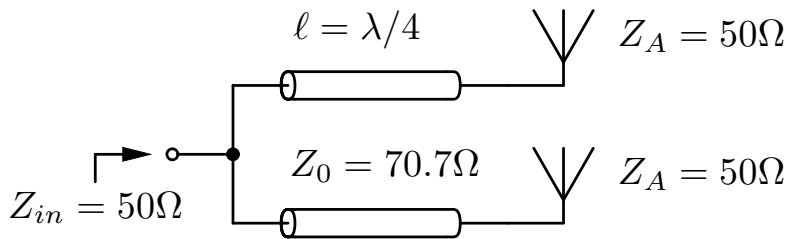
Figure 2.5: Lambda-quarter wave transformer used to match two parallel to 50 Ω

length is used to match the input of this circuit to 50 Ω. Here two antennas with the impedance $Z_A = 50\Omega$ each is to be connected in parallel to a source. But if these ere connected straight to each other the input impedance would be half (i.e. 25 Ω). We want each branch to have a input impedance of 100 Ω which in parallel comes to the wanted 50.[1] By using equation 2.16 on the facing page the characteristic impedance can be calculated. In this case the optimal solution is to have $Z_0 = 70.7\Omega$. A coaxial cable with this impedance has to be custom made, so a compromise of the much more common 75 Ω cables could be used to get an acceptable match.

---

[1] See appendix B on page 103 for an example on how this principle works on the antenna assembly for the antennas used in this thesis.

2.3.3   Input Impedance of $\lambda/2$ Transmission Line

Something very interesting happens to the input impedance of a half-wavelength transmission line. It becomes equal to the load impedance when the transmission line length is equal to $n \cdot \frac{\lambda}{2}$ where n i any natural number. This can be shown if we substitute $d = l_d + \frac{m\lambda}{2}$ and fill inn for $\beta = \frac{2\pi}{\lambda}$ in equation 2.11 on page 11.

$$Z_{in}(d) = Z_0 \frac{Z_L + jZ_0 tan(\beta d)}{Z_0 + jZ_L tan(\beta d)}$$

$$Z_{in}(l_d + \frac{m\lambda}{2}) = Z_0 \frac{Z_L + jZ_0 tan(\frac{2\pi}{\lambda}(l_d + m \cdot \frac{\lambda}{2}))}{Z_0 + jZ_L tan(\frac{2\pi}{\lambda}(l_d + m \cdot \frac{\lambda}{2}))}$$

$$= Z_0 \frac{Z_L + jZ_0 tan(\frac{2\pi}{\lambda}l_d + m\pi)}{Z_0 + jZ_L tan(\frac{2\pi}{\lambda}l_d + m\pi)}$$

Because the tangent function has a period of π, we get that $tan(\frac{2\pi}{\lambda}l_d + m\pi) = tan(\frac{2\pi}{\lambda}l_d)$. This show that the input impedance repeats every half wavelength and is equal to

$$Z_{in}(\frac{n\lambda}{2}) = Z_0 \frac{Z_L + jZ_0 tan(\frac{2\pi}{\lambda}\frac{\lambda}{2})}{Z_0 + jZ_L tan(\frac{2\pi}{\lambda}\frac{\lambda}{2})} = Z_0 \frac{Z_L + jZ_0 tan(\pi)}{Z_0 + jZ_L tan(\pi)} = Z_L \qquad (2.17)$$

If only one fixed frequency is used in a system with the condition $Z_S = Z_L \neq Z_0$, the source can me matched to the load if the transmission line i precisely a multiple of a half-wavelength in length.

Chapter 3

Scattering Parameters

the s-parameters (short for scattering parameters) is a useful tool for describing linear circuit networks. S-parameters are defined in terms of wave quantities consisting of incident wave a and reflected wave b. These wave quantities have units of $\sqrt{W}$ where the power delivered to DUT is given by $|a|^2$. [13, 8]

A 2-port network and the different wave quantities are illustrated in 3.1. In this 2-port network the relationship between the wave quantities and the s-parameters is given by

$$\begin{Bmatrix} b_1 \\ b_2 \end{Bmatrix} = \begin{bmatrix} S_{11} & S_{21} \\ S_{12} & S_{22} \end{bmatrix} \begin{Bmatrix} a_1 \\ a_2 \end{Bmatrix}$$
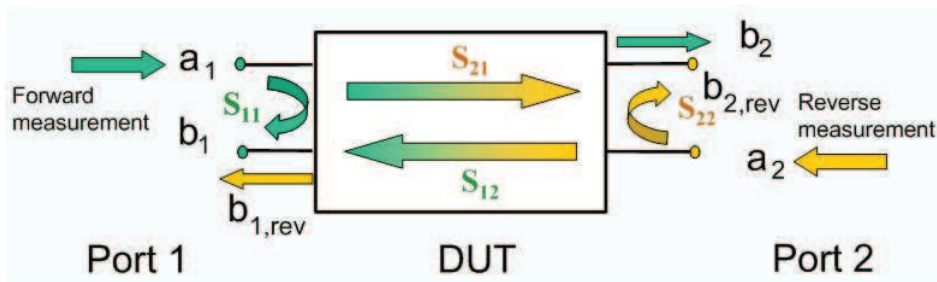
Figure 3.1: Illustration of s-parameters in a two-port network (Credit:R&S)

a_n is the incident normalized power wave and b_n is the reflected normalized power wave. The subscript n refers to port number. These waves are defined as follows:

$$a_n = \frac{1}{2\sqrt{Z_0}}(V_n + Z_0 I_n) \qquad \text{Normalized power wave}$$

$$b_n = \frac{1}{2\sqrt{Z_0}}(V_n - Z_0 I_n) \qquad \text{Reflected normalized power wave}$$

15

Where Z_0 is the reference impedance (usually 50 Ω). The S parameters for a two-port network are given by

$$S_{11} = \frac{b_1}{a_1}\bigg|_{a_2=0} \qquad\qquad \equiv \frac{\text{Reflected power wave at port 1}}{\text{Incident power wave at port 1}}$$

$$S_{21} = \frac{b_2}{a_1}\bigg|_{a_2=0} \qquad\qquad \equiv \frac{\text{Transmitted power wave at port 2}}{\text{Incident power wave at port 1}}$$

$$S_{22} = \frac{b_2}{a_2}\bigg|_{a_1=0} \qquad\qquad \equiv \frac{\text{Reflected power wave at port 2}}{\text{Incident power wave at port 2}}$$

$$S_{12} = \frac{b_1}{a_2}\bigg|_{a_2=0} \qquad\qquad \equiv \frac{\text{Transmitted power wave at port 1}}{\text{Incident power wave at port 2}}$$

For each s-parameter definition there are given conditions. For example in S_{11}, the input voltage reflection coefficient, a_2 is required to be 0. This condition can only be met if the transmission lines from port two of the network is terminated in its output characteristic impedance such that no reflection occur.

To calculate the S-parameters S_{11} and S_{21} the output side must be terminated with a load impedance equal to the line impedance Z_0 to avoid reflections at port 2. This is because the definition for these two parameters are given under the condition $a_2 = 0$. There must be no power reflected at the load end.

3.1 Useful S-parameter Equations

3.1.1 VSWR

If there are no reflection from the load of the DUT or if the DUT is the load (this occurs in a one- port measurement where S_{11} is the only parameter), then S_{11} is equal to the input voltage reflection coefficient Γ_{in}. Then VSWR is given by

$$VSWR = \frac{1 + |S_{11}|}{1 - |S_{11}|} \tag{3.1}$$

3.1.2 Return Loss

The return loss is usually abbreviated as RL. It defined the reflection loss (i.e. how much the reflected wave is attenuated relative to the incident wave at the input). The return loss can be found from the reflection parameter:

$$RL(dB) = -20log|S_{11}| \tag{3.2}$$

3.1.3 Forward Power Gain

The voltage at port 2 is directly related to generator voltage V_{RF} giving us the forward voltage gain. The forward power gain (G) is then given by

$$G = |S_{21}|^2 = \left|\frac{V_2}{F_{RF}/2}\right|^2$$

3.1.4 Insertion Loss

Equation 3.1.3 can also indicate loss of power and attenuation of voltage. Loss is normally defined by the insertion loss (IL) as

$$IL(dB) = -20log|S_{21}| \tag{3.3}$$

3.1.5 T-Parameters

When a system is described as multiple networks in cascade, it is more useful to use a chain scattering matrix representation which is described by so-called T-parameters. In this way the definition for the s-parameters from equation 3 on page 15 can be rewritten in terms of input and output ports in the following manner:

$$\begin{Bmatrix} a_1 \\ b_1 \end{Bmatrix} = \begin{bmatrix} T_{11} & T_{21} \\ T_{12} & T_{22} \end{bmatrix} \begin{Bmatrix} b_2 \\ a_2 \end{Bmatrix}$$

Where the T-parameters are given by:

$$T_{11} = \frac{1}{S_{21}} \qquad\qquad T_{21} = \frac{S_{11}}{S_{21}}$$

$$T_{12} = -\frac{S_{22}}{S_{21}} \qquad\qquad T_{22} = -\frac{Det(S)}{S_{21}}$$

Where $Det(S)$ is the determinant of the S-parameter matrix. Two or more networks in series can easily be described as one complete system by using matrix multiplication between each T-parameter matrix. This will give a single matrix describing the total system.

Chapter 4

Antenna Theory

In this chapter the basic theory of antennas is explained. Many antennas actually have a very simple physical design, but the process in which to design and analyze this can be very complex and nonintuitive. In this text there will be an emphasis on the components of the Yagi-Uda antenna.

4.1 What is an Antenna

An antenna is a transducer used as a means for radiating or receiving radio waves [1]. It does so by converting changing electrical current and voltage to coupled electromagenitc fields that propagate through space. The antenna can take many different forms based on a conductive material to achieve different characteristics. One of these arrangements is the simple wire antenna. A wire antenna used for generating radiation usually does so by having a time varying current applied to it. This follows from the following statement: *To create radiation, there must be a time-varying current or an acceleration(or deceleration) of charge* [1]. Radiation originating from a conducting wire exist under the following conditions:

1. If all the charge in a wire is static, there is no current and hence no radiation

2. If a charge is moving with uniform velocity($dI/dt = 0$):
   a. There is no radiation if the wire is straight and infinite in extent.
   b. There is radiation if the wire is curved, bent, discontinuous, terminated or truncated.

3. If charge is oscillating in a time-motion, it radiates even if the wire is straight.

Anywhere where there is an acceleration of charge there is potential for radiation. For a single source of accelerating charge there will always be induced
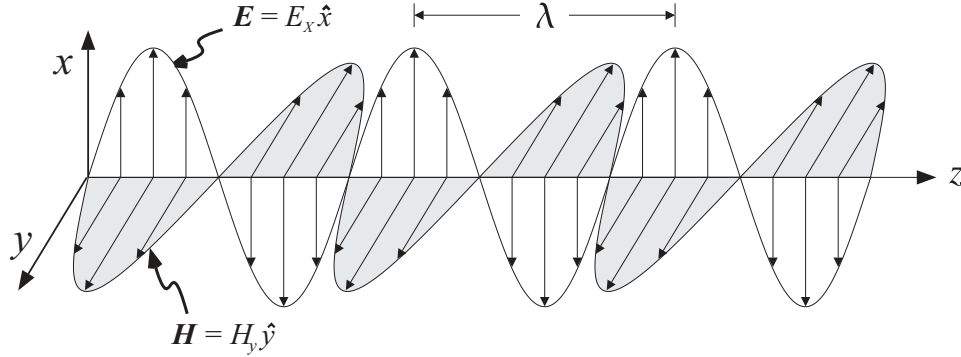
Figure 4.2: TEM wave propagating in free space

electric and magnetic fields, but if these are cancelled by other nearby filed sources with opposite polarity, radiation might not continue into free space. How antennas radiate electromagnetic waves seems very abstract and is hard to visualize. Figure 4.1 shows the electric field ($\vec{E}$) and the magnetic field ($\vec{B}$) emanating from a dipole ,which is excited by an electrical sinusoidal source. In this simplification the field lines can be thought of as being detached from the antenna as they form closed loops. This fields are then travelling in free space at the speed of light, being independent of the antenna source. Any device that performs this task can be classified as an antenna.

4.2   Electromagnetic Uniform Plane Wave

The representation of an electromagnetic wave propagating in free space can be seen in figure 4.2. This transverse electromagnetic mode (TEM) wave have orthogonal components of electric field **E** and magnetic field **H**. A sinusoidal form represent this wave by the following equations of the x-directed electric component E_x and the y-directed magnetic component H_y.

$$E_x = E_{0x}cos(\omega t - \beta z) \qquad (4.1)$$

$$H_y = H_{0y}cos(\omega t - \beta z) \qquad (4.2)$$

E_{0x} and H_{0y} are the constant amplitude factors given in units of V/m and A/m. ω is the angular frequency
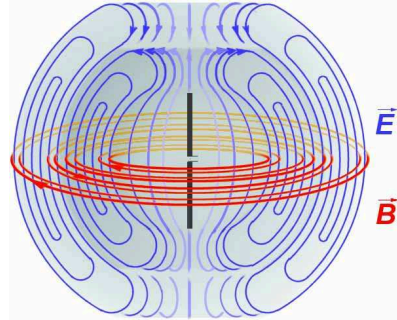
Figure 4.1: Electric and magnetic fields emanating from a dipole antenna(Credit: Wikipedia)

4.3 Maxwell's Equations

The electromagnetic behavior of an antenna and the fields it produces is governed by Maxwell's equations. James Clark Maxwell unified the theories of electricity and magnetism and presented this through a set of equations called the Maxwell's Equations in 1873. The fours equations are presented in differential form below. These must be solved for a specific antenna with a given electrical excitation to analyze and model the electromagnetic behavior of such a device. Typically, exact solutions of Maxwell's equations are not available and thus numerical modeling is often used to compute approximate solutions for practical configurations. The Maxwell's equations in differential form is:

$$\vec{\nabla} \circ \vec{E} = \frac{\rho}{\epsilon_0} \qquad \text{Gauss's law for electric fields} \qquad (4.3)$$

$$\vec{\nabla} \circ \vec{B} = 0 \qquad \text{Gauss's law for magnetic fields} \qquad (4.4)$$

$$\vec{\nabla} \times \vec{E} = -\frac{\partial \vec{B}}{\partial t} \qquad \text{Faraday's law} \qquad (4.5)$$

$$\vec{\nabla} \times \vec{B} = \mu_0 \left(\vec{J} + \epsilon_0 \frac{\partial \vec{E}}{\partial t} \right) \qquad \text{Faraday's law} \qquad (4.6)$$

There are basically two types of electric fields, the electrostatic field caused by static electric charge and the induced electric field which is created by a changing magnetic field. The main difference between these two fields can most easily be described by the use of field lines. While an electrostatic source has field lines starting on positive charges and ending on negative charges, the structure of induced electric field lines is more similar to magnetic field lines. These lines loop back on them self without any start or end. Such a field has no divergence. Gauss's law for magnetic field state that there exist no net divergence of a magnetic field. This implies that there does not exist a magnetic monopole. The maxwell's equations explain how a oscillating current source can create radiation and how this radiation behaves in the form of electromagnetic waves.[6]

4.4 Antenna Parameters

To avoid confusion, the coordinate system used throughout this text is shown in figure 4.3 on the next page. This is a spherical coordinate system where

any position in three dimensional space can be found by two angles and a radial distance. An rotator system analogy can be used to explain the parameters. Phi(ϕ) is then equal to the azimuth angle going counterclockwise from the x-direction. Theta (θ) is the elevation angle relative to the upwards z-direction and r is the magnitude of the vector aligned by the two previous mentioned angles. Antennas has many important parameters describing their
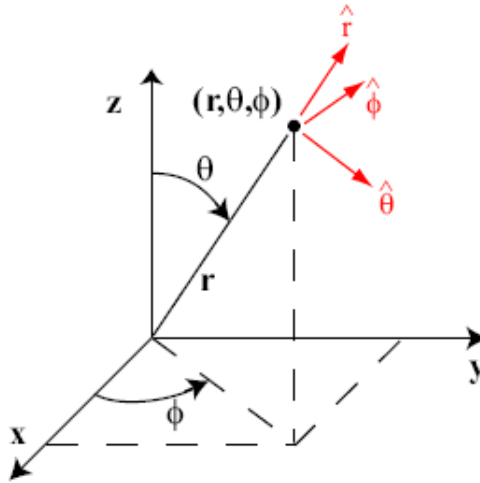
Figure 4.3: Spherical coordinate used in antenna calculations.

performance. It is not a single qualitative figure of merit that can describe how well an antenna will perform with all communication systems. There are often many trade-off's to consider. A well performing antenna installed in one specific system might underperform in another system. An example of this can be a simple dipole antenna which has practically no sensitivity in the same direction as the antenna is aligned. For this example the orientation of the antenna can play an important role. But ther are many more considerations to take into account as this chapter will describe.

4.4.1   Radiation Pattern

The antenna radiation pattern (sometimes abbreviated to just antenna pattern) is defined as *a mathematical function or a graphical representation of the radiation properties of the antenna as a function of space coordinates*[1]. The pattern described the far-field radiation. In figure 4.4 on the facing page an antenna pattern is shown. It has units of decibels and show the antenna directivity in the azimuth-plane. Because this is a directional antenna system it has one main lobe, several side lobes and a back lobe. For this system the
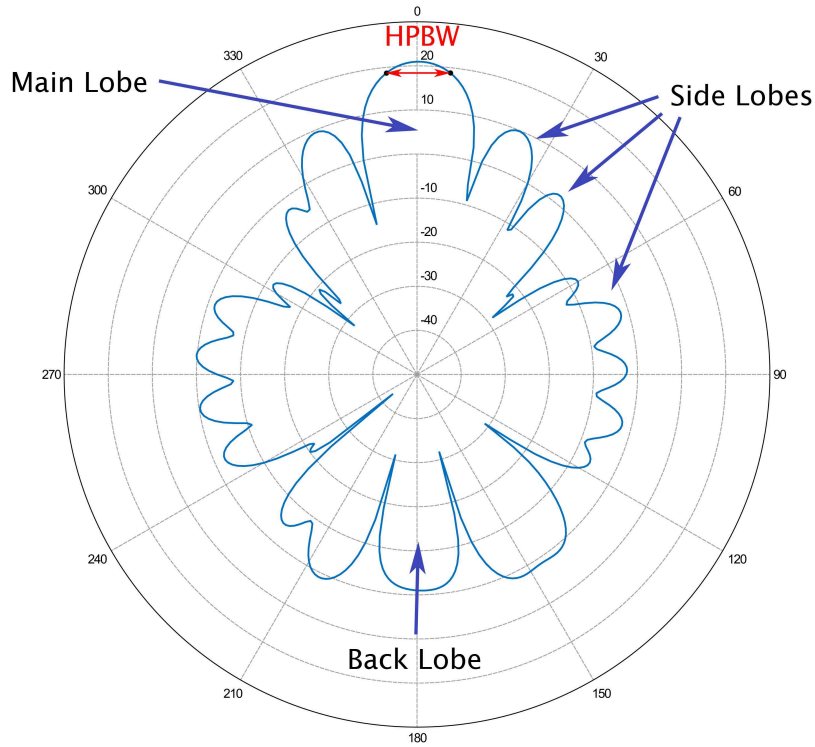
Figure 4.4: Simulated antenna radiation pattern for four stacked 436CP30 Yagi antennas (RHCP polarization, stacking distance of 1.2954 meters).

desired attributes would be only one single main lobe, but there are many other system where more than one main lobe is desired. Many antennas are desired to have omnidirectional radiation, which in theory will radiate equally in all directions. However in this text there will be an emphasis on the directional antenna. Often the difference of the maximum directivity for the biggest sidelobe to that of the main lobe is called the sidelobe level. In this case it is 10 dB (10 times less than that of the main lobe). The front to back ratio is very similar except that the back lobe is now compared to the main lobe. The bigger the main lobe is, the more gain of the desired signal is achieved. But the reason for wanting low side lobe and back lobe levels is to reduce the reception of unwanted signals and noise from other directions.

4.4.2 Beamwidth

The beamwidth is a parameter accociated with the antenna pattern. The half-power beamwidth (HPBW) is the angle between two separate points at -3 dB below the maximum in the main lobe of the antenna pattern. The HPBW is hown in 4.4.

4.4.3   Directivity

The radiation intensity is the power radiated from the antenna per unit solid angle. The radiation Intensity U of an antenna is given by

$$U = r^2 W_{rad} \tag{4.7}$$

Where r is the distance away from the source antenna in meters and W_{rad} is the radiation density at that point given in W/m^2. Knowing this, the directivity D can now be defined as

$$D = \frac{U}{U_0} = \frac{4\pi U}{P_{rad}} \tag{4.8}$$

Where U_0 is the radiation intensity of a isotropic source, which is constant in all directions, and P_{rad} is the average power radiated given in units of W/m^2. The directivity is often written in units of dBi (directivity relative to an isotropic source) or dBd (directivity relative to a theoretical dipole antenna). D is a function of the two angles θ and ϕ, but when presented as a single number it refers to the angle with the highest directivity (boresight).

4.4.4 Input Impedance

The antenna impedance is the impedance seen at the input terminals of an antenna. The antenna input impedance Z_A is given by

$$Z_A = R_A + jX_A = R_r + R_L + jX_A \tag{4.9}$$

Where R_r is the radiation resistance, R_L is the dissipative loss resistance and X_A is the reactance. A thevenin equivalent of a source transmitter connected
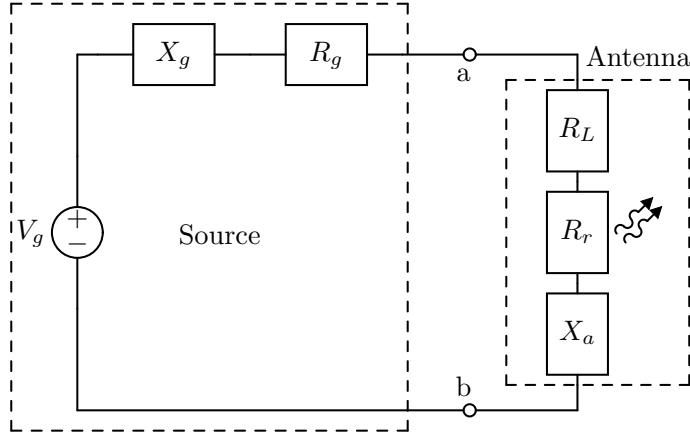
Figure 4.5: Thevenin equivalent for source generator connected to an antenna

to an antenna through terminal a and b is illustrated in figure 4.5. By deriving the current and voltages of this system it can be shown that the power delivered to the radiation resistance part of the antenna is given by [1]

$$P_r = \frac{|V_G|^2}{8} \left[\frac{R_r}{(R_r + R_L)^2} \right] \tag{4.10}$$

This only hold true when the source is a conjugate match to the antenna ($X_g = -X_A$) and $R_S = R_r + R_L$. If there was no loss in the antenna (ie. $R_L = 0$), then half of the power supplied by the source would be converted to radiation through R_r and the other half would be dissipated in the internal source resistor R_g. The behavior for receiving is very similar to the previous transmission example. Half the power which is captured by induced voltages due to R_r is delivered to the source resistance R_g. The portion of the received power remaining in R_r is then reradiated.

4.4.5 Antenna Gain and Efficiency

All dissipative losses in the antenna decrease the antenna efficiency. If mismatch loss is ignored, the efficiency of an antenna is a function of conduction

losses and dielectric losses in the antenna. This radiation efficiency is termed e_{cd} and is given by

$$e_{cd} = \frac{R_r}{R_L + R_r} \qquad (4.11)$$

The gain of an antenna, when presented as a single value, indicates the maximum gain. This is valid for a specific angle given by θ and ϕ. But the gain is a function of these two angles and is closely related to the directivity D. The gain G is defined as follows:

$$G(\theta, \phi) = e_{cd}D(\theta, \phi) \qquad (4.12)$$

4.4.6   Bandwidth

The bandwidth of an antenna gives the range of frequencies for which the antenna will perform better than a certain performance value. This value is often defined as no less than 3 dB of maximum power gain or the range over which the VSWR is no greater than 2:1. (Whichever is smaller of the two) [17].

4.4.6.1   Reciprocity Theorem

The reciprocity theorem states: *If a voltage is applied to the terminals of an antenna A and the current measured at the terminals of another antenna B then an equal current will be obtained at the terminals of antenna A if the same voltage is applied to the terminals of antenna B.*[17]. The parameters for an antenna can be used both for transmission and reception. But even though the antenna can be considered reciprocal, the propagation mechanism for the transmitted signal originating from an antenna A to an antenna B might be different than when a wave is transmitted from B to A.

4.4.7   Field Regions

Very close to the antenna ($r << \lambda$), the field patterns change very rapidly with distance. Here the field consist of radiative fields and reactive fields. At a distance far away from the antenna ($r >> \lambda$), the reactive fields are neglible and only the radiating energy is present [17]. The two regions are divided at a radius R given by

$$R = \frac{2L^2}{\lambda} \qquad (4.13)$$

Where L is the diameter of the antenna or of the smallest sphere which completely encloses the antenna(m) and λ is the wavelength(m). These two fields and the transistional field between them is called

1. Reactive near-field region.

2. Radiating near-field (Fresnel) region.

3. Radiating far-field (Frauenhofer) region.

The middle fresnel region can most easily be described as the region where the antenna radiation pattern changes with the distance from the antenna. In the far field this pattern remains unchanged. In the reactive near field the antenna characteristics are very sensitive to the presence of conductive material as it will reradiate and possibly alter the antenna impedance and radiation characteristics.

4.4.8 Polarization

The polarization of a radiated wave in the far field can be defined as: *Polarization is a property of a single-frequency electromagnetic wave; it describes the shape and orientation of the locus of the extremity of the field vectors as a function of time.*[23]. There are three main groups of polarization; linear, circular and elliptical. Visualization of linear and circular polarization is presented in figure 4.6 on the next page.

For linear polarization the electric or magnetic field vector must be oriented at the same straight line. A simple dipole is stated has having linear polarization because the far-field produced by this antenna will have field vectors that will oscillate along a single axis. The orientation of the linear polarized field can have any angle, but when it is oriented parallel to the earth surface it is usually denoted as horizontal polarization and if the antenna is aligned so that the electric field is normal to the earth surface it is called vertical polarization. When the field has circular polarization it must consist of two orthogonal components with the same magnitude and a phase difference of odd multiples of 90 degrees (if the phase difference is unequal to 90 degrees the polarization will be elliptical). If the these two orthogonal components have unequal magnitude and dont have a phase difference of multiples of 0 or 180 degrees, we end up with an elliptical polarization. For circular and elliptical polarization the sense of rotation can be determined by rotating the leading phase component towards the lagging component observed as the wave travels away from the observer. The clockwise rotation is called right hand circular polarization (RHCP) and counterclockwise is called left hand circular polarization (LHCP).

Polarization Loss

When the polarization of the incident wave is different from the receiving polarization of the antenna, then a loss due to polarization mismatch occurs. When sending signals between a linear polarized antenna and a circular polarized antenna, the theoretical polarization loss is 3 dB. If two circular polarized antenna, one with RHCP and the other with LHCP, the polarization loss is
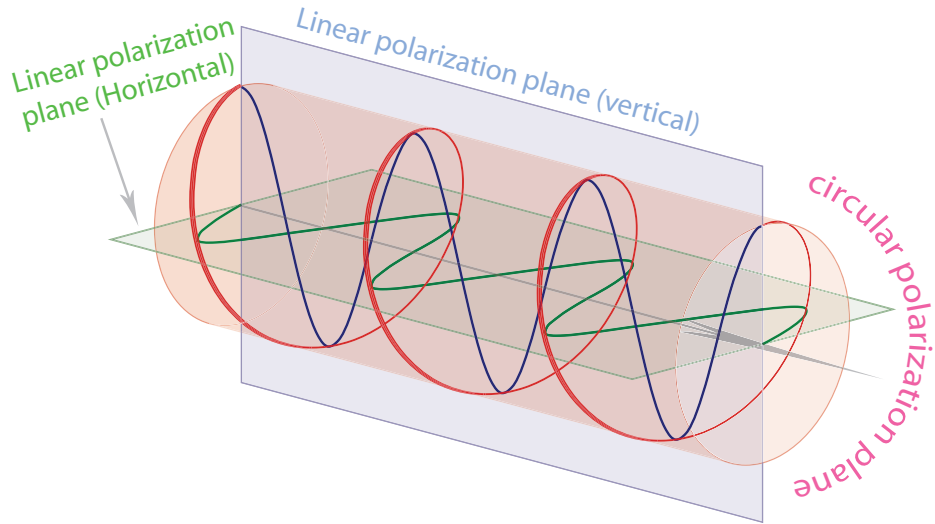
Figure 4.6: Polarization components of circular polarization (E-fieds). The two linear orthogonal polarization components (horizontal and vertical) are 90 degrees out of phase and combined form circular polarization.

30 dB or more [7]. Refer to [7] for an excellent nomogram used in finding the polarization loss from a link between two antennas with elliptical polarization.

4.5 Dipole Antenna

4.5.1 Hertzian Dipole Antenna

If we apply a sinusoidal current source to a infinitesimal length of a straight conductor we can assume that the current I is constant along its length at a given time. This small antenna is called a Hertzian dipole. Maxwell's equations can be solved for this antenna to find the electric and magnetic field components generated when a sinusoidal current source is applied. The magnetic field components is

$$H_r = H_\theta = 0 \tag{4.14}$$

$$H_\theta = \frac{I_0 l sin\theta}{4\pi} \left(\frac{jk}{r} + \frac{1}{r^2} \right) e^{-jkr} \tag{4.15}$$

And the electric field components are

$$E_r = \gamma_0 \frac{I_0 l cos\theta}{2\pi} \left(\frac{j\beta}{r} + \frac{1}{r^2} \right) e^{-jkr} \tag{4.16}$$

$$E_\theta = -\gamma_0 \frac{I_0 l sin\theta}{4\pi} \left(-\frac{\beta^2}{r} + \frac{j\beta}{r^2} + \frac{1}{r^3} \right) e^{-j\beta r} \tag{4.17}$$

$$E_\phi = 0 \tag{4.18}$$

$$\tag{4.19}$$

Where $\gamma_0 = (\mu_0 \epsilon_0)^{\frac{1}{2}}$ is the intrinsic impedance for free space (377 Ω)[2]. The different terms in the equations above corresponds to different types of fileds in the following manner:

$\frac{1}{r}$ - Radiation field.

$\frac{1}{r^2}$ - Inductive field.

$\frac{1}{r^3}$ - Electrostatic field.

Removing the inductive and electrostatic field components from the equations will give the far field radiation field. For a hertzian dipole this will look similar to the radiation pattern for a half-wave dipole shown in figure 4.7 on the following page. But the radiation resistance (R_r) of this antenna is very small.

$$R_r = 80\pi \left(\frac{l}{\lambda} \right) \tag{4.20}$$

This makes it hard to match the antenna to a transmission lines as the characteristic impedance required from the line is to low. The half-wave dipole on the other hand has equal characteristics, but a much higher input impedance.

4.5.2 Half-Wavelength Dipole Antenna

A dipole antenna and its simulated radiation pattern is shown in figure 4.7 on the next page. The half-wavelength antenna is a very simple yet effective antenna. It is a type of thin wire antenna consisting of two wires of a quarter-wavlength each. The two wires are aligned to almost form a half-wavelength piece except with a small separation between the two. The two wires have each their feed point towards the center. When the antenna is precisely 0.5Λ long the input impedance is capacitive ($Z_A = (73 + j42.5)\Omega$), but is the length is reduced to between 0.47-0.48Λ(depends on the radius of the antenna wire) the input impedance becomes purely real ($Z_A = 70\Omega$) [1]. This can easily be matched to a transmission line. The voltage and current distribution on a dipole is shown in figure 4.8 on the following page.
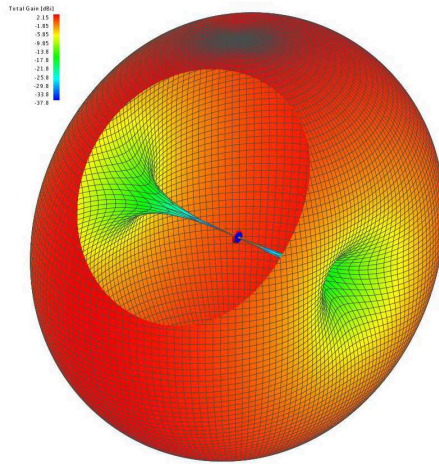
Figure 4.7: The far-field radiation pattern of a $\lambda/2$ length dipole simulated in FEKO

(a) Voltage distribution

(b) Current distribution
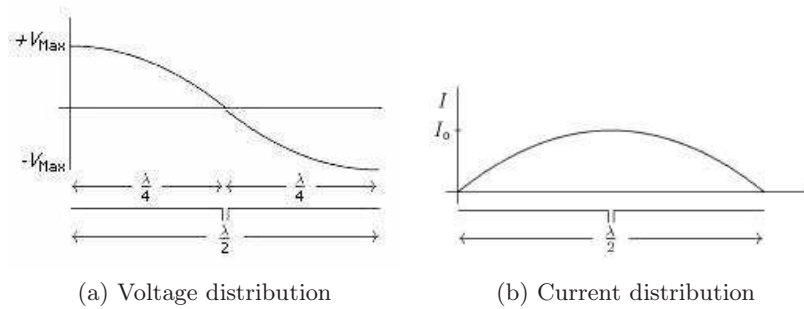
Figure 4.8: Voltage and current distribution on a dipole antenna.

4.6 Yagi-Uda Antenna

The Yagi-Uda antenna consist of a number of linear dipole elements. The usual structure can be seen in figure 4.9. It has a driven element which normally is a regular half-wave dipole or a folded dipole. Behind is something called the reflector and in front if it is a number of elements called directors. The Yagi-Uda antenna was first described by Professor S. Uda in japanese then was later described in english by his colleague H. Yagi. Hence the name Yagi-Uda refers to these two inventors [1]. The desired function of the Yagi-Uda antenna

(a) Yagi 1   (b) Yagi 2   (c) Yagi 3

(d) Yagi 4
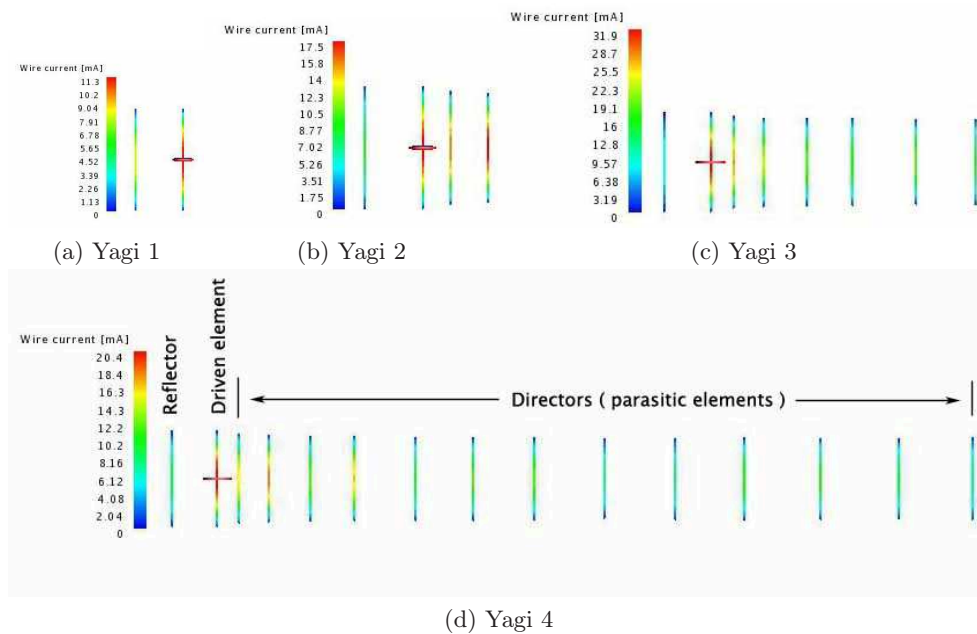
Figure 4.9: Development of a Yagi-Uda antenna which is modeled and simulated in FEKO

is to form a narrow beam with high gain in front of the antenna (in the antenna boresight) and have as little as possible gain in all other directions. The reflector is slightly longer than its resonant length and hence its impedance is inductive and the phase of the current lag behind that of the induced electromotive force (emf). The directors, also called parasitic elements, are a bit shorter than their resonance length and has a capacitive impedeance which leads the current relative to the induced emf. Thus the structure support a travelling wave a there will be a progressive phase shift along the antenna reinforcing the travelling electromagnetic wave. The induced emf comes from the radiation orginating from the driven element when transmitting and from an incoming electromagnetic wave and reradiation by the individual elements when receiving. Some of the most important design parameters of the Yagi-

Uda antenna is the element lengths and diameters, the distance between them
and the number of directors used. These are tuned to adjust the antenna pa-
rameters such as gain, input impedance, bandwidth, front-to-back ratio and
magnitude of minor lobes. There has shown to be very little increase in perfor-
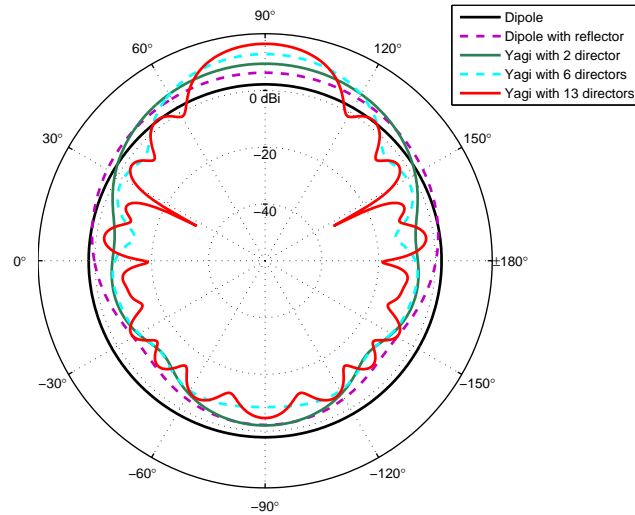
Figure 4.10: Radiation patterns for Yagi-Uda antenna with different number
of parasitic elements (Simulated in FEKO)

mance by using more than one reflector elements. The reflector has a strong
influence on backwards gain as it reduce this. The directors have a big influ-
ence on the forward gain and the antenna radiation pattern in general. All the
elements affect the input impedance due to the mutual inductance between
the elements.

A Yagi-Uda antenna can be seen as a array of passive elements with one
active driven element where the contribution of the reradiated fields from each
of the directors reshape the radiation pattern from the original dipole pat-
tern seen in figure 4.7 on page 30. By stacking more than one antennas, at
appropriate distances from each other, the overall radiation pattern is the
vector addition of all the radiation patterns for each of the stacked antennas.
Then the main lobe of the antenna pattern can be concentrated to increase the
maximum gain which also usually reduce the beamwidth. Using the simulation
software FEKO, a Yagi-Uda antenna was built and the radiation pattern and
input impedance was simulated. The antenna was built in four stages which
can be seen in figure 4.9 on the previous page. The corresponding radiation
pattern in the E-plane is shown in figure 4.10. The maximum gain is increased
every time additional parasitic elements is added. When doubling the number
of elements the maximum gain can be seen to increase by roughly 3 dB. This
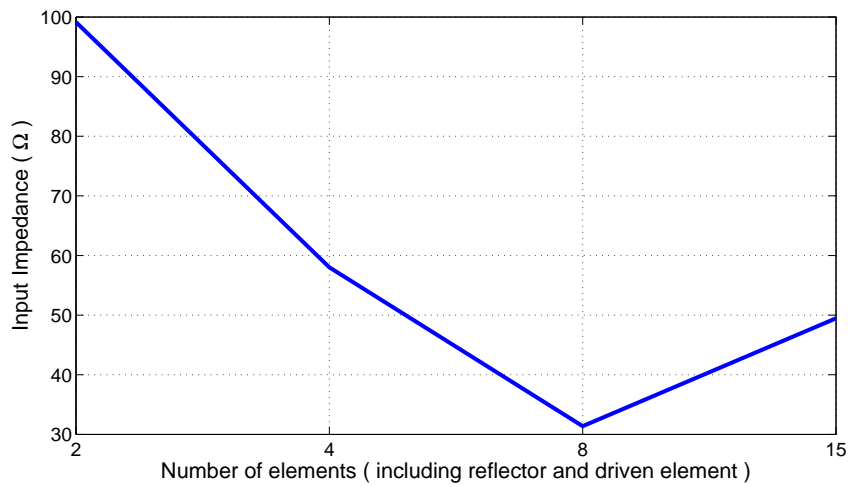
Figure 4.11: Antenna input impedance for different number of elements (Simulated in FEKO)

effect can also be achieved by stacking several antennas side by side as each doubling of number of antennas will add a maximum of 3 dB to the maximum gain. The input impedance into the driven element is also strongly affected by the precense of additional parasitic elements. The input impedance at the driven element terminal is plotted in figure 4.11.

Chapter 5

Satellite Communication Theory

This chapter presents some important principles and parameters relevant to the communication link between a satellite and a ground station.

5.1 Orbital Mechanics

The ability to describe the orbit of satellites is crucial for determining the position and movement of a satellite. For a satellite in a stable orbit around the earth there are two dominating forces acting on the satellite. These are the centrifugal force and the centripetal force [20]. The centrifugal force is due to the kinetic energy which has a force vector going outward from earth. The centripetal force is a result of the gravitational forces acting on the satellite resulting in a force vector going inward towards earth. When these two forces are balanced, the satellite moves in a stable circular orbit around the earth.

5.1.1 Kepler's Laws of planetary Motion

Johannes Kepler (1571-1630) developed three laws based on observations of planetary motion. These laws describe the orbit of for example a satellite orbiting the earth. The three laws are

1. The orbit of any smaller body about a larger body is always an ellipse, with the center of mass of the larger body as one of the two foci.

2. The orbit of the smaller body sweeps out equal areas in equal time.

3. The square of the period of revolution of the smaller body about the larger body equals a constant multiplied by the third power of the semi-major axis of the orbital ellipse. That is, $T^2 = (4\pi^2 a^3)/\mu$ where T is the orbital period, a is the semimajor axis of the orbital ellipse, and μ is Kepler's constant.

If the two foci of the elliptic orbit of a smaller body is both at center of the larger body, the orbit is circular and the period of revolution is then given by

$$T = \sqrt{\frac{(2\pi r^{3/2}}{\mu^{1/2}}} \qquad (5.1)$$

5.1.2   Keplerian Elements

Keplerian elements are a set of orbital elements that can describe the orbit of a satellite moving in a keplerian orbit. There are different sets of elements used to describe an unique orbit, usually consisting of six or more terms. A commonly used set with eight elements is described here. With these elements, the orbit can be calculated. This elements exclude orbital perturbations such as influences from the asymmetry of earth's gravitational field, gravitational fields of the sun and moon and solar radiation pressure. The effects of these must also be included to get entirely precise prediction. An illustration showing an explanation for some of the elements can be seen in figure 5.1 on page 38. The reference plane is based on a geocentric equatorial system.

Epoch

The keplerian elements are given in reference to a specific time stamp. The epoch simply states this time.

Eccentricity

The Eccentricity (e) describe the flatness of an ellipse. A perfect circle can be modeled as an ellipse with eccentricity of 0, which is the case for LEO orbits.

Argument of Perigee

Apogee is the point where the satellite is farthest away from earth while perigee is the point where the satellite is closest. These two points are always opposite of each other [20]. The argument of perigee is then simply the angle between the ascending node and the perigee measured in degrees along the orbital plane.

Mean Anomaly

The mean anomaly is the arc length the satellite has travelled since the perigee passage at a given time. This value increase linearly from 0 to 2π. For a elliptic orbit with eccentricity $\neq 0$, the mean anomaly relate to the travelled distance a satellite would have travelled along a circumscribed circle with radius equal to the semi-major axis length of the elliptic orbit and with the center in the center of the same elliptic orbit. For a circular orbit the mean anomaly relate

to the actual travelled distance of the satellite and is given by

$$M = \eta(t - t_p) \tag{5.2}$$

Where t is current time and t_p is the time of perigee. The true anomaly is the angle from perigee to the instantaneous position of the satellite.

Mean Motion

The mean motion is the average travelling speed for the satellite. A satellite in circular orbit travel at a nearly constant speed which is equal to the mean motion. Using the previous elements the distance from the earth to the satellite can be calculated from this element.

Inclination

Inclination is the angle between the orbital plane and the equatorial plane.

Right Ascension of the Ascending Node

right ascension (RA) is the angular distance measured eastward in the equatorial plane from the x axis (Seen in figure 5.1 on the next page). right ascension of the ascending node (RAAN) is the RA from the x-axis to the ascending node.

Drag

The earths atmosphere cause drag on an orbiting satellite, causing the satellite to spiral towards the earth. The unit is measured in $((revolutions per day)^2$ and is usually very small, in the order of 10^{-4} for LEO satellites. This term is sometimes referred to as decay rate.

5.2 Transmission Theory

To understand the margins and requirements for a satellite communication system, an equation describing the received power at the ground station from a transmitting satellite orbiting the earth is crucial.The link equation describe this relationship and it can be derived the following way.Consider a theoretical isotropic source transmitting P_t watts. Given a lossless transmitting antenna with the gain G_t, the flux density crossing the surface of a sphere with radius R is given by

$$F = \frac{P_t G_t}{4\pi R^2} \qquad \left(\frac{W}{m^2}\right) \tag{5.3}$$
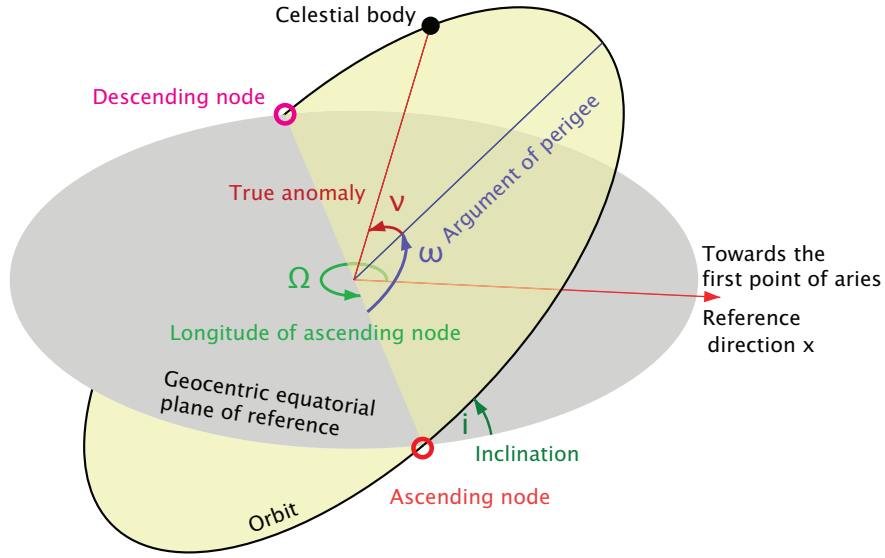
Figure 5.1: Keplerian elements for a satellite in orbit (Credit:Wikipedia, modified)

The term P_tG_t is known as the effective isotropically radiatied power (EIRP). It describe the combined transmitted power and gain of the transmitting antenna radiated uniformly in all directions. But this simplifications is only valid as long as we operate within the boresigth of the antenna (The direction in the antenna pattern with maximum gain). A real antenna is not lossless as some of the energy travelling towards the antenna is reflected due to impedance mismatches and absorbed by lossy components.These effects reduce the efficiency, η_A, of an antenna and its more useful to describe an effective aperture of the antenna as

$$A_e = \eta_A A_r \qquad \left(m^2\right) \tag{5.4}$$

As the received power by an receiving antenna with effective aperture A_e is given by $P_r = F \times A_e$. The received power can now be describes as

$$P_r = \frac{P_t G_t A_e}{4\pi R^2} \qquad (W) \tag{5.5}$$

A fundamental relationship in antenna theory is that the gain and area of an antenna are related by $G = 4\pi A_e/\lambda^2$ [20]. Substituting this in to the previous equation gives us the link equation which is dependent upon the antenna gain

and frequency of operation.

$$P_r = \frac{P_t G_t G_r}{(4\pi R/\lambda)^2} \qquad (W) \qquad (5.6)$$

Where G_r is the receiver antenna gain. The term $(4\pi R/\lambda)^2$ is know as the path loss, L_p. This is describes as a loss that relates how the effect how the transmitting energy spreads out like a sphere reducing the flux density of a constant area A at the surface of this sphere while travelling away from the source. It is very useful to write the link equation in the form of decibels as each loss and gain can be added or subtracted. A link equations describing the received power at the LNA input can be written as

$$P_r = EIRP + G_r - L_p - L_a - L_c \qquad (dBW) \qquad (5.7)$$

Where L_a is atmospheric losses and L_c is losses in the transmission lines between the antenna and the LNA.

5.3 System Noise Temperature

To analyze the noise in a receiving communication system, a term known as system noise temperature,T_s, is used. A black body, which does not reflect or emit any visible light, with the physical temperature of T_p Kelvins generate constant electrical noise up to frequencies of 300 GHz[20]. The noise power it it delivers is given by

$$P_n = kT_p B_n \qquad (W) \qquad (5.8)$$

Where k is boltzmann's constant and B_n is the noise bandwidth. In a receiver chain with several amplifiers in series, the succeeding stages contribute less and less of the total system noise temperature. If there is a noise source, with noise temperature T_{in}, connected to three amplifiers in series, the system noise temperature T_{system} is given by

$$T_{system} = T_{in} + T_1 + \frac{T_2}{G_1} + \frac{T_3}{G_1 \cdot G_2} \qquad (K) \qquad (5.9)$$

Where the gain of the two first amplifiers is given by G_1 and G_2. And the noise temperature of the three amplifiers is given by T_1, T_2 and T_3. So for a system with large gain on the first amplifier, the simplified system in figure 5.2 on the following page can be used to model the system noise temperature for most systems. Then the system noise temperature T_s is given by

T_a
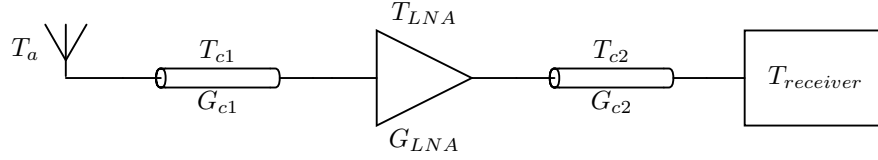
Figure 5.2: Noise model of a receiver

$$T_s = T_a G_{c1} + T_c G_{c1} + T_{LNA} + \frac{T_{receiver}}{G_{LNA} G_{c2}} \qquad (K) \qquad (5.10)$$

The total noise power referred to the input of the receiver is then given by

$$P_{no} = k T_s B_n G_{rx} \qquad (W) \qquad (5.11)$$

Where B_n is the narrowest filter bandwidth in the system. The SNR can be calculated by the following formula

$$\frac{S}{N} = \frac{P_r}{k T_s B_n} \qquad (5.12)$$

5.3.1 Noise temperature contributions

Three of the major contributions which make up the system noise temperature are

1. T_A - Antenna noise temperature.

2. T_C - The transmission line noise temperature arising from the noise generated in the coaxial cables between the antenna and the LNA.

3. T_{LNA} - The equivalent noise temperature cause by the LNA.

These three components are presented in the following sections.

Antenna Noise Temperature (T_A)

The antenna noise is created by unwanted noise sources. We divide the sources into sky temperature T_{sky} and T_{earth} which is the earth temperature. The sky background noise consist of random radiation from galactic sources, the sun and other terrestrial sources. These effects give rise to a sky noise temperature which decrease with the increase in operating frequency. The mean temperature of the sky is at 37 K and the expected or most likely temperature is 20 K. Less than 1 % of the sky has a temperature that exceeds 200 K [18]. Most of

the hot spots are in the direction towards the center of the milky way galaxy. The sky temperature changes as the antenna points at different places in the sky. The total antenna temperature is integrated and weighted according to the antenna gain pattern and the sky temperature T_{sky}. The equation for this relationship is presented in spherical coordinates below

$$T_A = \frac{\int_0^{2\pi} \int_0^\pi T_{sky}(\theta, \phi) G(\theta, \phi) sin\theta d\theta d\phi}{\int_0^{2\pi} \int_0^\pi G(\theta, \phi) sin\theta d\theta \phi} \qquad (K) \qquad (5.13)$$

Where G is the antenna gain pattern.This equation only holds true for the sky portion of what is covered by the antenna gain pattern. All other noise sources coinciding within this pattern such as the earth and man made noise must also be accounted for to get the correct antenna noise temperature. The process of calculating the exact antenna noise temperature is a difficult and tedious process. Measurements is a better alternative.

Noise From Coaxial Cables (T_c)

In a lossy line such as a coaxial cable, the degradation in SNR is a result of the attenuation of the signal alone. The noise remains fixed as long as the temperature in the line is equal or less than that of the source. The effective noise temperature in a lossy line is given as

$$T_L = (L-1)290K(T_g) \qquad (5.14)$$

LNA Noise temperature (T_{LNA})

a Low Noise Amplifier (LNA) is an amplifier specifically designed for having a low noise characteristics. As all the noise sources in the subsequent stages after a LNA is divided by the the LNA gain, it is also important to have high gain.

5.3.2   Noise Figure

The noise figure gives the ratio between input SNR and output SNR, usually in decibels. This is measure of how much the SNR is degraded by a device such as for example an amplifier. The noise temperature T_d can be calculated from the linear noise figure value by the following equation

$$T_d = T_0(NF-1) \qquad (K) \qquad (5.15)$$

5.3.3   G/T and C/N Ratio

The ratio between the gain of a receiver system and its noise temperature gives the G/T ratio given in units of dB/K. This term can be classified as a figure of merit for the receiver as it describe the quality of the receiving system. The relationship between carrier to noise(C/N) ratio is given by

$$\frac{C}{N} = \left[\frac{P_t G_t}{kB_n}\right]\left[\frac{\lambda}{4\pi R}\right]\left[\frac{G - r}{T_s}\right] \tag{5.16}$$

The C/N ratio is proportional to the G/T ratio.

5.3.4   Atmospheric and Propagation Effects

Attenuation due to Atmospheric Gases

The gases in the atmosphere may attenuate radio frequency signals. Water (H_2O) contains polar molecules which align with the varying electromagnetic field and cause energy loss to the signal. Oxygen contains non-polar molecules which also might absorb electromagnetic energy due the existence of magnetic moments [17]. The attenuation due to atmospheric gases at frequencies below 10 GHz and at elevation angles above 10 degrees is neglible [14].

Rain attenuation

At UHF frequencies rain attenuation is caused mainly by absorption by the rain drops. Because the drops also act as noise sources (Black body radiators). This will increase the receiving antenna noise temperature. Using the calculation methods recommended by ITU [9] for finding attenuation due to rain at 1 GHz, the attenuation was found to be neglible.

Faraday Rotation

In the ionosphere between about 40 km and 600 km above the earth surface, there are a large amount of electrons and ions. This can have an effect in linearly polarized waves entering this area. The incoming wave are excited into two characteristic polarizations travelling at different velocities until the end of the ionosphere. This may cause a change in the polarization of the wave. This effect is called faraday rotation. This effect can be combated in a communication system with the use of circular polarization.

Ionospheric Scintillations

The ionosphere is the upper level of the atmosphere. A region with almost no air pressure where there are free electrons and ions moving around. The ultra-violet radiation from the sun is the main cause of ionization in this area [12].

The total electron count (TEC) grow during the day and reduce throughout the night [20]. These charged concentrations can cause passing though signals to be fluctuate rapidly as it vary in amplitude and phase. This effect is called ionospheric scintillation. The magnitude of this effect varies through the day and location. It is worst around $\pm 20°$ of the geomagnetic equator and over the poles.

Doppler Shift

When a transmitting source has a motion relative to a receiving station, the received frequency varies by Δf given by the following equation

$$\Delta f = \frac{V_T f_T}{c} = \frac{V_T}{\lambda} \qquad (Hz) \qquad (5.17)$$

Where V_T is the velocity of the transmitter and λ is the wavelength of the transmitted signal. For satellites in a LEO orbit, this effect is significant due to the high velocity of the satellite relative to a static ground station.

5.4 Modulation Schemes

Modulation is the process of conveying a digital signal into a high frequency carrier. The reason for using a high frequency carrier involves the required dimensions of the transmitting or receiving antenna. The antenna performance is dependent upon the wavelength of the carrier frequency meaning that the size of the antenna can be reduced as the frequency increase. There are many different modulation schemes that each have different trade-off's.

5.4.1 Frequency Shift Keying

frequency shift keying (FSK) modulation involves changing the carrier frequency in accordance to a baseband signal. The analytical expression for this modulation can be described as [19].

$$s_i(t) = \sqrt{\frac{2E}{T}} cos(\omega_i t + \phi) \qquad\qquad 0 \leq t \leq T \qquad (5.18)$$

Where T is the period of the carrier frequency, ω_i is a frequency in radians and the phase term ϕ is an arbitrary constant. The subscript i has M discrete values each corresponding to a specific frequency. The term E stands for energy in joules/T seconds. It is derived from the root mean square (RMS) amplitude of the signal normalized to 1 Ω. An illustration of Binary FSK modulation is shown in figure 5.3 on the next page. In this scheme there are only two different frequencies ω_1 and ω_2. the highest frequency can represent a one
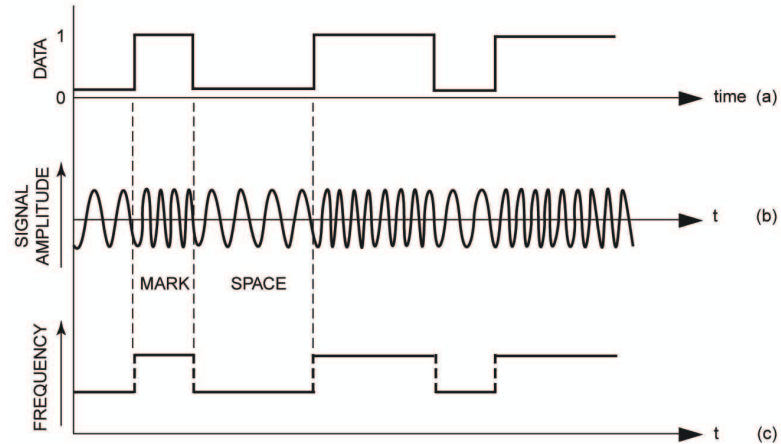
Figure 5.3: FSK modulation.

(mark) and the other a zero (space). The output signal in b has continuous phase , but in regular FSK this is not an requirement. As a result there can be quite abrupt changes in phase which cause more out of band radiation. FSK is usually not used in satellite communication. phase shift keying (PSK) is preferred because of its lower bit error rate (BER) rate for a given C/N ratio [19]. But it requires more complex communication systems and for that reason FSK is often used in amateur satellites.

5.4.2   Bandwidth of FM Signals

The frequency spectrum of an FSK signal is difficult to calculate. An expansion of a FM waveform leads to an infinite number of harmonic terms with magnitudes that can be calculated by bessel functions. This indicate an infinite bandwidth, however the magnitude of frequency components beyond the frequency deviation fade very quickly. Carson's rule state that the required bandwidth B for transmitting a FM signal is

$$B = 2(\Delta f_{pk} + f_{max}) \qquad (Hz) \tag{5.19}$$

Where Δf_{pk} is the peak frequency deviation and f_{max} is the highest frequency in the modulating signal.

5.4.3   Gaussian Frequency Shift Keying

An FSK Modulator is much the same as a GFSK Modulator ,but GFSK uses a Gaussian filter as well. In a GFSK modulator everything is the same as a FSK modulator except that before the baseband pulses (-1, 1) go into the FSK

modulator, it is passed through a gaussian filter to make the pulse smoother so to limit its spectral width. This process is called pulse shaping and it takes place in the baseband part of a communication link.

The general idea behind this effect can be compared to the fourier transform of a sinc function. The sinc function $(\frac{sin(\pi\theta)}{\pi\theta})$ is similar to the impulse response of a gaussian filter except that the sinc has symmetrical oscillating tailes with infinitie length as can be seen in figure 5.4. The fourier transform of the sinc function gives a perfectly rectangular function. This means that if a sinc

(a) Gaussian filter impulsee response.

(b) Sinc function.

(c) Fourier transform of sinc function.
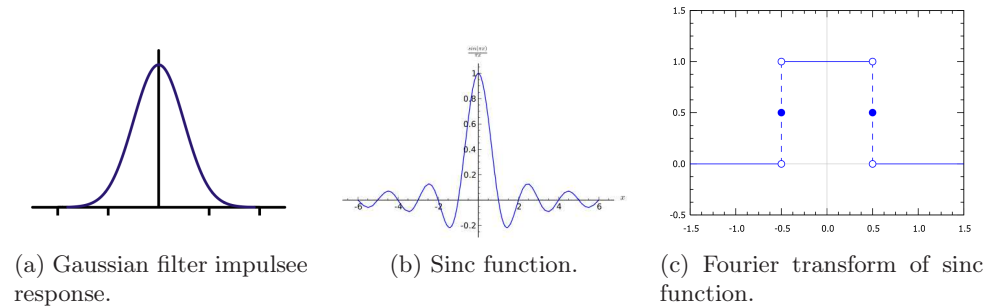
Figure 5.4: Different shapes in time and frequency domain (Credit:Wikipedia)

signal is presented in time domain, the rectangular shape will describe the frequency domain behaviour of this signal. While spectral width of a FSK signal is unlimited, the spectral width of an GFSK signal can be said to be bandlimited which in turn give a higher spectral efficiency $(\frac{\text{bit rate}}{\text{bandwidth}})$.

5.4.4 On-Off Keying

on off keying (OOK) is a basic form of amplitude-shift keying. For a binary setup, transmitting simply the carrier can represent a one (On) and turning the transmitter off can represent a zero (Off). When this scheme is used for transmitting morse code it is called continous wave (CW). Most amateur satellites use CW as a downlink beacon signal.

5.4.5 S/N and E_B/N_0

SNR($\frac{S}{N}$) is a figure of merit which describe the average signal power to average noise power ratio. It is most commonly used in analog communication to describe the quality of the link. In digital communications on the other hand a ratio called the energy per bit over the noise power spectral density. This is a more useful quantity for use in digital communication as it is very useful for use in comparison between different types of modulation. The two quantities are related as follows

$$\frac{E_B}{N_0} = \frac{S}{N}\left(\frac{W}{R}\right) \tag{5.20}$$

Where W is the system bandwidth and R is the baseband bit rate. The advantage of the SNR parameter is that it accounts for the actual implemented filter bandwidth in the receiver which influence the amount of noise power that is passed to the demodulator. The $\frac{E_B}{N_0}$ ratio is a normalized version of SNR and it assumes a perfectly matched filter.

5.4.6   Bit Error Performance

A very important parameter in communication theory is the probability of bit error P_b. This gives the relationship between bit error rate and $\frac{E_b}{N_0}$. For noncoherently detected FSK signal the bit error probability is given by[19]

$$P_b = 0.5 e^{-\left(\frac{E_b}{2N_0}\right)} \tag{5.21}$$

Usually this relationship is plotted graphs as can seen in figure 5.5.
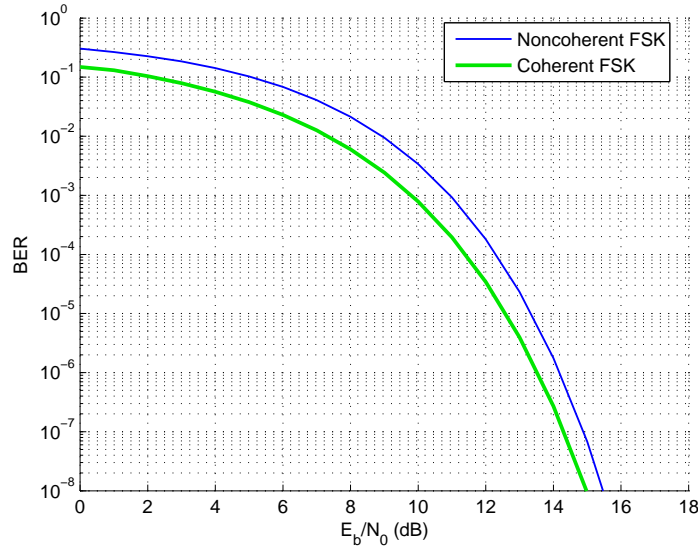
Figure 5.5: Bit error rate vs E_B/N_0

Chapter 6

Antenna Simulation

The effects on antenna radiation for different stacking distances between four identical circular polarized Yagi-Uda antennas have been investigated through simulations. Also the effects of the antenna frame and its material choice was evaluated. The input impedance has not been evaluated in these simulations as it could be measured and tuned after installation.

6.1 Introduction

The radiation pattern shown in figure 6.1 on the following page was supplied by the manufacturer "M2 Antenna Systems". In this simulation only the rear horizontal driven element is excited by a voltage or current source (linear polarization). The plot termed E-plane is equivalent to the horizontal plane and the plane termed H-plane is the orthogonal vertical plane. The two driven elements are modeled as two simple half-wave dipoles instead of the folded dipoles which is on the real physical antenna. More details on the antenna is described in 8.2.1 on page 66. Initial simulations was done and compared with the pattern shown in figure 6.1 on the following page to verify its correctness. All other simulations was based on the real antenna model with circular polarization as this is the polarization both the ground station antennas and the satellite antenna will use. There was an attempt to model the whole roof and mast structure to see the effects it had on the antennas, but it proved too difficult. The meshing grid would require extensive amounts of computational resources and memory and it was too difficult to find the appropriate electrical properties of the roof and building material. But the antennas are elevated several wavelengths above the rooftop and it is assumed to have very little impact on the antenna radiation characteristics. A perfect ground conductor was used instead to simulate effects of ground. The subsequent sections go through the different simulation scenarios. Everything was simulated at the frequency assigned to the CubeSTAR project (437.465 MHz).
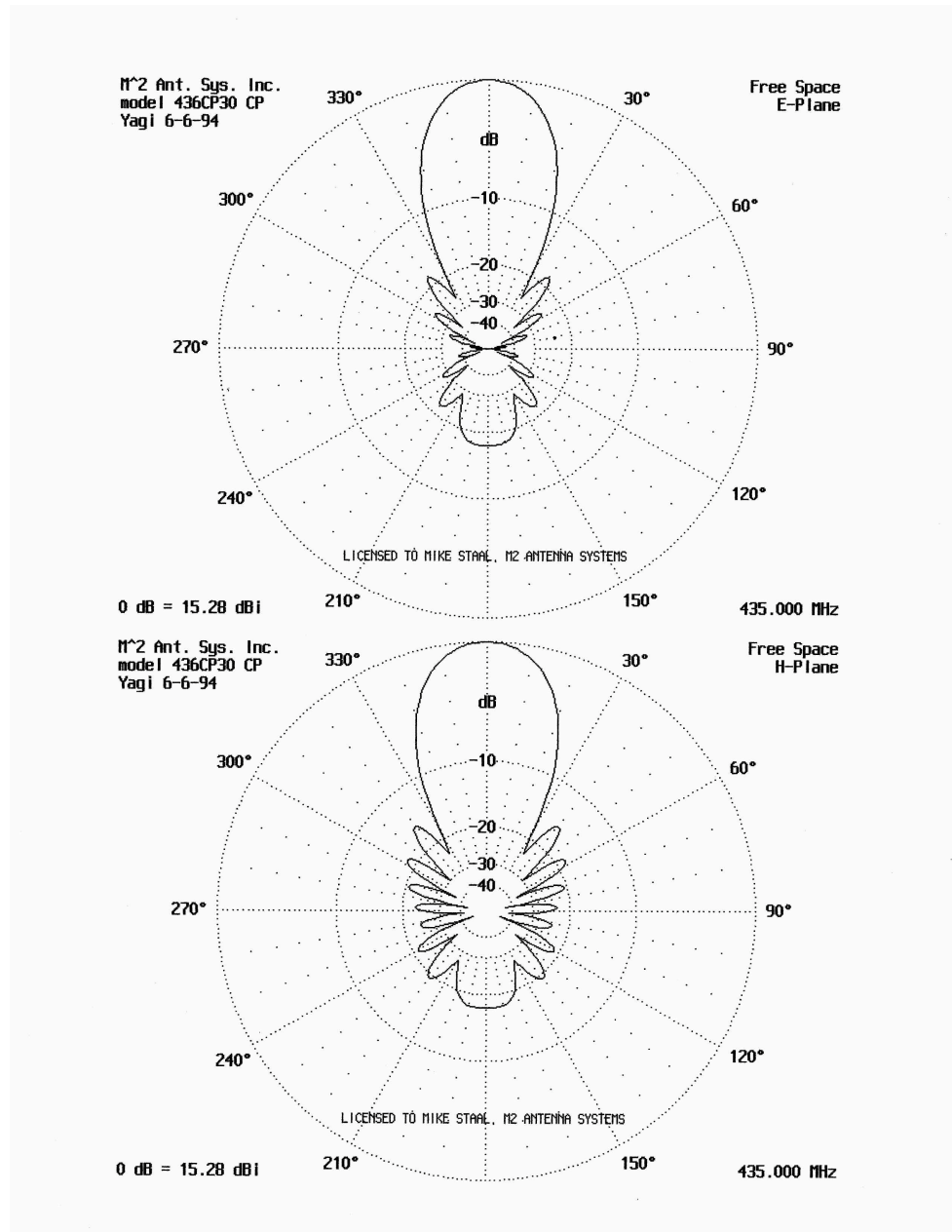
Figure 6.1: Antenna radiation pattern for the 436CP30 antenna (linear polarization).

6.2 Simulation Software

The electromagnetic simulation software FEKO from "EM Software & Systems - S.A. (Pty) Ltd." was used for the simulations. Multiphysics from "COMSOL"

and SuperNEC from "Poynting Software (Pty) Ltd." was also evaluated. But the decision fell on FEKO because of its many features mainly focused on antenna applications and it's excellent graphical user interface. The program is based on the method of moments (MoM) to solve maxwell's integral equations (on segments for thin wires in this case)[5].

The FEKO software was not readily available so a free academic trial license was attained from the supplier.

6.3 Radiation Pattern for a Single Antenna

The 436CP30 circular polarized antenna is the basis for all the simulations. The antenna was modeled in FEKO in accordance to the dimensions given in the antenna datasheet. The modeled antenna and its equivalent meshed model can be seen in figure 6.2. The accuracy of the simulations results in FEKO depends on the quality of the mesh, so the mesh size was set according meshing guidelines in the FEKO user guide. The recommendations are to use segment lengths smaller than a tenth of the free space wavelength of the signal in question. After a simulation the mesh resolution was increased to verify that the results converged to the same results as with the previous chosen mesh size. The excitations consisted of two voltage sources, one on each of the

(a) Yagi-Uda model in FEKO.   (b) Meshed Yagi-Uda model in FEKO.
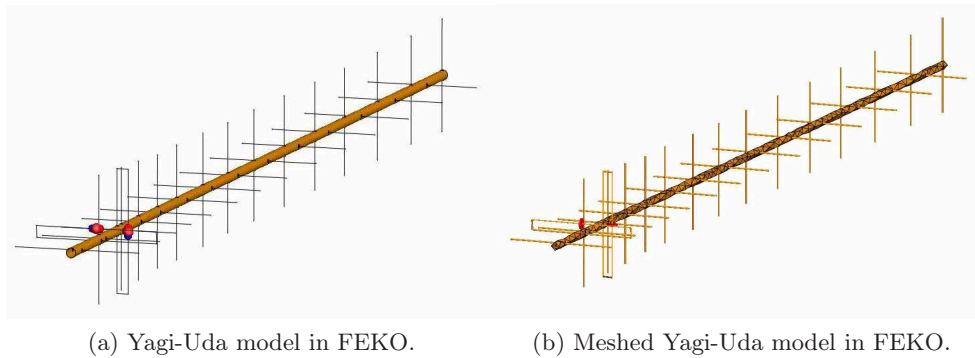
Figure 6.2: Models used in antenna simulations.

vertical and horizontal driven elements (The folded dipoles). The two elements are physically placed apart by 90 degrees so the excitations on the two dipoles can be set with equal phase to achieve circular polarization. The simulated radiation pattern is shown in figure 6.3 on the following page. This result is based on free space (ie. equivalent to outer space without any air, interfering materials or reflecting planes).

(a) E-plane.   (b) H-plane.
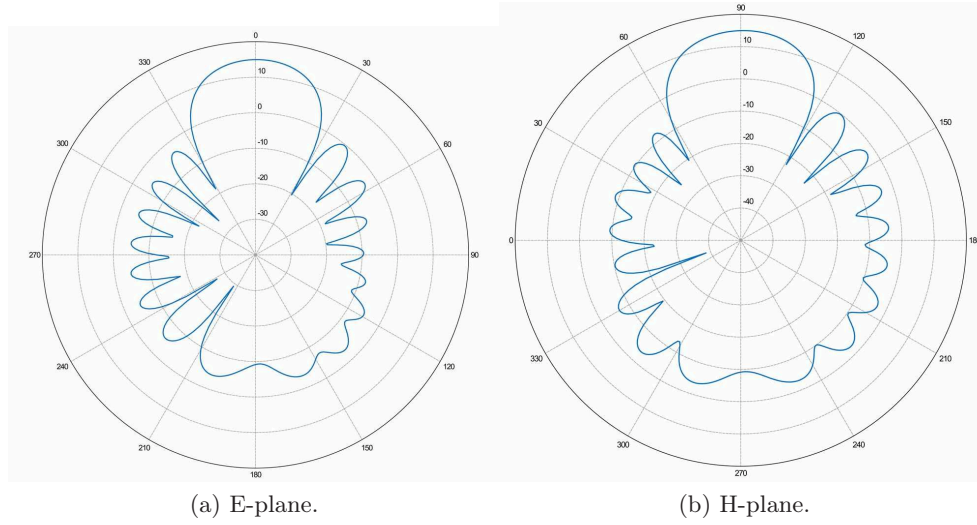
Figure 6.3: Simulated radiation pattern in free space for single antenna with circular polarization (RHCP).

6.3.1   Polarization Loss

There are imperfections to the circularity of the polarizations of the antenna. The ellipticity of the field is stated in the datasheet to be typically 1.5 dB. This gives a axial ratio of less than 4 dB. If a receiving antenna has a axial ratio equal to 1 (ie. perfect circular) the polarization loss will be approximately less than 0.3 dB [7], a very small value. The software takes this deviation into account so it will not be addressed any further.

6.3.2   Dissipative Loss in Antenna

In these simulations the radiation efficiency of the antenna was ignored and hence the simulated directivity was assumed equal to the gain of the antenna. The high frequency resistance R_{hf} of the wire of the folded dipoles in the antennas are given by

$$R_{hf} = \frac{l}{2\pi r}\sqrt{\frac{\omega \mu_0}{2\sigma}} \qquad (6.1)$$

Where r is the radius of the cross section of the antenna wire, l is the length of the antenna, ω is the radian frequency, μ_0 is the permeability of free space and σ is the conductivity of the wire metal. The antenna elements use an aluminum alloy called 6061-T6. It has a slightly lower conductivity than pure aluminum of approximately $2.5 \cdot 10^7$ S/m. The folded dipole has a length of approximately 0.7 meters (approximately one wavelength at 437.465 MHz). If

the current distribution on the antenna is sinusoidal the loss resistance of the antenna R_L is given by

$$R_L = \frac{1}{2}R_{hf} = \frac{0.7}{2\pi \cdot 2.4 \cdot 10^{-3}}\sqrt{\frac{2\pi \cdot 437.465 \cdot 10^6 \cdot 4\pi \cdot 10^{-7}}{2 \cdot 3.5 \cdot 10^7}}$$

$$= 0.3261\Omega$$

The input impedance of the folded dipole (Z_{in}) is approximately 300 Ω. The radiation resistance R_r dominates this term and is therefore set equal to the input impedance. Then the antenna radiation efficiency e_{cd} is calculated the following way

$$e_{cd} = \frac{R_r}{R_r + R_L} = \frac{300}{300.3261} \approx 0.9989 = 99.89\%$$

Assuming no mismatch losses between a transmission line and the antenna, the gain is given by $G = e_{cd} \cdot D$, where D is directivity. But because the efficiency is so high the gain is set equal to the directivity through out this text. Simulations using the variables for the aluminum showed marginal small differences and all the simulations was based on a perfect conducting material.

6.4   Antenna Stacking Distance
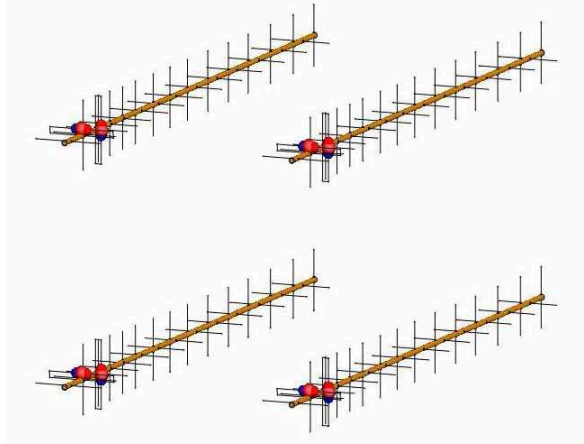
Figure 6.4: Quad antenna array model in FEKO.

Different separation distances between the fours antennas can have drastic alterations of the antenna characteristics. In this simulation the focus was to compare mainly two different stacking distances, 45 inches (1.14300 meters) and 51 inches (1.2954 meters). The maximum possible gain is achieved with 51 inches of separation. This information is given by the manufacturer, but it

was also verified by sweeping the separation parameter in FEKO to find the distance with the highest gain. But it is possible to sacrifice a small portion

(a) E plane   (b) H plane
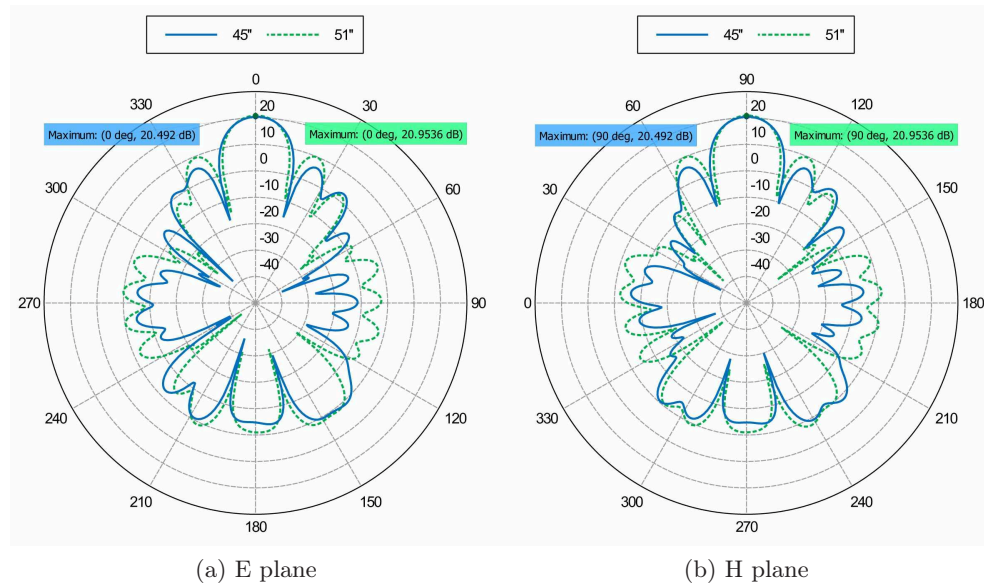
Figure 6.5: Simulated radiation pattern in free space for four stacked antennas with circular polarization (RHCP).

of the gain to get smaller sidelobes which can decrease interference and noise. The simulated radiation plots can be seen in figure 6.5. The separation of 45 inches gives a small decrease in gain of less than 0.5 dB, but the sidelobe levels also decrease by almost 5 dB as well as the back lobe by about 4 dB. The separation of 45 inches was chosen for this setup because of smaller magnitude of the minor lobes. But the installed antenna frame has some margins which makes it possible to adjust this separation later if it is desired.

6.5 Effects from Antenna Frame
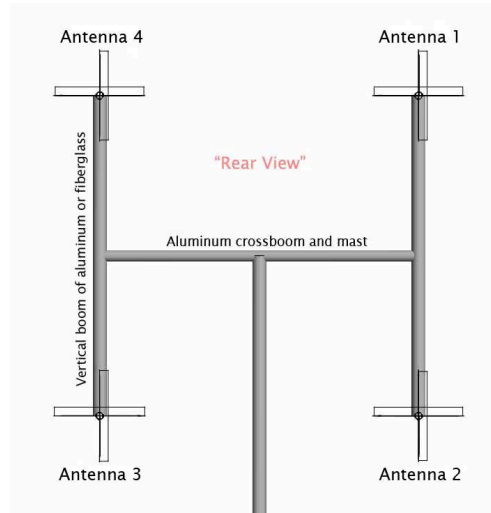
Figure 6.6: Antenna frame.

To install a stack of four antennas a frame for holding the antennas had to be constructed. A frame model was implemented in FEKO as seen in figure 6.6. The frame could be constructed with vertical booms of either metal or fiberglass material. When simulating the fiberglass, the vertical booms was simply removed as there is negligent electrical effects from fiberglass material. The results of the two simulations is shown in figure 6.7 on the next page. By using metal the maximum gain decrease by approximately 1.5 dB and the front-to-back ratio is 10 dB worse. Due to these conclusions fiberglass material was chosen to be used in the antenna frame.

(a) E-plane.   (b) H-plane.
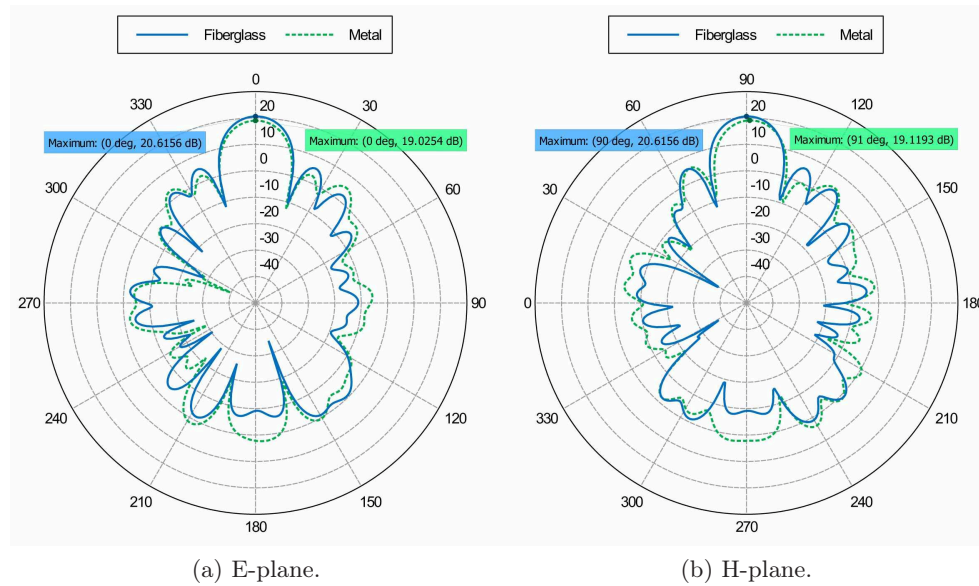
Figure 6.7: Simulated radiation pattern for fours stacked antennas with frame (RHCP polarization).

6.6 Effects from Ground and Different Elevation Angles

To investigate the antenna system in a more realistic environment a ground plane was added to the model. The antenna system was also tilted at three different elevation angles as shown in figure 6.8 on the facing page. During a satellite pass, where the satellite travel directly over the ground station site, the antenna rig is expected to move through these angles. The simulated patterns give a good indication on the changes in the radiation pattern. The ground plane was set at 4 meters below the two lower antennas. This is based on the actual distance between the antennas and the building rooftop. The results show small changes in the minor lobes, but the main lobe is relatively stable throughout all elevation angles (see figure 6.9 on the next page). Based on these results the antenna rig should perform well at all angles.

(a) 15° elevation.   (b) 45° elevation.   (c) 90° elevation.
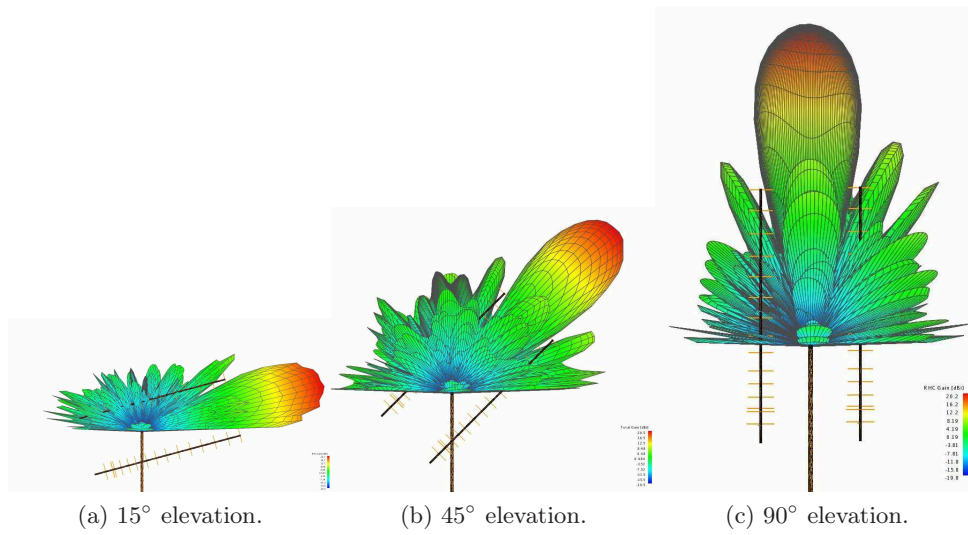
Figure 6.8: Simulated radiation pattern with perfect ground at different elevation angles.

(a) E-plane.   (b) H-plane.
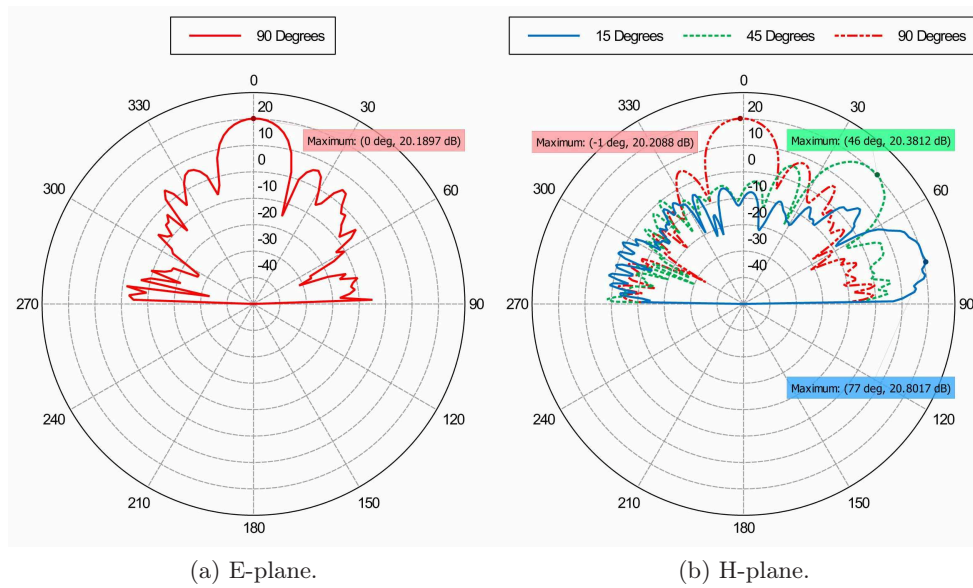
Figure 6.9: Simulated radiation pattern in with perfect ground at different elevation angles.
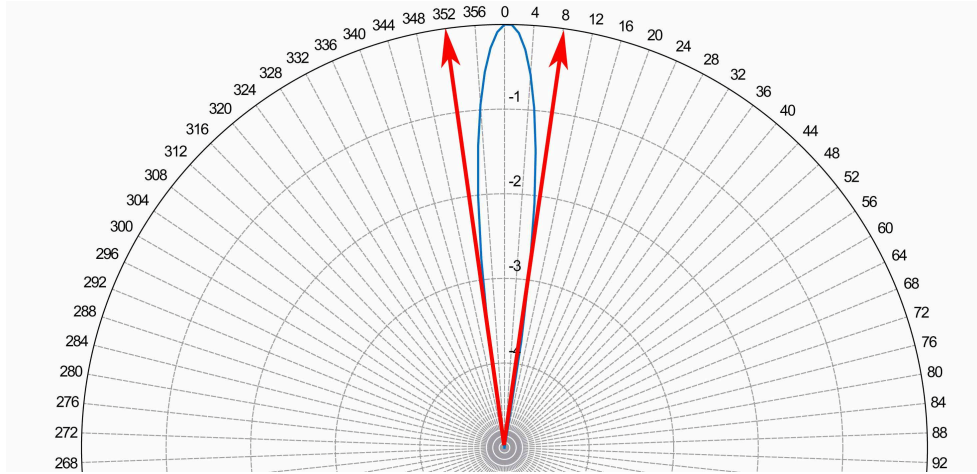
Figure 6.10:   The antenna pattern scaled down to better visualize the beamwidth

6.7   Final System

To conclude this section, the normalized antenna radiation pattern for the chosen separation distance is showed in figure 6.12 on page 58. Polarization switches are installed on the antenna to switch from RHCP and LHCP polarization. In figure 6.11 on the next page the radiation pattern for LHCP polarization is presented. These are the value used in the link budget calcal-

Parameter	Value	unit
Gain (RHCP)	20.5	dBi
Gain (LHCP)	21	dBi
$Beamwidth_{3dB}$	16	Degrees
Back to front ratio	20-25	dB

Table 6.1: Antenna system parameters

culations. But the real life values might differ from these results. There are elements such as coaxial cables and a ground structure which is not perfectly flat that can have some effect on the antenna patterns. But as there is not a proper way of measuring these precise values, this is the best foundation to work with. Ideally the antenna pattern of the whole rig could be measured in an anechoic chamber, but there are no one big enough available at our disposal. And this would only give the free-space pattern and not the pattern in its installed location.
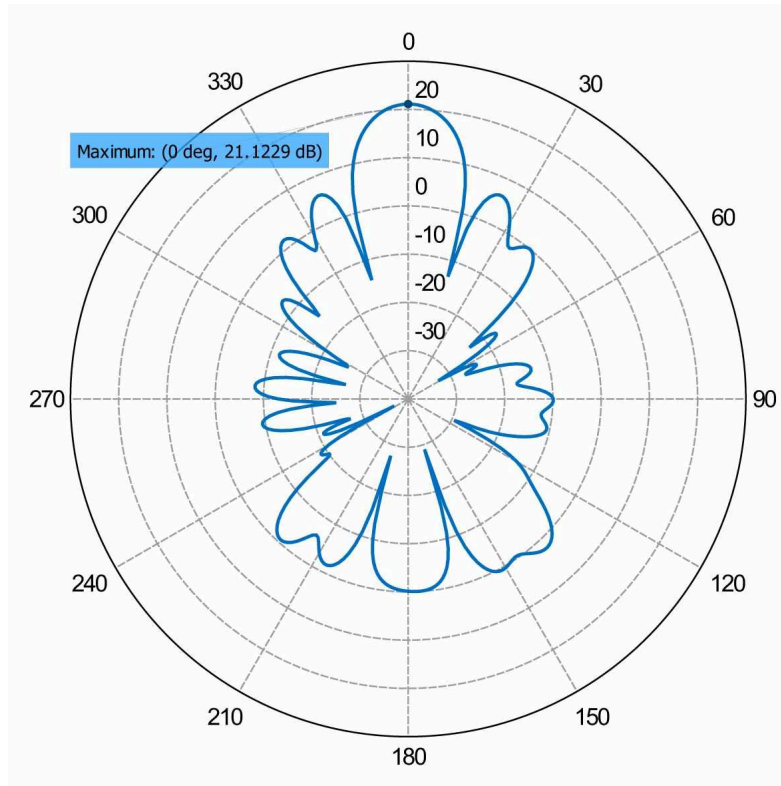
(a) Normalized E plane
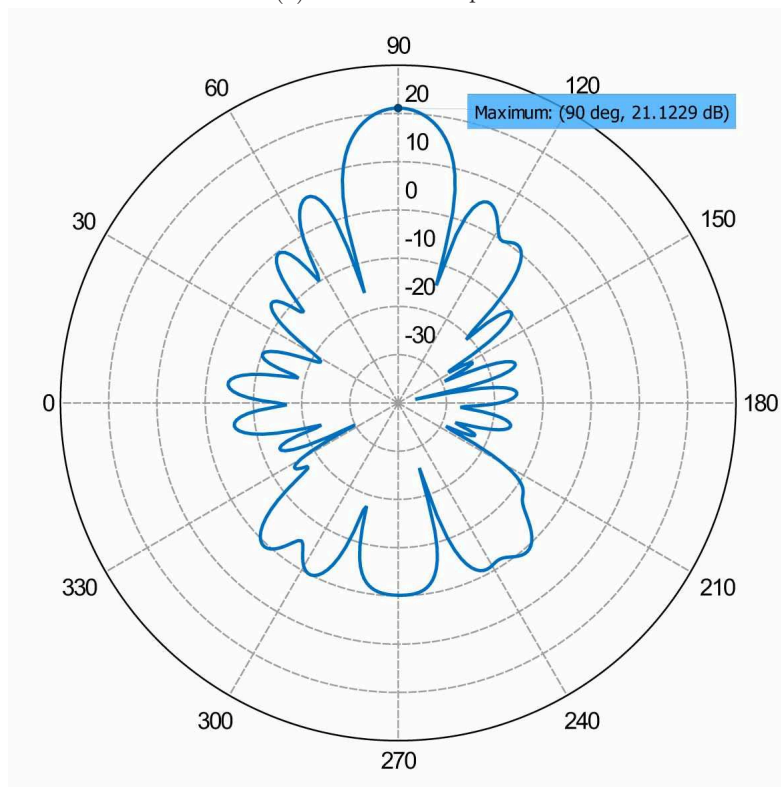
(b) Normalized H plane

Figure 6.11: Radiation patterns for final antenna setup in free space (LHCP)
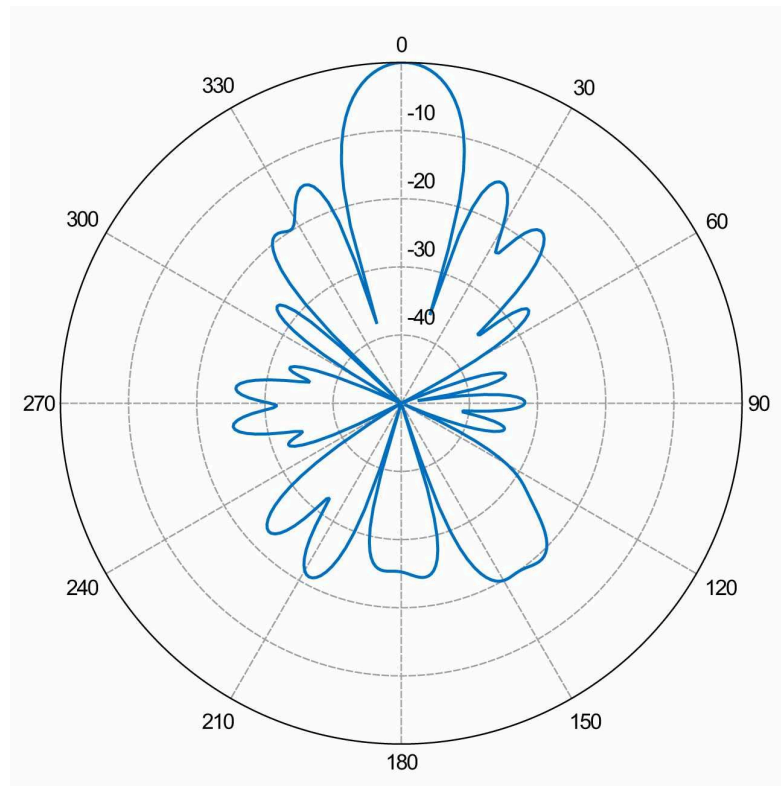
(a) Normalized E-plane.
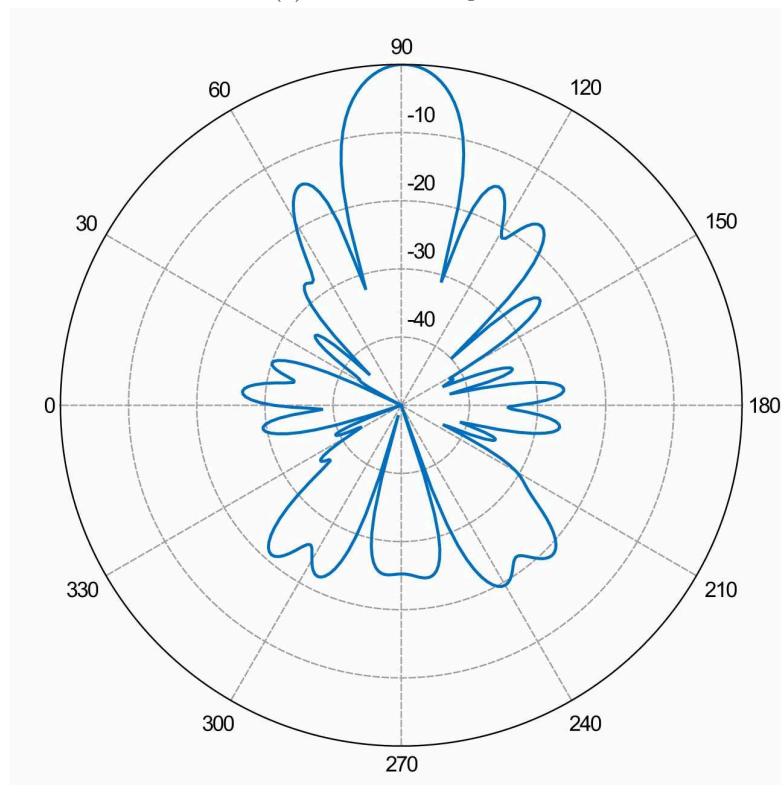
(b) Normalized H-plane.

Figure 6.12: Normalized radiation patterns for final antenna setup in free space (RHCP), 0 dB = 20.6 dBi

Chapter 7

Link Budget Calculations

In this chapter many of the calculations done for the link budget will be re-viewed. Certain paramters such as attenuation due to precipitation is ognored as this has minimal impact on the communication link as explained in 5 on page 35.

7.1   Dynamics of Path Loss During a Satellite Pass

The CubeSTAR satellite will travel in a LEO orbit. The altitude is expected to be around 600 km, but the precise value is not known until a specific launch vehicle is confirmed. The path loss is the dominant loss of the communication link. At all elevation angles above 10 degrees, the satellite communication link must be operational. The path loss used in the link budget is then based on the line of sight (LOS) distance from the ground station to the satellite at 10 degrees, the slant range S.

$$S = r_e \left(\sqrt{\left(\frac{r}{r_e}\right)^2 - cos^2(\delta)} - sin(\delta) \right) \qquad (m)$$

Where r_e is the earth radius in kilometers, r is distance from the satellite to the erth center given in kilometers and δ is the elevation angle in radians. Now the slant range for an elevation angle of 10 degrees (0.1745 radians) can be found

$$S_{10°} = 6378.14 \left(\sqrt{\left(\frac{6978.14}{6378.14}\right)^2 - cos^2(0.1745)} - sin(0.1745) \right) \approx 1932 \text{ km}$$

The path loss L_{max} can now be calculated using the equations given in section 5.2 on page 37.

$$L_{max} = \left(\frac{4\pi S_{10°}}{\lambda}\right)^2 = \left(\frac{4\pi \, 1932000}{0.685}\right)^2 \approx 1.26 \cdot 10^{15} = 151 \text{ dB}$$

This gives the worst case loss. When the satellite comes closer, giving a shorter slant path, the path loss will decrease to a minimum at 90 degrees elevation. The path loss L_{min} is then

$$L_{min} = \left(\frac{4\pi S_{10°}}{\lambda}\right)^2 = \left(\frac{4\pi 600000}{0.685}\right)^2 \approx 141 \text{ dB}$$

There will be an 10 dB increase in link margin when the satellite is right over our heads (where the subsatellite point hits the ground station location). From these results one would think that the best link quality occurs when the satellite is at this point. This is not neccesarily the truth. In this case the relative distance between the ground station and the satellite gives the fastest change possible during the pass and therefore the doppler shift also change more rapidly, in accordance with equation 5.17 on page 43, which might cause some problems for the frequency compensation in the receiver. Also the antenna rotor system must be fast enough to be able keep the antenna boresight aimed at the satellite as it passes to avoid excessive pointing losses. The orientation of the satellite antenna also might cause pointing losses. If the satellite antenna is circularly polarized it might even change the sense of the orientation which can give around 30 dB in losses if the ground station does not switch orientation. Sometime the most stable link can occur when the satellite passes by with a significant distance more to the east or west.

7.2 Downlink Calculation

The weakest link in the link budget is the data downlink communication. This is due to the fact that the link budget calculation process gives similar results both ways for two identical systems. But the ground station will have a much higher transmit power and the uplink will therefore have a better link margin than the downlink. The satellite will also send a downlink OOK beacon, but this modulation scheme has very good performance even at a very low SNR ratio. The data downlink will use GFSK modulation and send at a datarate of 9600 bps. Packets will be sent according to the AX.25 data protocol.

7.2.1 Power Received at LNA Input

First the signal power at the ground station LNA input, P_{LNA}, is calculated.

$$P_{LNA} = EIRP_{satellite} - L_{propagation} + G_{antenna} - L_{pointing} - L_{polarization} - L_c$$

$$= 31dBm - 152 \text{ dB} + 20 \text{ dB} - 1 \text{ dB} - 3 \text{ dB} - 0.4 \text{ dB}$$

$$= -105.4 \text{ dBm} = -135.4 \text{ dBW}$$

The parameters in the equation above and their values is shown in table 7.1. The parameter L_c includes all loss between the antenna connector and LNA input. This includes the lightning arrestor, the power splitter and all the interconnecting coaxial cables.

Parameter	Value	Unit
$EIRP_{satellite}$	31	dBm
Propagation loss ($L_{propgation}$)	152	dB
Receiving antenna gain (G_a)	20	dBc
Cable loss (L_c)	0.4	dB
Polarization loss ($L_{polarization}$)	3	dB
Antenna pointing loss ($L_{pointing}$)	1	dB

Table 7.1: Parameters for calculating received power at LNA input.

7.2.2 Noise calculation

All electrical circuits generate noise that increase the noise characteristics of a receiver which in turn degrade the sensitivity and performance. The ground station can be modeled as shown in figure 5.2 on page 40. Here the coaxial cable from the antenna, the power combiner, the subsequent two coaxial cables and the lightning arrestor is modeled as a single transmission with the gain $G_{c1} = \frac{1}{L_{c1}}$ and the noise temperature T_{c1}. Very often the stages that follow the LNA is usually assumed to have no significant influence of the overall effective system noise temperature. But the large attenuation due to a very long coaxial cable after the LNA and a high noise temperature of the ICOM 910H transceiver, these must be included into the calculation. To calculate the received noise the values in table 7.2 on the next page has been used. The overall effective system noise temperature is calculated as follows

$$T_{system} = (T_a G_{c1}) + (T_{c1} G_{c1}) + T_{LNA} + \left(\frac{T_{c2}}{G_{LNA}} \right) + \left(\frac{T_{receiver}}{G_{LNA} G_{c2}} \right)$$

$$= (200 \cdot 0.912) + (28 \cdot 0.912) + 75 + \frac{2747}{100} + \frac{1000}{100 \cdot 0.0955}$$

$$= 415.12 \approx 415 \text{ K}$$

The effective received noise power is then

$$P_n = 10log(k \cdot T_{system} BW)$$

$$= 10log(1.38 * 10^{(-23)} \cdot 415 \cdot 25 \cdot 10^3)$$

$$= -158.44 \approx -158.4 \text{ dBm}$$

Parameter	Value	Unit
LNA noise temperature ($TLNA$)	75	K
Antenna noise temperture (T_a)	200	K
Cable noise temperature(T_{c1})	28	K
Cable 1 linear gain(G_{c1})	0.912	Linear ratio
Cable noise temperature(T_{c2})	2747	K
Cable 2 linear gain (G_{c2})	0.0955	dB
Receiver noise temperature(T_r)	1000	K
LNA gain (G_{LNA})	100	Linear ratio
Receiver bandwidth (BW)	25	KHz

Table 7.2: Parameters for calculating equivalent system noise temperature.

7.2.3   Link Margin

The SNR is then given by the following calculation

$$SNR = P_s - P_n = -135.4 + 158.4 = 23 \text{ dB}$$

The E_b/N_0 is then given by the following calculation

$$\frac{E_b}{N_0} = \frac{S}{N}\left(\frac{W}{R}\right)$$

$$= 23 + 10log(25000/9600)$$

$$= 23 + 4.16 \approx 27 \text{ dB}$$

The wanted BER for this link is $P_B = 10^{-5}$. To achieve this then we need the following relation to hold true

$$\frac{E_B}{N_0} \geq 14dB$$

This is based on a noncoherent detection of a orthogonal FSK signal [19] and the value can be found in figure 5.5 on page 46. This value is theoretical and therefore an implementation margin should be included. For the AX.25 standard made by G3RUH an implementation margin of 4 dB should be added to the threshold. The link margin is then

$$\text{Link margin} = \frac{E_b}{N_0} - \text{ Threshold} - \text{ Implementation margin} \qquad (7.1)$$

$$\text{Link margin} = 27 \text{ dB} - 14 \text{ dB} - 4 \text{ dB} = 9dB \qquad (7.2)$$

There is no law which say precisely how much link margin each communication system should have. The link margin is required to compensate for link parameters with high variance (such as attenuation due to propagation mechanisms) and errors in the system characterization. Atmospheric condition have very little impact on the communication link so 9 dB should be sufficient to maintain a stable link.

7.3 Results

The complete link budget is calculated with the AMSAT/IARU Annotated Link Model System developed by Jan A. King, (W3GEY/VK4GEY). The results of this link budget work sheet is presented in appendix F on page 113.

Chapter 8

UiO Ground Station

This chapter introduce the reader to a general description of the ground station,its components and the installation of the station. The part list is presented in appendix D on page 107.

The station is named "UiO Ground station" which is short for "The University of Oslo Ground Station".

8.1   Overview

A sketch of the whole ground station can be seen in Figure 8.1 on the next page. the Control room is situated on the fourth floor in the west wing of the building for department of physics. The radio, rotor controller, computer and all belonging interfaces all reside here, while the antenna mast is installed on the roof. The antenna rig is seen from the rear as if the four Yagi-Uda antennas where pointing directly in to the paper. When the elevation rotator turns from 0 to 180 degrees, the mounted splitter follow the rotation so that the coaxial cables going from the splitter to the antennas remains unchanged relative to the rotational plane. This is because the splitter is fastened to the elevation boom. This setup allows for short solid copper core coaxial cables between the splitter and the antennas as there will not be applied any stress or tension to the cables during operation of the rotor system. Precautions must be taken so that none of the other cables are subject to stress and tension while the rig turns. This can cause severe damage to cables and connectors, possibly lowering or completely crippling the system performance.

The computer controls both the radio and the rotor controller through various interfaces. All the cabling and connections is shown in figure 8.1 on the following page. The software and setup is described in more detail in subsection 8.3 on page 74.
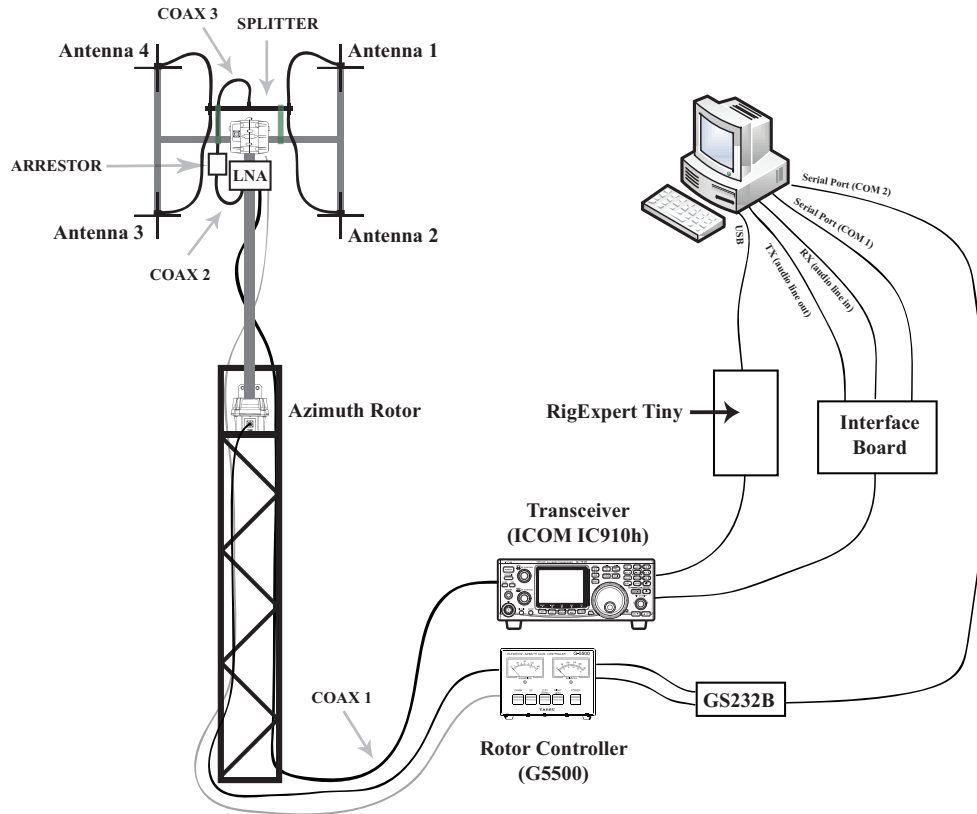
Figure 8.1: Overview of UiO Ground Station

8.2   Hardware

Some of the key components chosen for use in this station, such as the transceiver and rotor system, was chosen mainly because of the compatibility for use with the GENSO software. The cost also played a small role in making the decision on which parts to buy.

Besides describing the components this section goes through some requirements and arguments for why the selected hardware was chosen.

8.2.1   Antennas

The chosen antenna is the 436CP30 model from M2 Antenna Systems. It is a 3 meter long circular polarized yagi antenna with 2x15 elements. A polarity switch upgrade kit, PS-70CM also from M2 Antenna Systems, was installed on all four antennas to allow polarity switching between right and left hand circular polarization. There was set some practical limitation on the antenna dimensions. A very long antenna is impractical with regards to installation

and maintenance. The benefit with a longer antenna is usually more gain, due to increase in directivity, and a narrower beamwidth. More gain usually increase system performance, but without sufficient pointing accuracy of the rotor system to align the antennas the gain can quickly fade to levels below even that of a single antenna. In figure 8.3 on page 69 the simulated radiation plots

D.E. BLOCKS ARE IN RHC
POSITION WITH RELAY OPEN

REAR D1

NEW D.E. ROD

MOVE 'T' BLOCK

3/4 WAVE
LINE

BOOM EXTENSION

1/4 WAVE LINE

NEW BALUN

+12 VDC CONTROL
WIRE

NEW D.E.
BLOCK

MAIN
FEEDLINE
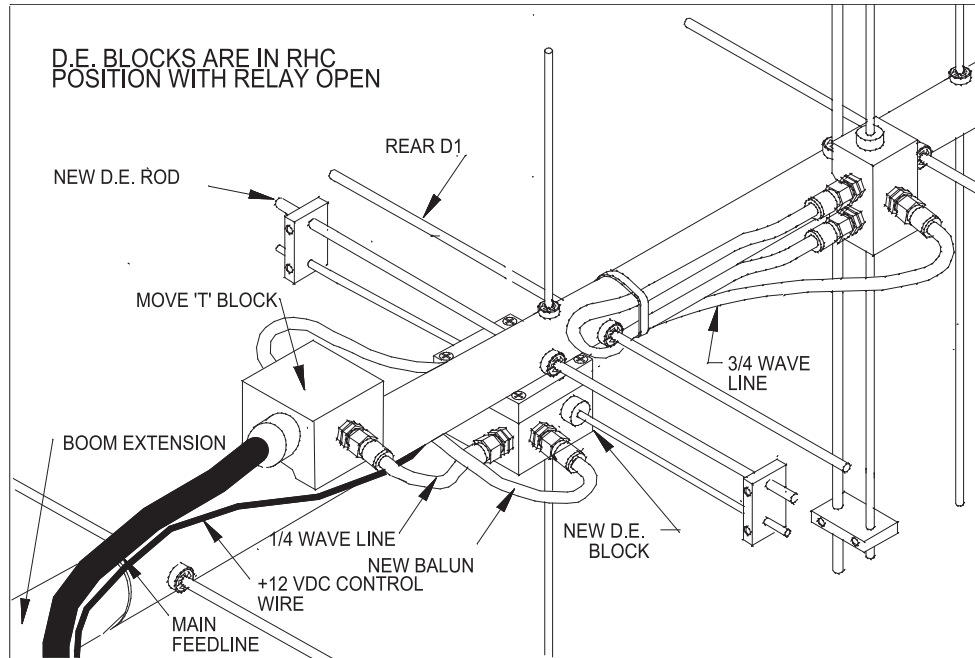
Figure 8.2: Antenna Assembly

for the chosen antenna (System A) and the almost 6 meters long 436CP42UG (M2 Antenna Systems) antenna (System B) can be seen. Both are based on a stack of 4 antennas with linear polarization. The 3 dB beamwidth of system B is approximately 8 degrees and the rotor used has a given pointing accuracy of $\pm 4°$. This would not be an ideal setup as the pointing accuracy would just barely remain inside the beamwidth. If the effects from calibration, wind, rotor backlash and small antenna misalignments during installation also are included, an offset of several degrees must be added to the given pointing accuracy. Under certain conditions a pointing error as big as 10 degrees could occur. Using system B with this error could cause a huge drop in gain (more than 20 dB), while the same error with system A would only cause about 4 dB decrease in gain. System A gives a more stable system and makes it easier to track satellites. Other features of the 436CP30 antenna includes a 3-port power splitter for dividing the input signal between the horizontal driven element and vertical driven element. Included RG6-U quad-shielded coaxial cables ensures correct phase for circular polarization and matches the input close to 50 Ω. There is also a half-wavelength balun for each folded dipole incorporated in the

driven element blocks. This balun works as a 4 to 1 transformer which divide the input impedance of the folded dipole by four. The balun also ensure that no current flow from the antenna into the coaxial cable ground shield. All of these features gives a complete setup which is easy and quick to install. The assembly setup with the polarization switch can be seen in figure 8.2 on the previous page[1]. The most relevant parameters for a single 436CP30 antenna is given in table 4.4 on page 21.

Parameter	Value	Unit
Bandwidth	432-440	MHz
Beamwidth	30 Circular	Degrees
Feed impedance	50	Ω
Boom length	3	meter
Weight	2.3	Kg
Gain	14.15	dBdc
Polarity	Circular	
Elements	15H, 15V	
Wind Area	0.093	m^2
VSWR	1.6:1 Max	Ratio

Table 8.1: Antenna parameters

---

[1]See appendix B on page 103 for an explanation on how the impedance to the antennas is matched
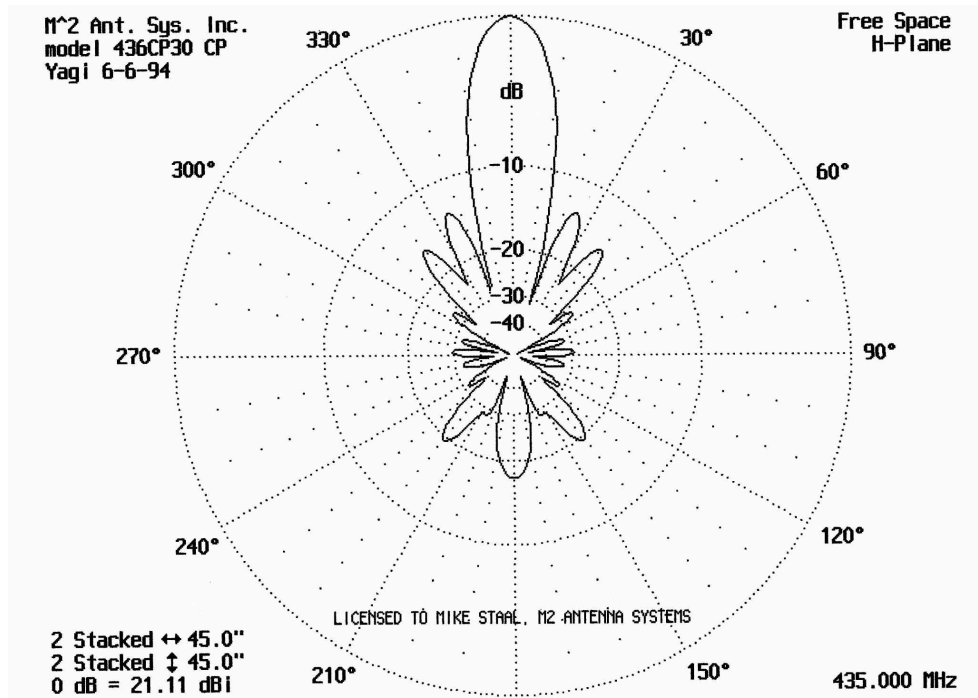
(a) System A (436CP30).
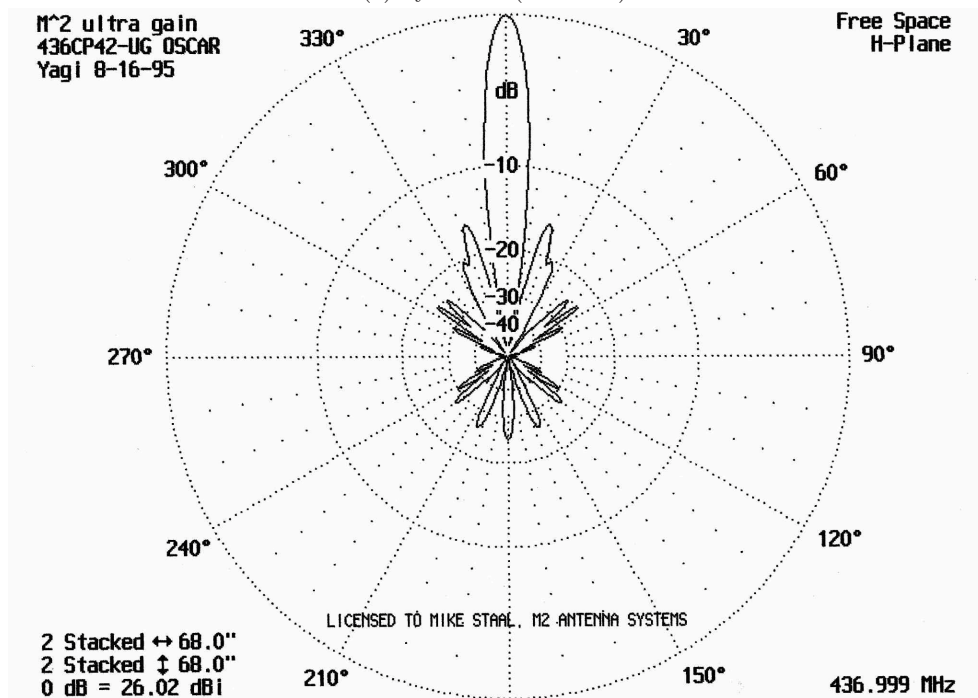
(b) System B (436CP42UG).

Figure 8.3: Simulated radiation plots (free space) in H-plane for 4 stacked antennas (Credit: M2 Antenna Systems)

8.2.2   Low Noise Amplifier

The mast-mounted preamplifier SP-7000 with integrated switch from SSB was chosen for this installation. This LNA is rated with an excellent performance and is very practical. It is powered from the radio through its coaxial connection with a DC voltage at 13.8 Volts applied to the center conductor. This eliminate the need for an additional power cable. If no DC voltage is applied to the LNA, the internal relays disconnect the amplifier and connect the input directly to the output. It also has a built in RF switching capability meaning that the amplifier will automatically disconnect if the radio transmit while the amplifier is powered on. A helical resonator type filter is integrated to the amplifier, which is a passive device that can achieve high Q-factors. Relevant parameters for this amplifier is presented in table 8.2. The s-parameters de-

Parameter (Rx)	Value	Parameters (Tx)	Value
Gain	20 dB	Capacity	100 W (RF Switching)
Noise Figure	0.9 dB	IL	0.3 dB
Bandwidth	430-440 MHz	Supply Voltage	12-14 V

Table 8.2: LNA parameters

scribing reflection(S_{11}) and transmission (S_{21}) are shown in figure 8.4 on the next page. The amplifier has a very good gain flatness over the operating frequency. there is an considerable mismatch at the input. At 435MHz with a source impedance of 50 Ω, the reflection parameter S_{11} is approximately -4 dB. This means that more than half the power delivered to the amplifier is reflected. But preamplifier are usually designed for lowest possible noise figure which often results in a tradeoff with the ideal matching of the input impedance.

8.2.3   Power Splitter

The power splitter/combiner used is based on two parallel quarter wave transmission line stubs. This is a reactive type splitter delivering equal phase to all output ports. An illustration of the device can be seen in 8.5 on the facing page. On each side two and two antennas are connected in parallel through a simple T-junction. If the input impedance to these antennas are 50 Ω, the input impedance at the T-junction is 25 Ω. To get an input impedance of 50 Ω, the two quarter wave transformers must convert each branch to an input impedance of a 100 Ω. Then the parallel combination of these two will give the desired input impedance. The required characteristic impedance Z_0 of the quarter wave transmission lines can be calculated from the equation 2.16 on page 12.

$$Z_0 = \sqrt{25\Omega 50\Omega} = 50\Omega \tag{8.1}$$
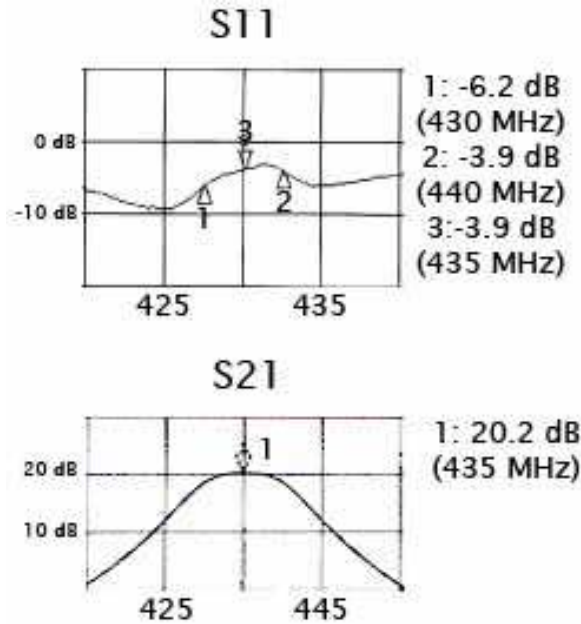
Figure 8.4: LNA S-parameters: reflection (S11) and transmission(S21) (Credit:SSB electronics, modified).
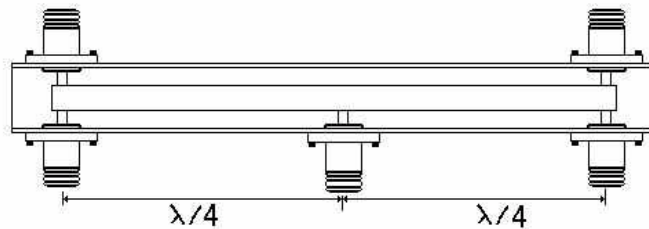
Figure 8.5: Internal structure of power splitter.

This splitter could have been made by just splicing appropriate lengths of coaxial cable together. But the advantage of the used splitter is the construction, which gives a very low insertion loss. This is because the construction allow a true air spaced transmission line which minimize dielectric losses. The disadvantage is the low isolation (approximately 3 dB) between adjacent ports. As long as the antennas are well matched close to 50 Ω this is not a big problem, but if one antenna short circuit it will strongly degrade the performance of the others antennas as well. The performance of the splitter is examined in more detail in chapter 9 on page 85.

8.2.4   Coaxial Cables

Three types of coaxial cable are used in the ground station installation. RG6-U in the antenna assembly, RG213 between the LNA and the lightning arrestor (COAX2) and Westflex W103 in the rest. The only reason for using RG213 type is because of its stranded center conductor which is much more flexible than the W103 which has a solid copper core. This is because the cable (COAX2 in figure 8.1 on page 66) bends during the operation of the elevation rotor. In figure 8.6, the composition of the W103 cable is shown. The advan-

Plastic Jacket   **Copper Foil**

Inner Conductor
Plain Copper (2.65mm)

Copper Braid   **Dielectric Insulator**
Semi Air Spaced five cell extrusion
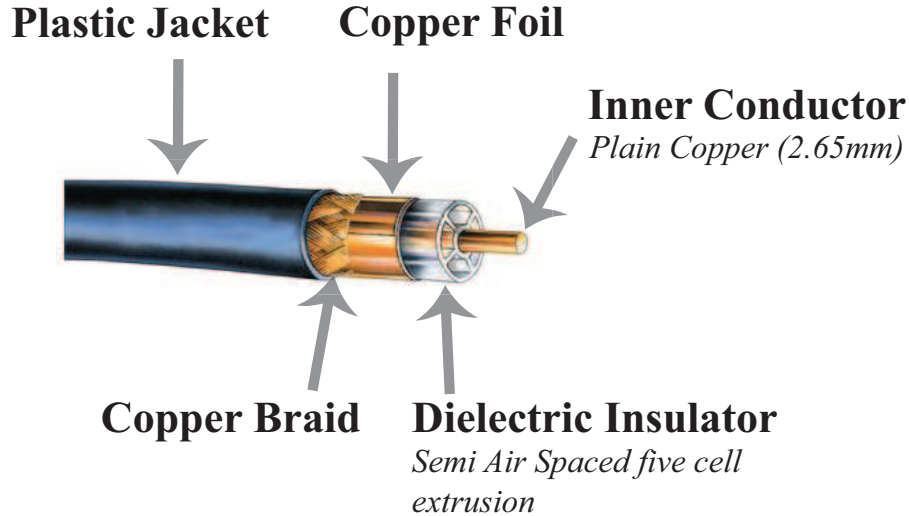
Figure 8.6: Composition of the Westflex W103 coaxial cable (Credit: Modified image from SSB).

tage of this cable is lower resistance in the center conductor, less dielectric loss and lower radiation loss. The cable has an solid copper core which reduce the resistance. Air spaced design for low dielectric loss and copper foil in addition to the stranded to reduce radiation loss. The only real downside is less flexibility. The copper core can withstand a certain amount of bending before it breaks, but the copper foil will very quickly develop cracks and tears if care is not taken during installation or storage. The loss per 100 meters for each of the cables is shown in table 8.3.

Cable type	Z_0	Loss/100m at 400 MHz (dB)
W-103	50 Ω	7.2
RG213	50 Ω	15.4
RG6-U	75 Ω	15

Table 8.3: Coaxial cable loss.

8.2.5 Rotor Controller

The G-5500 rotator and controller system from Yaesu is used in combination with GS-232B computer control interface. This is a reasonable priced complete Azimuth-Elevation rotation system for small to medium installations.

Between the two rotors, the elevation rotor is the weakest link with regards to how much size of weight and wind loads it can handle. The system is therefore constrained by its requirements. It can handle a maximum vertical load of 30 Kg and a maximum wind load of about $1m^2$. The wind load of the system attached to the elevation rotor is less than $0.6m^2$, well below the limit. And the combined weight of the antennas and the antenna frame is less than 20 Kg.

Yaesu introduced a parameter called the K-factor which is derived by multiplying the turning radius of the antenna by the weight of the antenna. This takes into account weight distribution along the length of the antennas which give a larger contribution to rotational torque. The K-factor is defined as

$$K = \text{(Turning Radius of antennas)(Weight of Antennas)} \qquad (8.2)$$

For the G5500 kit the K factor of the rig must be less or equal to 60 meter-Kg. Given the total weight of antennas and rig of approximately 20 Kg with a turning radius of 1.6 m the K-factor of the ground station is

$$K_{Station} = 1.6x20 = 32 \leq 60 \qquad (8.3)$$

This is well within the limits of the rotor. This should indicate a good performance of the rotor with good margins. It is very important to have a good margin as snow and ice during winter can increase the weight of the system, leading to an increased system k-factor.

8.2.6 Transceiver

Two types of modulation is of relevance for this system. CW for morse code and frequency modulation (FM) for data transfer. The ICOM IC910H is based on the superheterodyne principle, delivering double conversion on CW and triple conversion for FM. Some basic parameters for this radio is presented in table 8.4.

Parameter	CW	FM
Sensitivity	0.11 μ V	0.18 μ V
Selectivity	2.3 KHz	15 KHz
Output Power	5-75 W	5-75 W

Table 8.4: Basic transceiver parameters.

8.3 Software and Interface Connections

This section briefly describes the software used in satellite tracking operation.

8.3.1 Rotor and Radio Control Program

Ham Radio Deluxe (HRD) is used for and controlling the rotor controller. It also calculates the frequency doppler shift and adjust the transceiver frequency accordingly. This software is developed by Simon Brown (Amateur license ID:HB9DRV). For determination of the satellite positions, HRD uses a Two-Line Element (TLE) file which contains the keplerian elements and identification. The layout of this file for the satellite HO-68 is shown in figure 8.7. The keplerian elements explained in 5.1.2 on page 36.

Figure 8.7: TLE 2-line keplerian element set

8.3.2 Communication Setup

There are two types of communication protocols to be used for the link between the satellite and the ground station. These are a downlink CW beacon and a half-duplex gaussian frequency shift keying (GFSK) link for sending and receiving AX.25 packets. Currently two different schemes are used in connecting the hardware for these two modulation types. In both cases the RigExpert Tiny interface is used to control the transceiver.

Reception of Downlink Beacon

To decode the morse coded beacon signal the program CwGet is used. The signal is sent as sound signals over a cable connected to the microphone input of the computer sound card. Confer to figure 8.8 on the next page for the physical setup for this mode. In this setup the "CW" and "SPK" cables are left unconnected because they are used for transmission of CW signals. Only reception of the beacon signal is currently used.
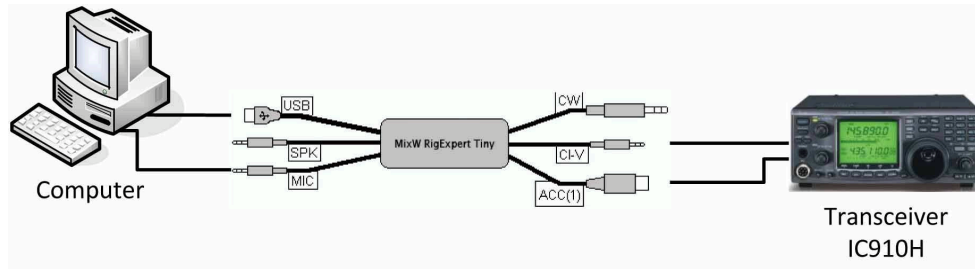
Figure 8.8: Hardware configuration for reception of CW beacon

Reception of Downlink Data

To decode the AX.25 data packet, The program mixW is used. The physical connection required for this is shown in figure 8.9. The MixW RigExpert Tiny is only used for software control of the radio in this setup, While another custom data interface[2] card is used to connect the "data in", "data out" and "push to talk" pins from the DIN connector on the transceiver.
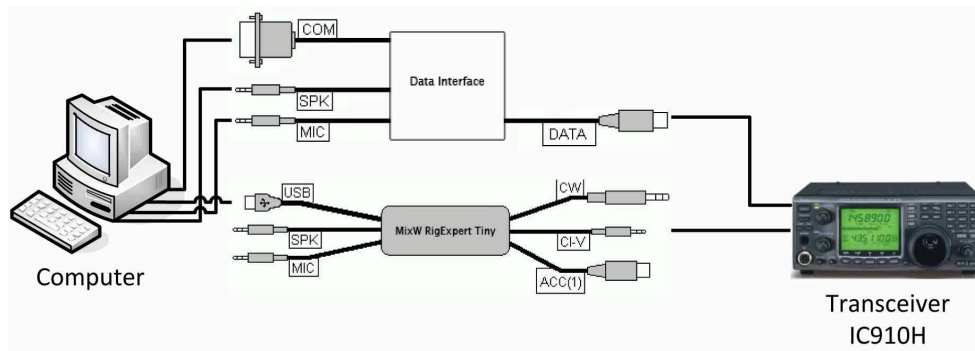
Figure 8.9: Hardware configuration for half duplex GFSK data communication

---

[2]Made by Johan L. tresvig

8.4   Installation

The antenna rig was installed on the roof of the building for the department of physics. Antenna, mast and tower installation is pictured in figure 8.10.

The installation was done during days with good weather forecast to avoid working in rain. It took several days to complete, so the equipment was covered with tarpaulin each night to protect from rain. The installed rig can handle rain when complete, but during the installation not all connectors where water proofed yet and the rotators has implicit recommendation not to be left outside laying in a sideways position due to possible water intrusion. Several people is required in the process of raising and lowering the antenna mast which made it unpractical to make several small adjustments as this required to organize help from other people every time. All the installation and measurements was done in three sessions. I made an effort towards making the entire rig durable over a long time period by securing all cables and wires with extra strips and tape. Some additional precautions were also taken to make future work on the rig easier. All cables and wires connected to the rig has been coiled up with some extra length both in the top and the bottom of the antenna tower. This will ensure that there is enough material to work with if any of the mentioned must be cut or extended due to damage or any other reasons. Key components such as screws and nuts and the small ropes fastened to the coaxial cables between the antenna and the splitter should be inspected at a later instance. The instrumentational workshop at the department of physics could be consulted to get further advise on this.

Figure 8.10: UiO ground station installation

8.4.1 Tower, Mast and H-Frame

The antenna tower is a straight type of a steel lattice structure. It provides great strength combined with low weight and wind resistance. Two antenna towers where already present, constructed many years ago. These where real-located to slightly higher positions (Where they are now) to get an elevated position with less nearby clutter and to get an easier mechanism for lowering and raising the mast. The H-frame for mounting the antennas is shown in fig-

(a) Antenna frame used for mounting the antennas

(b) Pulley system for lowering and raising the antenna tower
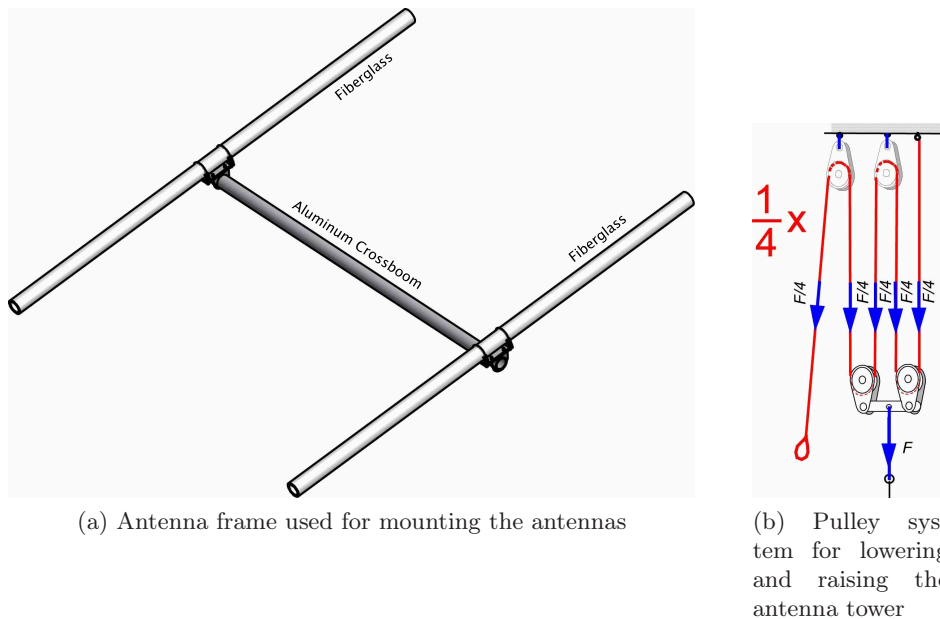
Figure 8.11: Components in installation

ure 8.11[3]. The cross boom is an aluminum tube, while the two vertical lengths are made of fiberglass to reduce the impact on the antenna radiation patterns.

Hoisting the Antenna Mast

At least two people, preferably three people, are required to safely lift and lower the antenna mast. A pulley system is installed which reduce the instantaneous force by four in exchange for having to pull a longer stretch of rope. This principle is shown in figure 8.11.

One person should be on the rope securing and pulling while the other person holds on the tower itself and contribute as well. The rope alone should not be relied to be the only thing securing the entire rig while lowering or raising. When lowering the rig a table should be placed over something flat to avoid the any sharp edged from the table feet to damage or penetrate the top

---

[3]The frame is made by the instrumentational workshop located at eh dept. of physics

material on the roof. This can cause leaks through the ceiling. When lowered, the antenna tower can be rested on the table ensuring that the antennas do not touch the roof top. Prioritize safety rather than speed as a single slip can cause damage to people and totally destroy the entire installation.

8.4.2   Wind Loading and Mast Strength

The estimated weakest point on the antenna installation is on the antenna mast at the thrust bearing. The mast is made of steel which has a yield strength of 36000 psi[16]. First the total moment of the mast at the thrust bearing is calculated by the following formula [21]

$$M_{Total} = \sum FD \tag{8.4}$$

$$(F_{ant1} \cdot D_{ant1}) + (F_{ant2} \cdot D_{ant2}) + (F_{ant3} \cdot D_{ant3}) + (F_{ant4} \cdot D_{ant4}) \tag{8.5}$$

Where D is the height from the thrust bearing to the antenna in question and F is the force on each antenna given by

$$F = \frac{Velocity_{wind}^2 Area_{antenna}}{390} \tag{8.6}$$

Then the mast stress at the thrust bearing can be calculated by the following equation

$$f = \frac{M_{Total}c}{I} = \frac{M_{Total}c}{(\frac{\pi}{64})(D^4 - d^4)} \tag{8.7}$$

Where:

- c is half the mast diameter in inches.

- d is the inner diameter of the mast in inches.

- D is the outer diameter of the mast in inches.

The relevant parameters of the rig for this calculation is gathered in table 8.5 on the facing page. First the force on each antenna is found. The highest wind velocity recorded in february 2011 (See weather statistics in appendix G on page 117).

$$F = \frac{29^2}{390} \approx 474$$

This is the same for all the antennas, so $F_{ant1} = F_{ant2} = F_{ant3} = F_{ant4}$. The the total moment M_{Total} is found

$$M_{Total} = 2 \cdot 2.16(37 + 77) = 492.5$$

Parameter	Value	Unit
Mast inner diameter (d)	1,79	Inches
Mast outer diameter (D)	1,97	Inches
Antenna wind area	1	square feet
D_{ant2} and D_{ant3}	37	Inches
D_{ant1} and D_{ant4}	77	Inches
$velocity_{wind}$	29	miles per hour

Table 8.5: Parameters for yield stress calculation.

The mast stress at the thrust bearing is then found to be

$$f = \frac{491.5 * 0.984}{\left(\frac{\pi}{64}\right)\left(1.97^4 - 1.79^4\right)} \approx 2060$$

The mast stress at the thrust bearing is much less than the yield strength rating ($2060 << 36000$) which concludes that it can handle much more load and higher wind speeds than what it is subject to date.

8.4.3   Coaxial Cables

Phasing the COAX4_x Cables

The four coaxial cables between the splitter and the antennas is required to have the same electrical length. If the electrical length is equal the phase of the applied signal arriving at the antenna will be equal and the antenna will have the simulated characteristics shown in 6 on page 47. To be able to achieve this, four approximately equal lengths of coaxial cable was cut and then terminated with connectors on one end. Then the phase change through the first reference cable was measured by measuring the phase of the reflected signal. Then the other cables was connected to the VNA while cutting small pieces of length of the open end until it had the same phase change as the reference cable. With this process the four cables ended up with less than 1 degree difference in electrical length.

Connectors

(a) Step 1	(b) Step 2	(c) Step 3
(d) Step 4	(e) Step 5	(f) Step 6
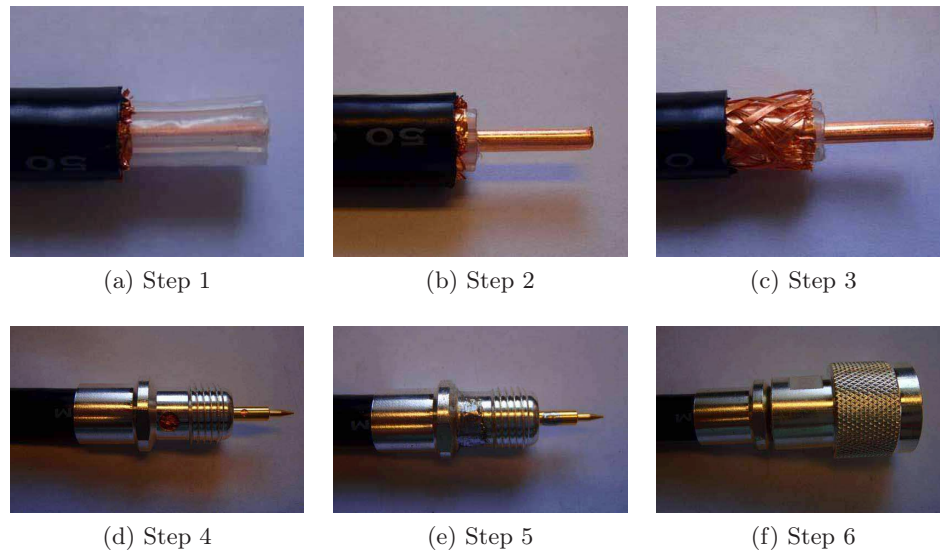
Figure 8.12: Procedure for installing coaxial connector on Westflex W103 cable.

The connectors used are a two-piece N-type connector with heavy silver plating. This connector performs well and is relatively easy to install. The procedure for installing the coaxial cable connector used in the Oslo Ground Station (OGS) installation is described below. Illustrations for these steps can be seen in figure 8.12.

1. Cut 14.3 mm from the end and remove the wire braid and copper foil.

2. Cut the dielectric insulator 12.7 mm from the end.

3. Cut down additional 8 mm of the plastic jacket.

4. Screw on piece (1) of the coaxial connector. Use a multimeter and check the conductivity through the center conductor and ground. Make sure there is not a short cut between the center conductor and ground. checked for continuity between the ends.

5. Solder the connector on the connector as shown in figure 8.12 on the facing page. If there is a lot of excess solder file it down to a smooth surface such that piece (2) can be easily screwed on. Wait until it cools down before the next step.

6. Screw on piece (2) of the connector and tighten with two wrenches. Avoid turning part (1) any further around the plastic jacket after soldering.

Weatherproofing

All connector joints should be weatherproofed to avoid water intrusion into the coaxial cables and connectors. A water intrusion might short circuit and severely degrade the transmission line. If the line is short circuited, there will be a voltage reflection coefficient close to -1 at this point and all power will be reflected back to the source. This can potentially damage the radio as more power is dissipated in the radio than what it is rated for. Two types of tape

(a) Step 1   (b) Step 2   (c) Step 3
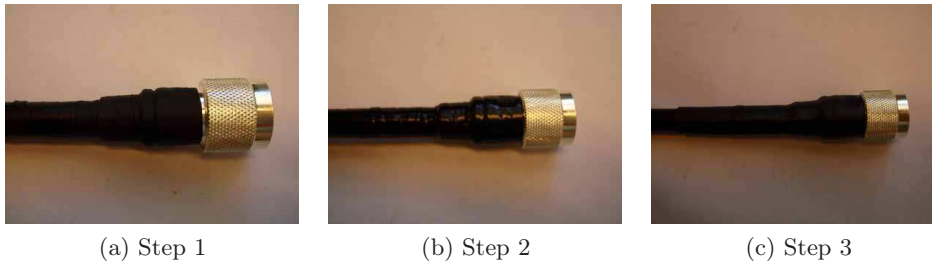
Figure 8.13: Procedure for weatherproofing coaxial connectors.

are used. An all weather "Scotch Super 88+" from 3M [4] and a conformable self-fusing rubber insulating tape. Finally a shrink tubing is placed over both the two previous layers of tape to protect the electrical tape from UV light and hinder the tape from unwinding. with this method the connectors should have a reliable water seal. It is easy to remove the seal by carefully cutting it open and just peeling it off. A substance called plastidip and liquid electrical tape was experimented with to see if it would create an even better seal. But these substances work best on metal alone as they teared up the underlying

---

[4]Thanks to 3M for supplying several free samples

tape when applied due to the fact it shrunk when drying while pulling the tape apart.

The following procedure describe the chosen way of weatherproofing the coaxial connectors.

1. Before starting one the first layer slide on the shrink tube. Always wrap in the direction from smaller to larger diameter ("uphill") where possible and wrap in the direction that tend to tighten the connectors. Dont stretch the tape to hard as it might compress the cable and change its characteristic impedance at that point. First apply a layer of the self-fusing tape. Place by a tape width before the end of the connector and stretch out the tape until its between half and a third of the original width. Then wrap around overlapping by half the width for each turn.

2. Start with the next layer one inch below the first. Apply the super 88 electrical tape with half the tape width in overlap for each turn. The tape can be slightly stretched when applying and try to avoid any wrinkles or open spots.

3. Slide the shrink tube in place and heat it with a heat gun to make it sit tight around the tape.

8.4.4   Calibration of the Rotators

To calibrate the rotators a 5mW laser was assembled in a custom waterproof structure that could be placed on the antenna frame. This was connected to a red and blue wire (100 meters) going all the way down to the UiO ground station control room. The laser was tested in the assembly with the 100 meters of wire, prior to the installation, to verify the function. There was approximately a voltage drop of 0.2 Volts over the cable. As the laser required an input voltage in the range 3 - 4.5 volts, the range 3.2-4.7 could be applied to the input of the supply wires. The general idea for calibration of the azimuth rotator was to point the laser at a given point, calculate the azimuth angle on a map and find the offset to compensate for this in software. But after installation there has probably formed dew on the plastic cover in front of the laser beam which spread out all the light making it impossible to get a light beam visible on a far away structure. The calibration was instead aligned with the local structures on the roof. The azimuth rotor points 10 degrees counter clock wise (-10) from true north. This can be compensated for in the software. If the antenna rig is lowered for inspection or any other reason at a later time, the laser assembly can be reviewed and repaired so to make a more precise calibration. The laser pointer is rated for the range -40 to 80 degrees for storage, so it should be operational as long the custom housing remains water tight. Dont try to operate the device at temperature lower than -10 degrees though.

Figure 8.14: 5 mW laser pointer in custom housing.

When the antenna rig is not used it should be parked in the direction such that the effective wind are is minimized. In figure G.3 on page 118 the average wind at blindern is shown in a polar plot. This shows that the most common wind direction is 30 degrees from north (±180 degrees). When the antennas are aligned with or against the wind direction their effective wind are will decrease and there wil be less stress on the azimuth rotor.

Chapter 9

System Testing and Verification

9.1 System Characterization

To verify the performance of the ground station hard ware, the S-parameters for each component was found by measurements done with a network analyzer (see explanation about this instrument in 9.1.2 on the following page).

It is possible to first assemble everything between the antenna and the radio and then measure the S-parameters for the combined system. But if for example there is a faulty connector at one of the coaxial cable ends, the measurement would not tell us where to find this. Measuring every coaxial cable would also reveal if the connectors was installed correctly.

9.1.1 System Overview

All the parts between the radio transceiver and the antennas will be modeled as two-port networks, each with their names in accordance with the parts seen in figure 9.1. Throughout this chapter the the individual parts for the system
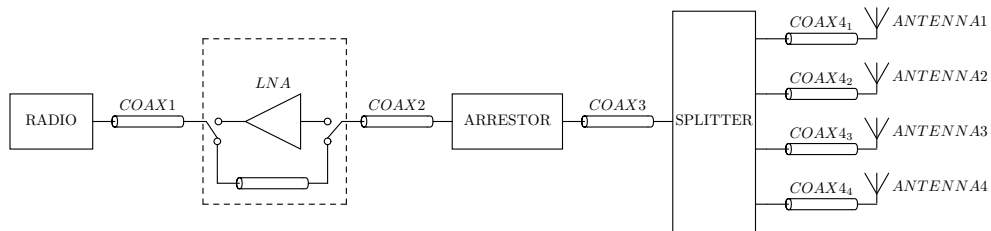
Figure 9.1: Overview of ground station

will be called by the names given in figure 9.1.

9.1.2 Vector Network Analyzer

A VNA is an instrument that can measure network parameters in terms of magnitude and phase with a high level of precision. Examples of such parameters are impedance, loss, gain, etc. The main focus in here is to measure the S-parameters, which under certain conditions can be used to find the parameters previously mentioned. In figure 9.2 the ZVL combined network analyzer and spectrum analyzer can be seen. This is used to measure the S-parameters for the ground station system.

Figure 9.2: Vector Network Analyzer.

9.1.3 TOSM Calibration

For the measurements of a VNA to be accurate, the instrument in questioned must be calibrated. This process use a technique called vector error correction. In this method standards are measured to find error terms that can be used to calculate and remove systematic errors[8]. Even though the repeated errors will be compensated for, there will still exist random errors caused by noise and repeatability of switches, connectors and adapters. Other measures must be taken to further reduce this uncertainty if desired.

After a successful calibration, an interface between the DUT and the test port cables with its connectors, is established. Figure 9.3 shows this boundary. The parameters measured and presented only represent all that exist after this plane(i.e. the DUT). Everything between the reference plane and the VNA will be removed from the results by error correction. There are several calibra-
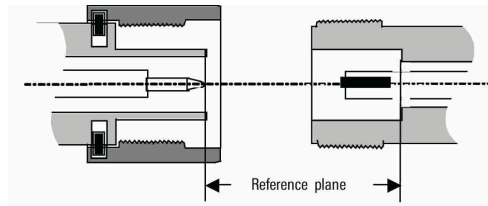
Figure 9.3: Reference plane in N-type connector (Credit: R&S)

tion procedures, but the one used here is called TOSM. It stands for Through,

Open, Short and Load. This is the four calibration standards required for performing this calibration. These can be seen in figure 9.4. The instructions for this calibration procedure is presented in 9.1.4. It is not possible to construct perfect standards. For example, the open standard have fringing capacitances causing negative imaginary parts to measurements. So these standards has to be described by special coefficients and stored on the VNA prior to calibration.
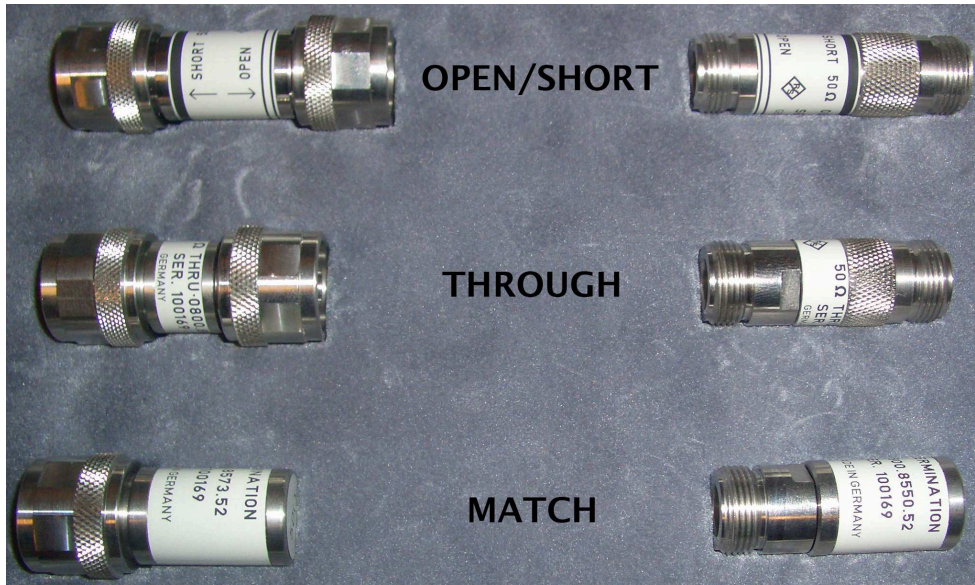
Figure 9.4: N-type calibration standards from ZCAN kit.

9.1.4 Measurement Procedure

If certain conditions have changed since the previous calibration, the calibration must be performed again with the same settings that will be used in the subsequent measurements. The TOSM calibration procedure needed for a two-port measurement is described below. This is the setup used when measuring the ground station components.

1. The VNA must have been stored at least three hours at ambient temperature before another 30 minutes warm-up time after the VNA is turned on. This is required to reach a stable operating temperature.

2. Make sure the test port cables and adapters that will be needed during the following measurement are connected.

3. Set the frequency span to 435-438MHz.

4. Set the frequency step size to 5 KHz linear sweep type.

5. Set the IF bandwidth to 10KHz. This setting determine the dynamic range of the measurements.

6. Set Average factor to 10 and enable average. This will remove some of the additive white gaussian noise (AWGN) from the measurement results.

7. Set power bandwidth to -10 dBm.

8. Start the TOSM calibration procedure. For N-type connectors use the calibration standards from the ZCAN calibration kit. Caution must be used so not to cause damage which might alter the characteristic behavior of the calibration standards.

9.2   Measurement Results

All the components in the ground station was measured using the procedure described in 9.1.4 on the previous page. The results was stored in .s2p files given names in accordance with the ones in figure 9.1 on page 85. These files are basic text files that store columns for frequency and all the S-parameters for a 2-port network. They store the real and imaginary part of the parameters so that phase information is accessible at a later time if needed. The files can be found in appendix H on page 119.

A matlab script called "Sparameters" was created to handle and present the S-parameters for the system. A screen print and background theory for this is presented in appendix E on page 109. The total insertion loss between the radio and the antenna is

$$IL_{system} \approx 11 \text{ dB}$$

9.2.1   Converting the 5-port Power Splitter into a 2-port Network

The 4-way power splitter is really a 5-port network. But the network analyzer only has the ability to make 2-port measurements. All the output ports of the power splitter is matched for 50 Ω. So measurements was done between the input and one output port at a time while the other output ports was connected to 50Ω loads. The measurement verified that all the S-parameters where equal for the measurements between port1 and port 2, 3, 4 and 5. So if the antenna impedances is close to 50 Ω the 2-port measurement between the input port and port 2 of the power splitter was assumed to be valid for all the four different branches out towards the antennas.

9.2.2   Antenna Measurements

The first input reflection measurements for the antennas showed unsatisfactory results. Therefore the shorting bars connecting the two straight aluminum rods

into the folded dipole (driven element) was moved to increase the electrical length. The antenna input impedances was improved from the range 20-30 to 40-50 Ω. The antenna measurements was done while the antenna tower

(a) Antenna input reflection coefficient.

(b) VSWR at antenna input.
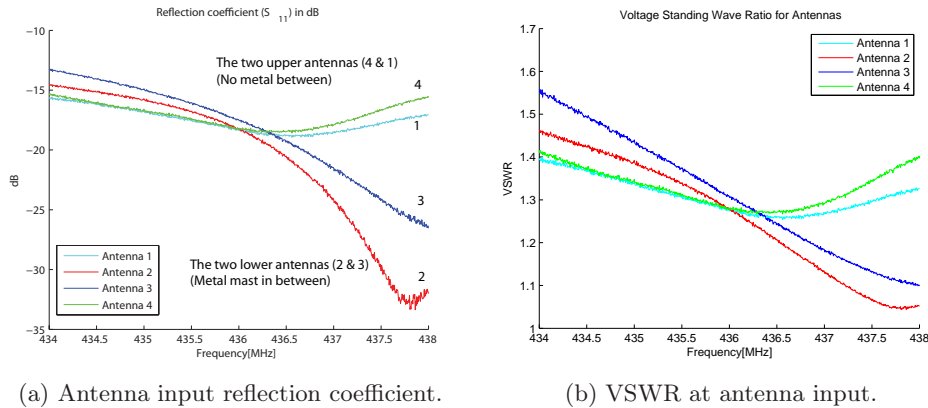
Figure 9.5: Antenna measurement results. The difference between the almost identical antennas is probably caused by the metallic antenna mast which will be in between the two lower antennas in the rig (antenna 2 and 3) while the two upper antennas (antenna 1 and 4) dont have this metal interfering with their near-field in the same manner.

was tilted down on the roof. A measurement was also performed while the tower was erected to ensure the results would be valid. To be able to measure while the antenna was raised, a 15 meter long coaxial cable was used and the VNA was calibrated to have the reference point at the end of this cable. There was minimal differences. Although when the elevation of the antenna rig was raised towards 90 degrees the reflection coefficient was consistently worse by about 3dB. The most likely reason is the interacting effects of the aluminum antenna mast which come close to the antennas as it rotate towards to align with the mast. This Means that the input impedance of the antennas will be altered while tracking a satellite. This degradation is very small and even if the reflection at the antennas increase slightly while the satellite passes over our heads, the path loss between the ground station and the satellite will be reduced by a much greater factor. The input impedance seen at the input of the splitter of the Yagi-Uda antennas is hown in figure 9.6 on the next page.

9.2.3 Varying Reflection Coefficient for COAX1

Most of the coaxial transmission lines showed a constant reflection constant over the frequency span of 434 to 438 MHz close to -30 dB except for the COAX1 cable. The reflection coefficient varied over the frequency span as can be seen in figure 9.7 on page 91. At first i did not understand this behavior.
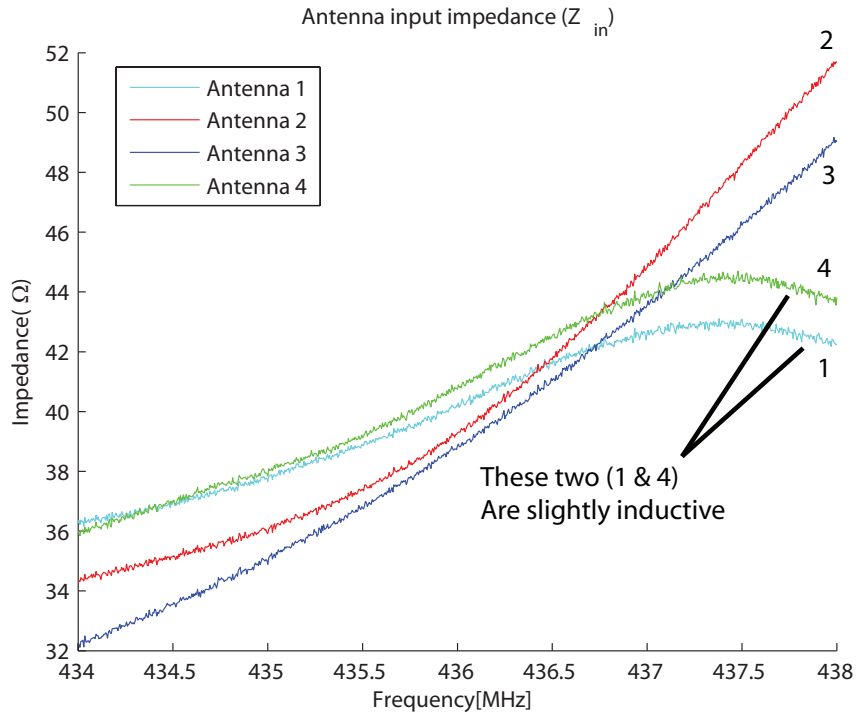
Figure 9.6: Antenna Input Impedance.

But there was a simple explanation. I assumed the characteristic impedance of the transmission line to be near perfect to 50 Ω. But it clearly either had a few Ω higher or lower than 50 Ω. Equation 2.17 on page 14 shows that for every lossless transmission line with length multiples of $\frac{\lambda}{2}$ the input impedance is equal to the load impedance. The ports on the network analyzer has input impedance of 50 Ω. When the frequency changes in such a long coaxial cable as COAX1 (100 meters), the relative phase change on the other side will change rapidly moving through several multiples of half a wavelength. When the input sees the load impedance there would be no reflection at all if the line was lossless. But this line has some loss and some small irregularities along its length which gives the curve shown in figure 9.7 on the facing page.

The coaxial cable is likely to be shortened in the future as the total length of 100 meters is not needed. There are some cable gate ways being installed at the roof, and the cable will be cut down to the axact needed length after this is installed. When this takes place, care should be taken to try to match the length of the cable to the operating frequency for CubeSTAR at 437.465 MHz to minimize losses due to reflection.

The reflection coefficient measured here is not a good representation as there is considerable loss through the cable. This means that the measured
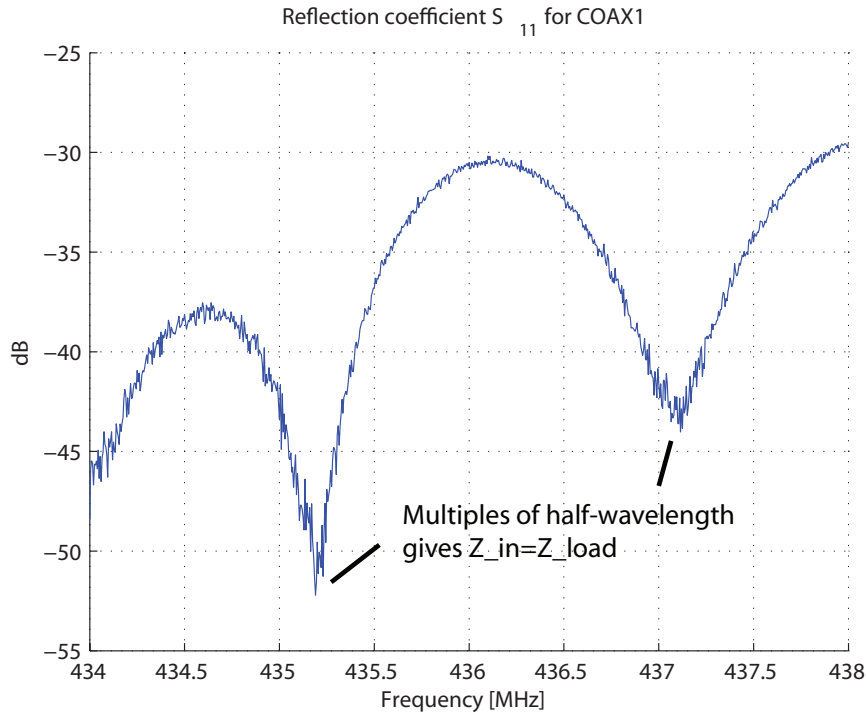
Figure 9.7: Reflection coefficient at input of COAX1

reflected signal due to reflection in the other end are attenuated by approximately 20 dB as the insertion loss through the cable is approximately 10 dB. This means that the power of these reflections are divided by 100.

9.2.4 System VSWR

The VSWR for the system, measured at the input of COAX1, is shown in figure 9.8 on the next page. It is calculated by the use of equation 2.10 on page 10 on the measured reflection coefficient S_{11}. The results look very good, but for VSWR to give a true meaning of the system performance, all the transmission lines between the radio and the antenna should be lossless. As VSWR is defined to be the ratio between the maximum voltage and minimum voltage in a transmission line, it will be different along a lossy line. Strictly speaking, VSWR can only be applied to lossless line [13]. But for systems with very low losses, it can be applied. Because there is more than 10 dB attenuation in COAX1, any reflection on the other end will be attenuated by more than 20 dB before it is returned to the input. This means that the results in figure 9.8 on the next page is not a good indication of match throughout the system. But this result can be used later for comparison to check for any serious system degradation which might occur due to water intrusion into the
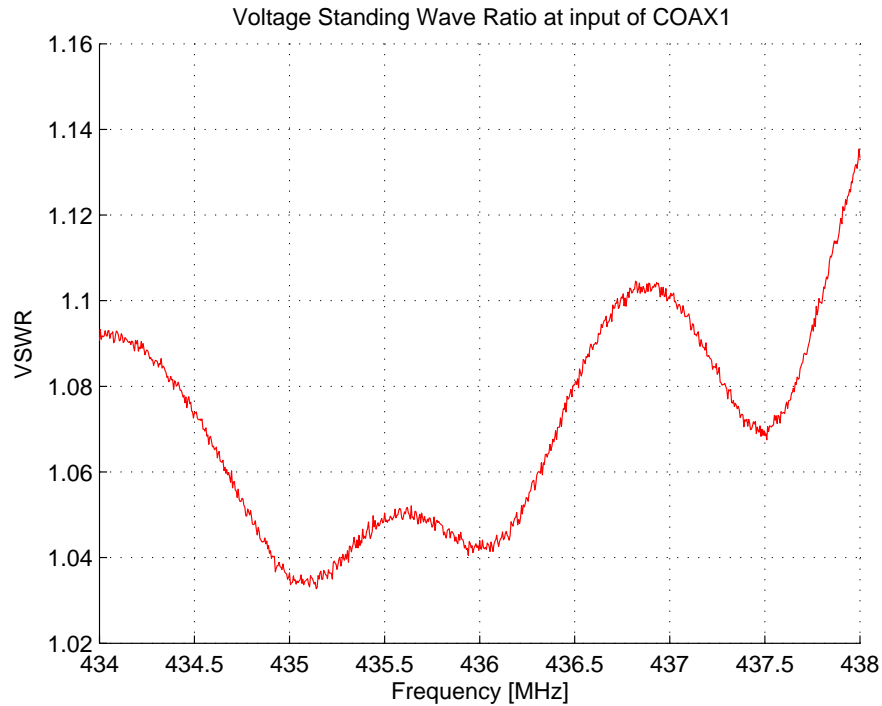
Figure 9.8: System VSWR (fluctuations is mainly due to the behavior of COAX1)

coaxial cables or other damages to the cables or connectors. The result also ensures that very little power will be returned to the radio output. This is important as most radios will be damaged if it transmit at full power with out any load attached. In that case all the output power will be returned to the radio and hence it must dissipate twice the amount of power it is meant to do.

9.2.5   Power Delivered to Antennas

The power delivered to the antennas was calculated to be approximately 1 W (see appendix E on page 109) when the radio transmited with an output power of 50 W. A Watt-meter was connected between the antenna and the transmission line connected the the power splitter. The Watt-meter had a very low resolution and I had to stand pretty close to the antenna which might have altered the characteristics somewhat. The reading was a little under 1W. This measurement does not give a high reliability or accuracy, but it gives a good indication of the performance.

The losses between the radio and the antenna has been calculated, but there might be additional mismatch losses which is very hard to analyze. This is due to the fact that because there are reflections in the transmission lines,

the forward and reflected voltage and current waves recombine into different magnitudes along the line length. Because the power loss in resistance is an exponential function ($P = I^2R$), the power loss does not have a linear relationship throughout the line. By adding a small margin due to this additional mismatch loss and due to the small imaginary parts of the antenna impedance, the power radiated by the antennas when the radio transmit at 75 W is approximated at 5W. When the COAX1 cable is cut shorter it is expected to se around 3 dB reduction in line losses which will increase the power delivered to the antennas to approximately 10W.

9.3 Communication Link Test

9.3.1 Reception of Downlink Beacon from HO-68

The satellite HO-68 had a relatively stable performace and was therefore used in verifying the downlink CW morse code communication link. HO-68 travel in a LEO orbit at an altitude of approximately 1200 Km. The downlink morse code CW beacon transmit at 200 milliWatt (23 dBm).

(a) HO-68 trajectory   (b) H0-68 elevation angle during pass
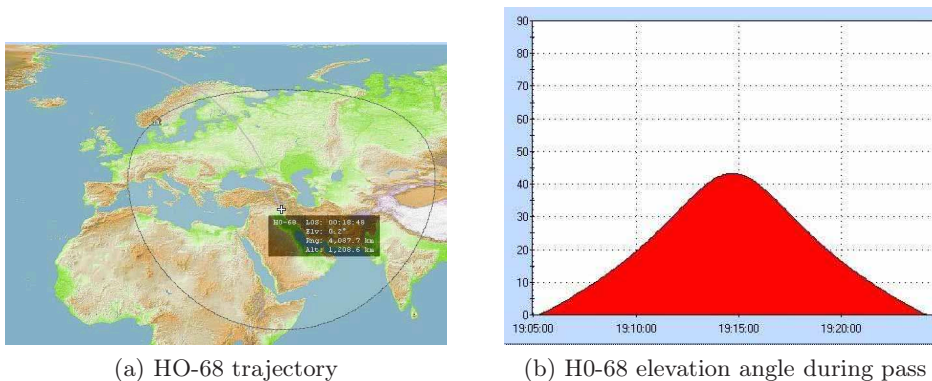
Figure 9.9: Path profile for HO-68 satellite during a pass

The received signal strength given in table 9.1 on the next page was read from the Icom 910-H s-meter and translated to dBm value through the s-meter calibration data in appendix C on page 105. The values might differ by a few dBm because of the resolution. But these values are a good indication of the system performance. A potential received morse code signal received from CubeSTAR if it transmit at 100 mW (20dBm) can be around -96 dBm (worst case from link budget) when the satellite is at an elevation of 10 degrees (Slanth path = 1900 Km).

El. angle (degrees)	Received signal (dBm)	Range (Km)	Path loss (dB)
10	-108	3100	155.2
16	-106	2690	153.9
24	-103	2250	152.3
28	-99	2070	151.6
44	-93	1600	149.4
43	-99	1620	149.5
36	-103	1800	150.4
31	-106	1960	151.1
11	-108	3050	155

Table 9.1: Received power from morse code beacon from HO-68

9.3.2   Noise source at 437.496 MHz

While in the process of tracking the Cubesat Oscar-66 (CO-66) satellite a noise source was discovered. The downlink beacon of CO-66 is 437.4850 MHz. The noise source center frequency was found to be around 437.496 MHz. A
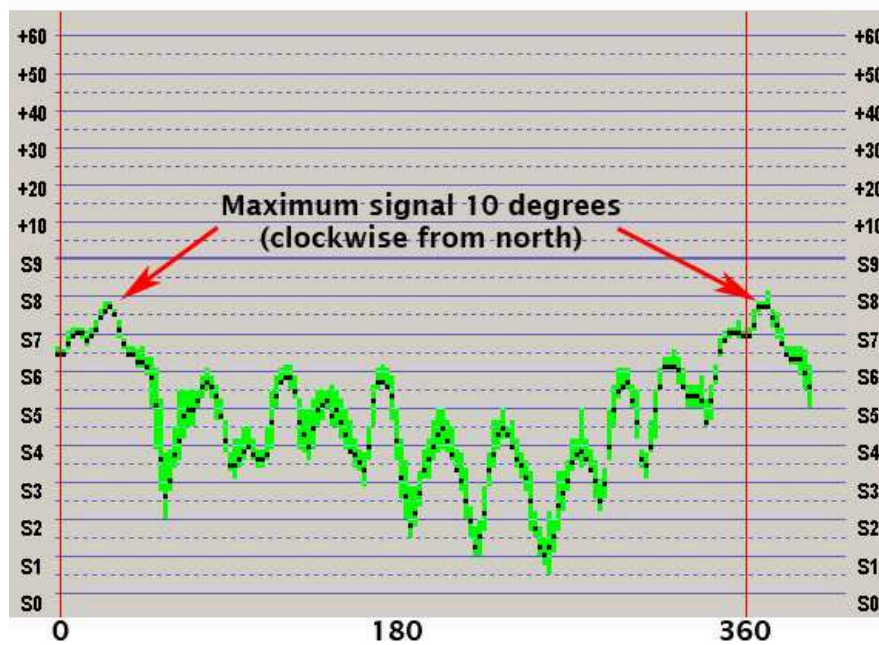
Figure 9.10: S-meter values for the noise source at 437.496 MHz. This figure is a screen print of the S Meter Lite software

sweep of the noise signal power read from the radio s-meter can be seen in figure 9.10. The antenna was set to 0 degrees elevation and was turned 360

degrees around while logging the s-meter levels.[1] The measurement indicate that the noise source might be somewhere close to the north. But this should not be of any concern for the CubeSTAR satellite as the bandwidth of the filters in the receiver system is narrow enough to exclude this when operating at the CubeSTAR frequency (437.465 MHz).

9.4 Measured Antenna Pattern

There are resources available to measure the antenna pattern for smaller antennas in an anechoic chambers. The chamber is a shielded room which is covered by material that absorb and scatter incident waves to simulate free space environments. But the stacked antenna rig was too big to fit in the chamber. A more primitive measurement was performed.

A signal generator was connected to a single Yagi-Uda antenna termed A. It was directed with the boresight direction towards our four stacked antennas which will be referred to as antenna B. The two stand at equal height 20 meters away from each other. Antenna B was then rotated 360 degrees while recording the s-meter values of the radio. The program "S Meter Lite" was used to record these values.

This test is performed in an uncontrolled environment as there might be reflections from the ground and surrounding objects creating an unknown applied field from antenna A. And there might be some near-field components present. But Antenna A has a very strong line of sight component as the gain of the antenna A is around 16 dBi. This can reduce effects from reflections coming from the sidelobes of the antenna. The measured result is shown in figure 9.11 on the following page. This test can give an indication of the antenna pattern. Because of the reciprocity of antennas the results apply to both transmission and reception. But this should not be used to validate the simulations as the test setup can have large error contributions. The pattern presented in figure 9.11 on the next page show a minimum value of -30 dB. This is because the measurment is taken from the s-meter on the Icom radio. This has a very limited dynamic range. This test procedure is relatively quick and simple to set up which makes it a valuable tool for troubleshooting possible future errors.

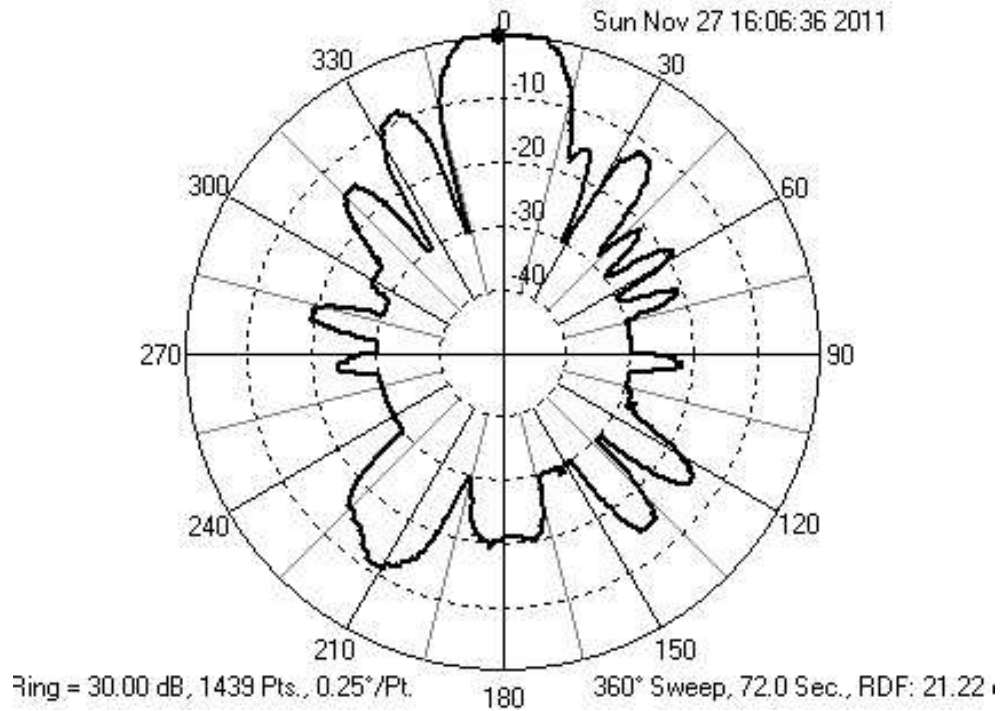[1]S Meter Lite Software was used to log the s-meter values.

Figure 9.11: Normalized measured antenna pattern. The s-meter values was read from the Icom radio while receiving a continous wave. The program S meter Lite was then used to record the values and plot this pattern

Chapter 10

Summary

A detailed analysis of the physical ground station setup has been performed. A tool for simulating and analyzing the antennas and their performance is now readily available through the use of the presented work. Received CW beacon signals from HO-68 gave indication that the station performs as was expected in terms of received signal strength.

10.1 Discussion

The results from the antenna measurements showed a deviation in the reflection seen at the antenna input. Small deviations are expected because there might have been small differences between the four antennas due to small inaccuracy's of the installed elements. But the big difference which is seen between antenna 1 and 4 vs. 2 and 3 is more than would be expected. The metal mast stands in between antenna 2 and 3 and this is close enough to the near field to possibly affect the antenna parameters. In this case it improves the antenna impedance. But there is no proof to this conclusion.

The antenna simulations was performed without simulating the input antenna impedance. This was done because the input to the Yagi-Uda antenna is looking into a matching network that connect to both the horizontal and vertical antenna to create a circular polarization. SO the input impedance will be different here than directly into each folded dipole antenna. If the input impedance had been simulated, it could have indicated what kind of effect the metal mast has on the input impedance of the surrounding antennas. As the simulation files are included in appendix H on page 119, this can easily be done for those who have a FEKO license. It might be possible to tune the antenna impedance to an even better matched condition, but all the antennas remain under a VSWR ratio of 1:1.6 (almost) which is the given performance in the datasheet.

10.2 Conclusions

The new UiO ground station is operational and should be capable of sustaining a communication link with the future CubeSTAR satellite. An important goal with this thesis was to create a document which made it easier for future students and participants in the project to understand the ground station parameters and how to operate it.

The HO-68 satellite was used for testing the received signal strength because it was very stable. But many more downlink beacon messages was decoded successfully from other student satellites, although their signal was much more unstable. There was strong fluctuations in signal strength. There might be several reasons for this behavior, for example if the satellite is not stable and spins. Then the antenna will be misaligned in a periodic behavior causing a varying received signal strength.

10.3 Future Work

The grounds station is operational in it's current state. But there are a few improvements to consider in the future. There are two relatively easy action items that should be considered first.

1. The 100 meter long COAX1 cable has been kept to it's full length until it is decided for certain what length is required. Between 20-30 meters of cable can probably be removed. Because the characteristic impedance of the cable is slightly different from 50 Ω, the final cable length should end up at a multiple of half a wavelength or whichever length give the best matching.

2. The laser installed on the cross boom should work by simply replacing the transparent plastic front cover by a more suiting material which let the laser beam through clear

Hopefully many students will take part in using this ground station in the future. It is very rewarding to hear "sounds from outer space" through the reception of morse code signals. And this might increase interest for new people to evaluate and contribute with additional improvements to the ground station.

Bibliography

[1] Constantine a. Balanis. *Antenna Theory - Analysis and Design.* John Wiley and Sons, 3rd edition, 2005.

[2] Constantine a. Balanis. *Modern Antenna Handbook.* John Wiley and Sons, 1st edition, 2008.

[3] Jøran Antonsen and Torbjørn Houge. The norwegian student satellite program ansat. In *ESA Symposium on European Rocket and Balloon Programmes and Related Research, Bad Reichall, Germany 2009.*, 2009.

[4] Tore André Bekkeng. Prototype development of a multi-needle langmuir probe system. Master's thesis, The University of OSlo, Norway, 2009.

[5] D.B. Davidson, I.P. Theron, U. Jakobus, F.M. Landstorfer, F.J.C. Meyer, J. Mostert, and J.J. Van Tonder. Recent progress on the antenna simulation program feko. In *Communications and Signal Processing, 1998. COMSIG '98. Proceedings of the 1998 South African Symposium on*, pages 427 –430, sep 1998.

[6] Daniel Fleisch. *A Student's Guide to Maxwell's Equations.* Cambridge University Press, 1st edition, 2008.

[7] Rastislav Galuscak and Pavel Hazdra. Circular polarization and polarization losses. *DUBUS*, pages 2 − 3, 2006.

[8] Michael Hiebel. *Fundamentals of Vector Network Analysis.* Rhode and Schwarz, 4th edition, 2008.

[9] Telecommunication Standardization Sector (ITU-T). Specific attenuation model for rain for use in prediction methods. *RECOMMENDATION ITU-R P.838-1*, 1992.

[10] T.Lindem J. L. Tresvig, T.A. Bekkeng. Cubestar - a nano satellite for space weather monitoring. 20010.

[11] G. Jönnson L. Sundström and H. Börjeson. *Radio Electronics.* Lund University, 1st edition, 2010.

[12] The Amateur Radio Relay League. *Antenna Book*. The ARRL inc., 3rd edition, 2009.

[13] Reinhold Ludwig and Gene Bogdanov. *RF Circuit Design - Theory and Applications*. Pearson Prentice Hall, 2nd edition, 2010.

[14] K. A. Norton A. P. Barsis P. L. Rice, A. G. Longley. *Transmission Loss Predictions for Troposheric Communication Circuits Volumes I*. National Burau Of Standards, 1967.

[15] Helen Page. Genso: A report on the early operational phase. 2010. http://www.genso.org/ (2011-02-25).

[16] R. Bruce Robert-Goodson. *The Complete Guide to Metal Boats*. International Marine and Ragged Mountain Press, 1st edition, 2000.

[17] Simon R. Saunders and Alejandro Aragón-Zavala. *Antennas and Propagation for Wireless Communication Systems*. John Wiley and Sons, 2nd edition, 2007.

[18] P.A. Schulz. Radar sensitivity, receiver calibration, and sky noise. In *Radar Conference, 2010 IEEE*, pages 1464 –1466, may 2010.

[19] Bernard Sklar. *Digital Communications - Fundamentals and Applications*. Prentice Hall, 2nd edition, 2001.

[20] Charles Bostian Timothy Pratt and Jeremy Allnutt. *Satellite Communications*. John Wiley and Sons, 2nd edition, 2003.

[21] Frank Travanty. Tower and antenna wind loading as a function of height. *QEX, ARRL*, pages 4 – 5, 2001.

[22] Hennig Vangli. Construction of a remotely operated satellite ground station for low earth orbit communication. Master's thesis, The University of OSlo, Norway, 2010.

[23] Dr. John L. Volakis. *Antenna Engineering Handbook*. McGraw-Hill, 4th edition, 2007.

[24] R. Walker, P. Galeone, H. Page, A. Castro, F. Emma, N. Callens, and J. Ventura-Traveset. Esa hands-on space education project activities for university students: Attracting and training the next generation of space engineers. In *Education Engineering (EDUCON), 2010 IEEE*, pages 1699 –1708, 2010.

Appendix A

Real and Imaginary Part of Antenna Input Impedance

Here the real and imaginary parts of the input impedance of the antennas are presented.
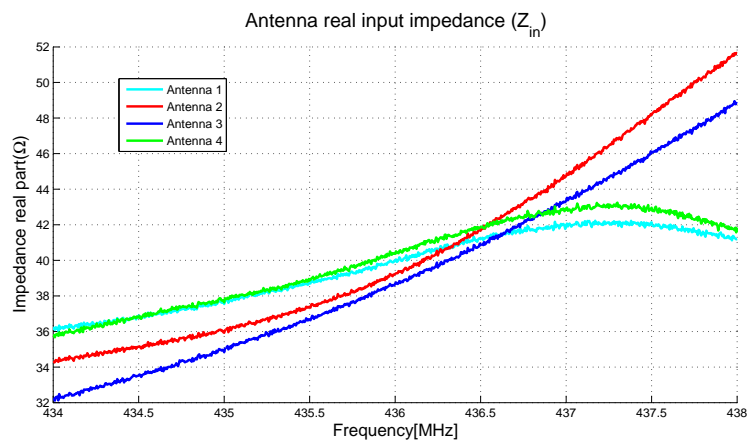
Figure A.1: Real part of antenna input impedance
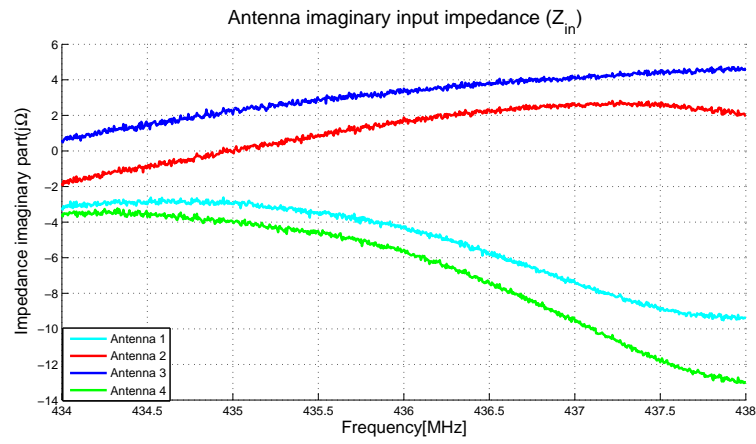
Figure A.2: Imaginary part of antenna input impedances

Appendix B

Explanation for the Antenna Assembly
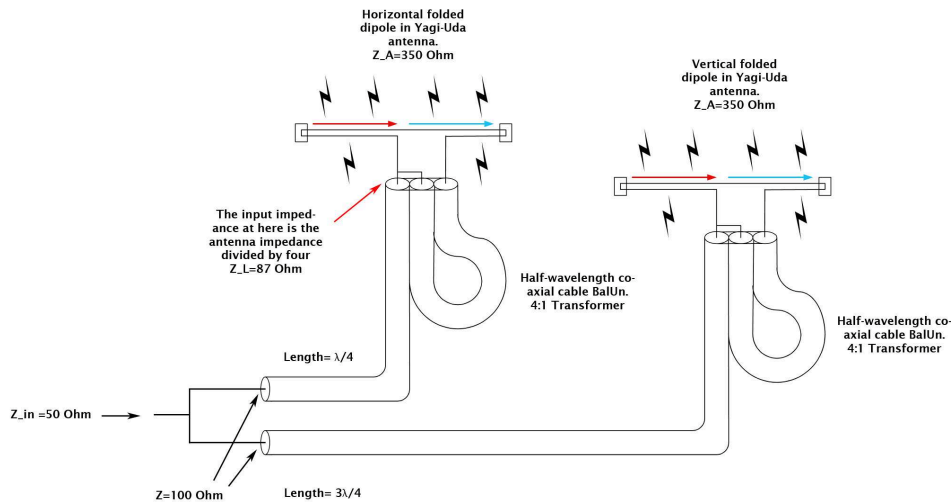
Figure B.1: An illustration on the matching in the antenna assembly on the 436CP30 antenna The two folded dipoles represent the two folded dipoles, one vertical and one horizontal, in the Yagi-Uda antenna (Credit: Wikipedia, modified)

The actual input impedance for the two folded dipoles in the Yagi-Uda antenna is not known. It is set to 350 Ω in this case to demonstrate the possibility to transform the parallel connection of these two to 50 Ω. The antenna assembly setup can be seen in figure B.1. This

The first step is a half-wavelength coaxial cable that works as a 4 to 1 transformer as well as an balun which transform the balanced antenna terminals to an unbalanced input conection. After this there are two cables with

lengths multiple of quarter wavelengths. Equation 2.16 on page 12 can now be utilized to calculate the impedance transformation.

Firstly the antenna impedance is divided by four because of the balun and ends up at a load impedance Z_L at approximately 87 Ω. Then the input impedance to each line is transformed by transmission lines of multiples of a quarter wavelength. Theese are the RG-6 coaxial cables in the antenna assembly, they both have the characteristic impedance Z_0 of 75 Ω. The input impedance to each branch is then

$$Z_{in} = \frac{Z_0^2}{Z_L} = \frac{87^2}{75} \approx 100\Omega$$

When these are connected in parallel the total input impedance Z_{in} becomes approximately 50 Ω. The reason for the extra half-wavelength of the cable to the vertical antenna is to get circular polarization.

Appendix C

Icom-910H S-meter Calibration Data

Table C.1 on the next page present the measured s-meter values on the ICOM 910H radio while applying a continous wave from a signal generator to the input of the radio. The input values are presented in dBm. In the column termed IARU show the recommendation for s-meter calibration from the International Amateur Radio Union (IARU).

Input	S-meter	IARU	Input	S-meter	IARU	Input	S-meter	IARU
-141	S0	S1	-107	S5.5		-73	S9+20	S9+20
-140	S0		-106	S6	S7	-72	S9+20	
-139	S0		-105	S6.5		-71	S9+20	
-138	S0		-104	S6.5		-70	S9+20	
-137	S0		-103	S7		-69	S9+20	
-136	S0		-102	S7.5		-68	S9+30	
-135	S0	S2	-101	S7.5		-67	S9+30	
-134	S0		-100	S8		-66	S9+30	
-133	S0		-99	S8	S8	-65	S9+30	
-132	S0		-98	S8.5		-64	S9+30	
-131	S0		-97	S9		-63	S9+30	S9+30
-130	S0		-96	S9		-62	S9+30	
-129	S0	S3	-95	S9		-61	S9+30	
-128	S0		-94	S9		-60	S9+30	
-127	S0		-93	S9	S9	-59	S9+40	
-126	S0		-92	S9.5		-58	S9+40	
-125	S0		-91	S9.5		-57	S9+40	
-124	S0		-90	S9.5		-56	S9+40	
-123	S0	S4	-89	S9.5		-55	S9+40	
-122	S0		-88	S9.5		-54	S9+40	
-121	S0		-87	S9.5		-53	S9+50	S9+40
-120	S0		-86	S9.5		-52	S9+50	
-119	S0		-85	S9+10		-51	S9+50	
-118	S0		-84	S9+10		-50	S9+50	
-117	S0	S5	-83	S9+10	S9+10	-49	S9+50	
-116	S0		-82	S9+10		-48	S9+50	
-115	S1		-81	S9+10		-47	S9+50	
-114	S1.5		-80	S9+10		-46	S9+50	
-113	S2		-79	S9+10		-45	S9+60	
-112	S3		-78	S9+10		-44	S9+60	
-111	S3.5	S6	-77	S9+20		-43	S9+60	
-110	S4		-76	S9+20		-42	S9+60	
-109	S4.5		-75	S9+20		-41	S9+60	
-108	S5		-74	S9+20		-40	S9+60	

Table C.1: S-meter calibration results.

Appendix D

UiO Ground Station Part List

Part	Model	Brand/Supplier
Antennas	436CP30	sm7sjr.se
Power splitter	Passive 4-port	sm7sjr.se
Polarization Switch	Integrated with antenna	sm7sjr.se
Preampliffier (LNA)	SP-7000	SSB/Permo electronics
Rotor	G-5500	Yesu/Permo electronics
Rotor RS232 interface	GS-232B	Yesu/Permo electronics
Lightning Surge arrestor	CA-23RS	Permo electronics
Coaxial Cable	WF103	Westflex/Permo electronics
Control Cable	PFK 6 leads	Permo electronics
Sound interface card	Rig Expert Tiny CI-V-1	Permo electronics
Az-El rotor	G-5500	Yaesu/Permo electronics
N-connector	55035	/Permo electronics
Transceiver	IC-910H	Icom

Table D.1: Partlist for UiO Ground Station

Appendix E

Matlab Script for Handling Measured S-parameters
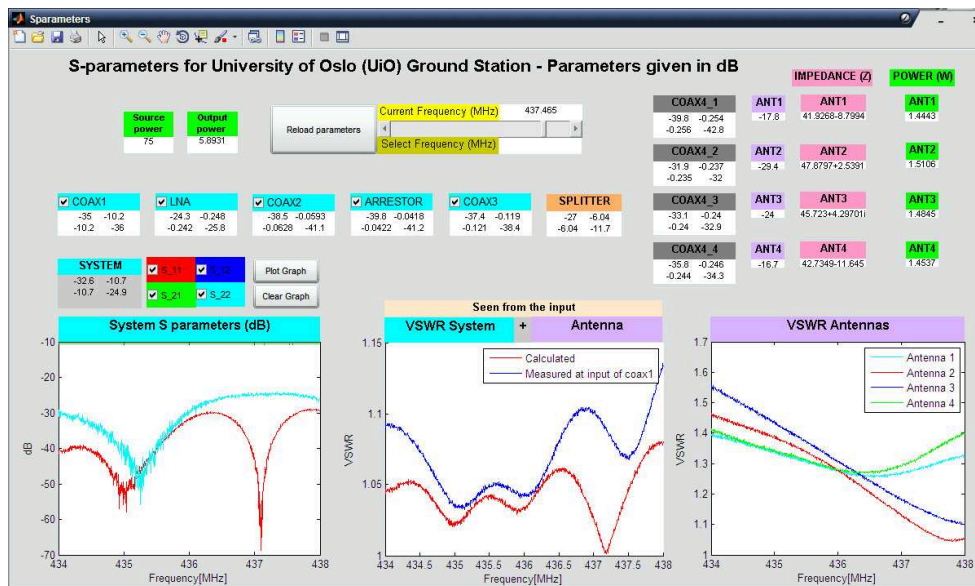
Figure E.1: Printout of the Sparam matlab script. This shows alle the Measured S-parameters in the ground station in decibels. The LNA is described in its off mode which makes thess results apply to transmission

This script uses the measured data for each component in th ground station system and present their measured S-parameters in dB. The measured data is found in the folder named data. All the names of each coincide with the presented overview throughout this text

E.1 Running the Script

To start the script, write "guide Sparmameters" in a matlab installation. Make sure to have the working directory in the same folder as the script. Press run figure to start the application and press the "Reload parameters" button in the window. Individual 2-port networks can be selected by pressing on the associated check boxes and pressing "Reload parameters" again. The chosen network will then appear in the system bar on the left and the different S-parameters can be plotted over the frequency range in the "System S parameters (dB)" by selecting the wanted s-parameters, pressing "Clear Graph" and then "Plot Graph". When selecting several networks the individual S-parameter matrixes is converted to T-parameters described in section 3.1.5 on page 17.Then these are combined and converted back to S-parameters and presented in the "SYS-TEM" box on the left. To change the frequency in question for all the boxes presenting S-parameters. Simply tap the yellow frequency slider and then press "Reload parameters" to load the new values.

E.2 The SPLITTER Component

The splitter component is showed in an orange colored box. Because this in reality is a 5-port network it has parameters that are dependent on the output of each port. The 2-port representation contain the following.

S_{11} shows the reflection on the input which is found by calculating the combined reflection at the input of the coaxial transmission lines COAX4_1, COAX4_2, COAX4_3 and COAX4_4. The attenuation of the incident wave is also accounted for to get the correcet magnitude of each reflected component.

$S_{12} = S_{21}$ presents the insertion loss from the input to each of the outputs. Because the power is divided out to four ports the theoretical minimum for this value is -6 dB. So if we want to describe the losses in the internal transmission line it selves, this is only 0.04 dB.

S_{22} shows the reflection looking in to either port 2,3,4 or 5 of the splitter.

E.3 Power Delivered to Antennas

The power delivered to each antenna is hown in green boxes on the right in figure E.1 on the previous page. They are calculated by finding the gain from the radio through each antenna branch. This is done by converting all the S-parameters to T-parameters and cascading the matrixes before converting back to a single S-matrix that describe each branch. Then the matlab function *powergain()* is used to find the gain. In this case the gain is off course less

than 1 as there is only loss and no gain through the coaxial cables when transmitting.

Appendix F

Link Budget Results

In this section the current link budget is presented. The worksheet can be found in appendix H on page 119.

Parameter:	Value:	Units:	Comments:
CubeSTAR - UiO Ground Station	NOTE:		**CubeSTAR - UiO Ground** **Date Data Last Modified:**
Downlink Telemetry Budget:			Version: 2.4.1 **2011 November 24**
Spacecraft:			
Spacecraft Transmitter Power Output:	1,0	watts	This value is transferred from "Transmitters" W/S, Cell [E50]
In dBW:	0,0	dBW	Transmitter power expressed in dB above one watt
In dBm:	30,0	dBm	Transmitter power expressed in dB above one milliwatt
Spacecraft Total Transmission Line Losses:	0,6	dB	This value is transferred from "Transmitters" W/S, Cell [I68]
Spacecraft Antenna Gain:	2,2	dBi	This value is selected at "Antenna Gain" W/S, Cell [E41]
Spacecraft EIRP:	1,6	dBW	Spacecraft Effective Isotropic Radiated Power (EIRP) [EIRP=Pt x Ltl x Ga]
Downlink Path:			
Spacecraft Antenna Pointing Loss:	0,1	dB	This value is calculated in the "Antenna Pointing Losses" W/S, and trasferred from Cell [K85]
S/C-to-Ground Antenna Polarization Loss:	3,0	dB	This value is calculated in the "Polarization Loss" W/S and is transferred from Cell [F60].
Path Loss:	151,0	dB	Lp = 22 + 20LOG(D/λ); Transferred from "Orbit & Frequency" W/S
Atmospheric Loss:	0	dB	This value is transferred from "Atmos. & Ionos. Losses" W/S, Cell [D23]
Ionospheric Loss:	1,0	dB	This value is transferred from "Atmos. & Ionos. Losses" W/S, Cell [D47:D50]
Rain Loss:	0,0	dB	This value should be estimated by the link model operator and place into Cell [B18]
Isotropic Signal Level at Ground Station:	-153,5	dBW	This is the signal level received at the Earth in the vacinity of the ground station using an omnidirectional antenna.
Ground Station (EbNo Method):			
------- Eb/No Method -------			
Ground Station Antenna Pointing Loss:	1,1	dB	This value is transferred from "Antenna Pointing Losses" W/S, Cell [K102]
Ground Station Antenna Gain:	20,5	dBi	This value is selected at "Antenna Gain" W/S, Cell [E58]
Ground Station Total Transmission Line Losses:	0,4	dB	This value is transferred from the "Receivers" W/S, Cell [J123]
Ground Station Effective Noise Temperature:	415	K	This value is calculated in the "Receivers" W/S and Transferred from Cell [J138]
Ground Station Figure of Merrit (G/T):	-6,1	dB/K	G/T = Ga-Ltl-10log(Ts). This is the uptimate measure of the receiver's performance.
G.S. Signal-to-Noise Power Density (S/No):	67,9	dBHz	**Boltzman's Constant:** -228,6 dBW/K/Hz
System Desired Data Rate:	9600	bps	Operator selects this value. Be Careful! This is the data rate, not the symbol rate.
In dBHz:	39,8	dBHz	This is simply = 10log(R); R= data rate
Telemetry System Eb/No for the Downlink:	28,0	dB	
Demodulation Method Seleted:	G3RUH FSK		Values selected in "Modulation-Demodulation W/S, Cell [E30]
Forward Error Correction Coding Used:	None		Value selected in "Modulation-Demodulation" W/S, also Cell [E30]
System Allowed or Specified Bit-Error-Rate:	1,0E-05		The selected value is transferred from the "Modulation-Demodulation W/S, Cells [E33:E50]
Demodulator Implementation Loss:	0	dB	This value is transferred from the "Modulation-Demodulation W/S, Cell[E52]
Telemetry System Required Eb/No:	18	dB	The selected value is transferred from the "Modulation-Demodulation W/S, Cells [F33:F50]
Eb/No Threshold:	18	dB	This is the result of the "Modulation-Demodulation" W/S and is transferred from Cell [H32]
System Link Margin:	10,0	dB	
Ground Station Alternative Signal Analysis Method (SNR Computation):			
---------- SNR Method ------------			
Ground Station Antenna Pointing Loss:	1,1	dB	This value is transferred from "Antenna Pointing Losses" W/S, Cell [K102]
Ground Station Antenna Gain:	20,5	dBi	This value is selected at "Antenna Gain" W/S, Cell [E58]
Ground Station Total Transmission Line Losses:	0,4	dB	This value is transferred from the "Receivers" W/S, Cell [J123]
Ground Station Effective Noise Temperature:	415	K	This value is calculated in the "Receivers" W/S and Transferred from Cell [J138]
Ground Station Figure of Merit (G/T):	-6,1	dB/K	G/T = Ga-Ltl-10log(Ts). This is the ultimate measure of the receiver's performance.
Signal Power at Ground Station LNA Input:	-134,6	dBW	Ps = Pso+Ga-Lpl-Ltl; This is the signal power that has arrived at the ground station receiver.
Ground Station Receiver Bandwidth (B):	25 000	Hz	Signal Spectrum Must Pass Through This Data Filter NOTE:
G.S. Receiver Noise Power (Pn = kTB):	-158,4	dBW	Pn = K + 10log(Ts) + 10log(B). This is the total noise power arriving at the ground station receiver.
Signal-to-Noise Power Ratio at G.S. Rcvr:	23,9	dB	Ps/Pn = Ps(in dBW) - Pn (in dBW)
Analog or Digital System Required S/N:	18,0	dB	If system is digital, use values from "Modulation-Demodulation" W/S. If analog, use appropriate value from text book.
System Link Margin	5,9	dB	

Figure F.1: Link budget downlink result

| Parameter:	Value:	Units:	Comments:
CubeSTAR - UiO Ground Station	NOTE:		**CubeSTAR - UiO G** — Date Data Last Modified:
Uplink Command Budget:			Version: 2.4.1 — 2011 November 24
Ground Station:			
Ground Station Transmitter Power Output:	75,0	watts	This value is transferred from "Transmitters" W/S, Cell [E15].
In dBW:	18,8	dBW	Transmitter power expressed in dB above one watt
In dBm:	48,8	dBm	Transmitter power expressed in dB above one milliwatt
Ground Stn. Total Transmission Line Losses:	11,5	dB	This value is transferred from "Transmitters" W/S, Cell [I33]
Antenna Gain:	20,5	dBi	This value is selected at "Antenna Gain" W/S, Cell [E11]
Ground Station EIRP:	27,8	dBW	Ground Station Effective Isotropic Radiated Power (EIRP) [EIRP=Pt x Ltl x Ga]
Uplink Path:			
Ground Station Antenna Pointing Loss:	1,1	dB	This value is calculated in the "Antenna Pointing Losses" W/S, and transferred from Cell [K43]
Gnd-to-S/C Antenna Polarization Losses:	3,0	dB	This value is calculated in the "Polarization Loss" W/S and is transferred from Cell [F40].
Path Loss:	151,0	dB	Lp = 22 + 20LOG(D/λ); Transferred from "Orbit & Frequency" W/S
Atmospheric Losses:	0,0	dB	This value is transferred from "Atmos. & Ionos. Losses" W/S, Cell [D23]
Ionospheric Losses:	1,0	dB	This value is transferred from "Atmos. & Ionos. Losses" W/S, Cell [D47:D50]
Rain Losses:	0,0	dB	This value should be estimated by the link model operator and place into Cell [B18]
Isotropic Signal Level at Spacecraft:	-128,3	dBW	This is the signal level received in space in the vacinity of the spacecraft using an omnidirectional antenna.
Spacecraft (Eb/No Method):			
------- Eb/No Method -------			
Spacecraft Antenna Pointing Loss:	0,1	dB	This value is transferred from "Antenna Pointing Losses" W/S, Cell [K63]
Spacecraft Antenna Gain:	2,2	dBi	This value is selected at "Antenna Gain" W/S, Cell [E24]
Spacecraft Total Transmission Line Losses:	0,4	dB	This value is transferred from the "Receivers" W/S, Cell [J52]
Spacecraft Effective Noise Temperature:	357	K	This value is calculated in the "Receivers" W/S and Transferred from Cell [J67]
Spacecraft Figure of Merrit (G/T):	-23,7	dB/K	G/T = Ga-Ltl-10log(Ts). This is the uptimate measure of the receiver's performance.
S/C Signal-to-Noise Power Density (S/No):	76,4	dBHz	Boltzman's Constant: -228,6 dBW/K/Hz
System Desired Data Rate:	600	bps	Operator selects this value. Be Careful! This is the data rate, not the symbol rate.
In dBHz:	27,8	dBHz	This is simply = 10log(R); R= data rate
Command System Eb/No:	48,7	dB	
Demodulation Method Seleted:	G3RUH FSK		Values selected in "Modulation-Demodulation W/S, Cell [E3]
Forward Error Correction Coding Used:	None		Value selected in "Modulation-Demodulation" W/S, also Cell [E3]
System Allowed or Specified Bit-Error-Rate:	1,0E-05		The selected value is transferred from the "Modulation-Demodulation W/S, Cells [E6:E23]
Demodulator Implementation Loss:	0,0	dB	This value is transferred from the "Modulation-Demodulation W/S, Cell[E25]
Telemetry System Required Eb/No:	18	dB	The selected value is transferred from the "Modulation-Demodulation W/S, Cells [F6:F23]
Eb/No Threshold:	18	dB	This is the result of the "Modulation-Demodulation" W/S and is transferred from Cell [H32]
System Link Margin:	30,7	dB	
Spacecraft Alternative Signal Analysis Method (SNR Computation):			← NOTE:
---------- SNR Method -----------			
Spacecraft Antenna Pointing Loss:	0,1	dB	This value is transferred from "Antenna Pointing Losses" W/S, Cell [K63]
Spacecraft Antenna Gain:	2,2	dBi	This value is selected at "Antenna Gain" W/S, Cell [E24]
Spacecraft Total Transmission Line Losses:	0,4	dB	This value is transferred from the "Receivers" W/S, Cell [J52]
Spacecraft Effective Noise Temperature:	357	K	This value is calculated in the "Receivers" W/S and Transferred from Cell [J67]
Spacecraft Figure of Merrit (G/T):	-23,7	dB/K	G/T = Ga-Ltl-10log(Ts). This is the ultimate measure of the receiver's performance.
Signal Power at Spacecraft LNA Input:	-126,6	dBW	Ps = Piso+Ga-Lpl-Ltl; This is the signal power that has arrived at the ground station receiver.
Spacecraft Receiver Bandwidth:	58 000	Hz	Signal Spectrum Must Pass Through This Data Filter. NOTE:
Spacecraft Receiver Noise Power (Pn = kTB)	-155,4	dBW	Pn = K + 10log(Ts) + 10log(B). This is the total noise power arriving at the ground station receiver.
Signal-to-Noise Power Ratio at G.S. Rcvr:	28,8	dB	Ps/Pn = Ps(in dBW) - Pn(in dBW)
Analog or Digital System Required S/N:	14,8	dB	If system is digital, use values from "Modulation-Demodulation" W/S. If analog, use appropriate value from text book.
System Link Margin:	14,0	dB	

Figure F.2: Link budget uplink result
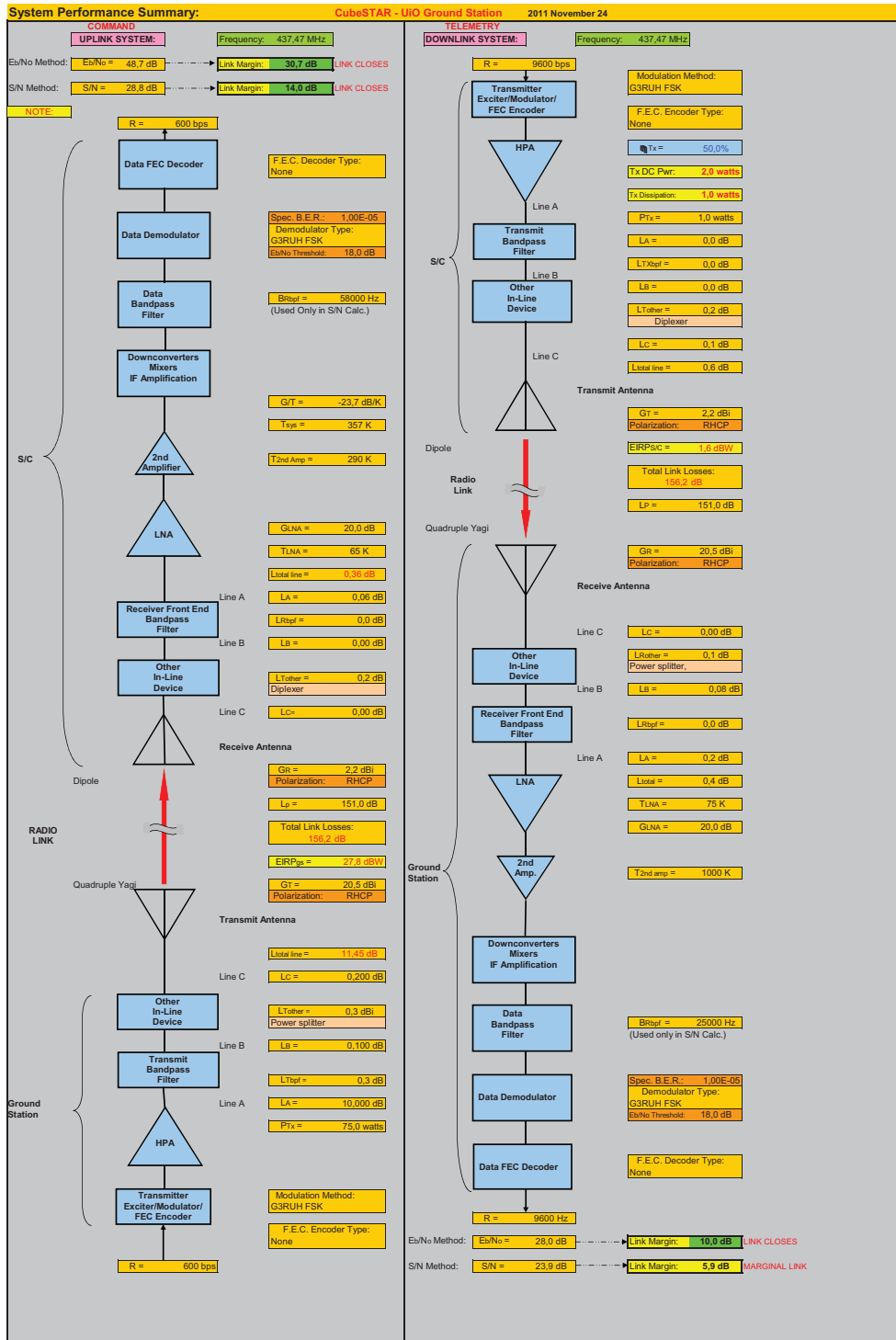
Figure F.3: Link budget system performance

Appendix G

Weather Statistics at the University of Oslo 2010/2011

Months	Temperature				Precipitation			Wind	
	Average	Normal	Warmest	Coldest	Total	Normal	Highest daily value	Average	Strongest wind
Sep 2010	11.3°C	10.8°C	19.6°C Sep 14	1.4°C Sep 29	89 mm	90 mm	30 mm Sep 25	2.8 m/s	9.6 m/s Sep 21
Oct 2010	5.7°C	6.3°C	16.1°C Oct 7	-5.0°C Oct 21	84 mm	84 mm	27 mm Oct 4	2.2 m/s	7.5 m/s Oct 15
Nov 2010	-2.0°C	0.7°C	9.2°C Nov 1	-12.1°C Nov 30	24 mm	73 mm	8 mm Nov 3	4.0 m/s	12.4 m/s Nov 10
Dec 2010	-9.2°C	-3.1°C	0.0°C Dec 16	-19.3°C Dec 22	15 mm	55 mm	4 mm Dec 5	2.2 m/s	10.6 m/s Dec 19
Jan 2011	-3.5°C	-4.3°C	5.1°C Jan 1	-12.8°C Jan 27	47 mm	49 mm	9 mm Jan 9	2.1 m/s	11.5 m/s Jan 1
Feb 2011	-4.9°C	-4.0°C	5.7°C Feb 3	-18.1°C Feb 13	53 mm	36 mm	15 mm Feb 11	2.3 m/s	12.9 m/s Feb 11
Mar 2011	0.6°C	-0.2°C	14.9°C Mar 23	-8.1°C Mar 6	18 mm	47 mm	5 mm Mar 9	2.5 m/s	10.0 m/s Mar 24
Apr 2011	9.4°C	4.5°C	20.3°C Apr 29	-0.8°C Apr 14	40 mm	41 mm	20 mm Apr 13	2.5 m/s	12.8 m/s Apr 8
May 2011	11.3°C	10.8°C	23.5°C May 9	0.0°C May 4	68 mm	53 mm	17 mm May 15	3.0 m/s	9.3 m/s May 24
Jun 2011	15.9°C	15.2°C	27.1°C Jun 3	8.0°C Jun 13	157 mm	65 mm	32 mm Jun 11	2.6 m/s	11.3 m/s Jun 2
Jul 2011	18.0°C	16.4°C	28.0°C Jul 28	9.6°C Jul 16	107 mm	81 mm	27 mm Jul 24	2.8 m/s	10.7 m/s Jul 22
Aug 2011	16.1°C	15.2°C	26.5°C Aug 1	6.7°C Aug 12	189 mm	89 mm	25 mm Aug 10	2.4 m/s	9.3 m/s Aug 28

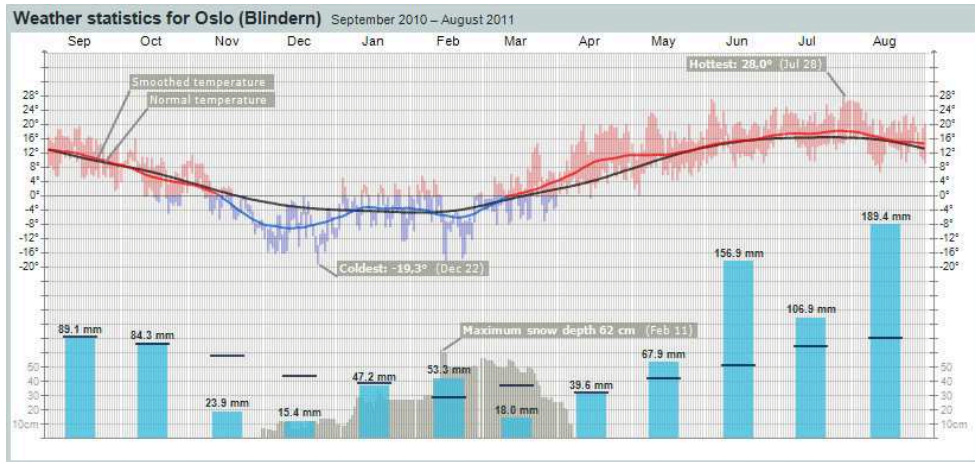Figure G.1: Weather statistics at the University of Oslo

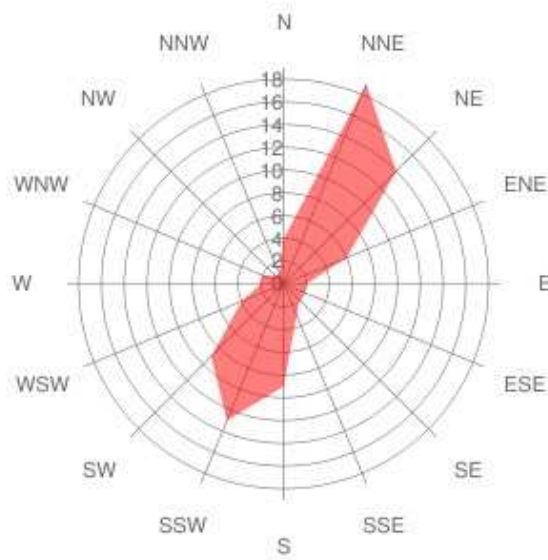Figure G.2: Weather statistics at the University of Oslo

Figure G.3: Average wind map at the University of Oslo

Appendix H

CD

The attached CD includes the following material

- FEKO simulation files.

- The link budget excel sheet.

- Sparam matlab script and all measured S-parameters (s2p and s1p files).

- Documentation to all components in UiO ground station (Datasheets).

- Pictures of antenna rig.

- PDF version of this document.

- 3D animations of the final antenna pattern.